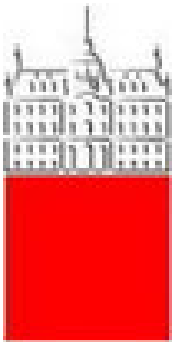
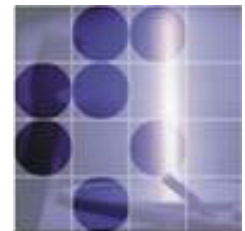

Photo-detectors

Peter Križan

Ljubljana



University of Ljubljana



"Jožef Stefan" Institute

Contents

Why (fast) single photon detection?

Photo-detectors

Some applications

Vacuum

- *Photomultiplier tubes (PMT)*
- *Microchannel plate photomultiplier tubes*

Solid-state photon detectors

Hybrid detectors

- *HPDs and HAPDs*
- *Other hybrid photosensors*

Gaseous photon detectors

Examples of applications

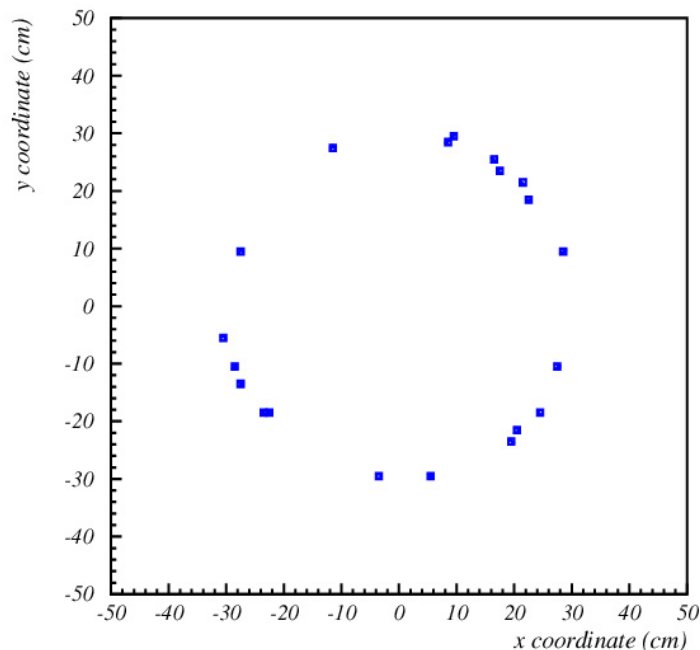
- *RICH detectors*
- *TOF counters*
- *Calorimeters*
- *Fiber trackers*
- *Non-accelerator experiments*

Example: photon detection in RICH counters

RICH counter: measure photon impact point on the photon detector surface

→ detection of **single** photons with

- sufficient **spatial resolution**
- **high efficiency** and **good signal-to-noise ratio**
- over a **large area** (square meters)



Special requirements:

- **Operation in magnetic field**
- **High rate capability**
- **Very high spatial resolution**
- **Excellent timing (time-of-arrival information)**

Parameters of photo-sensors

Photon detection efficiency (PDE)

- quantum efficiency
- collection efficiency / Geiger discharge probability

Granularity

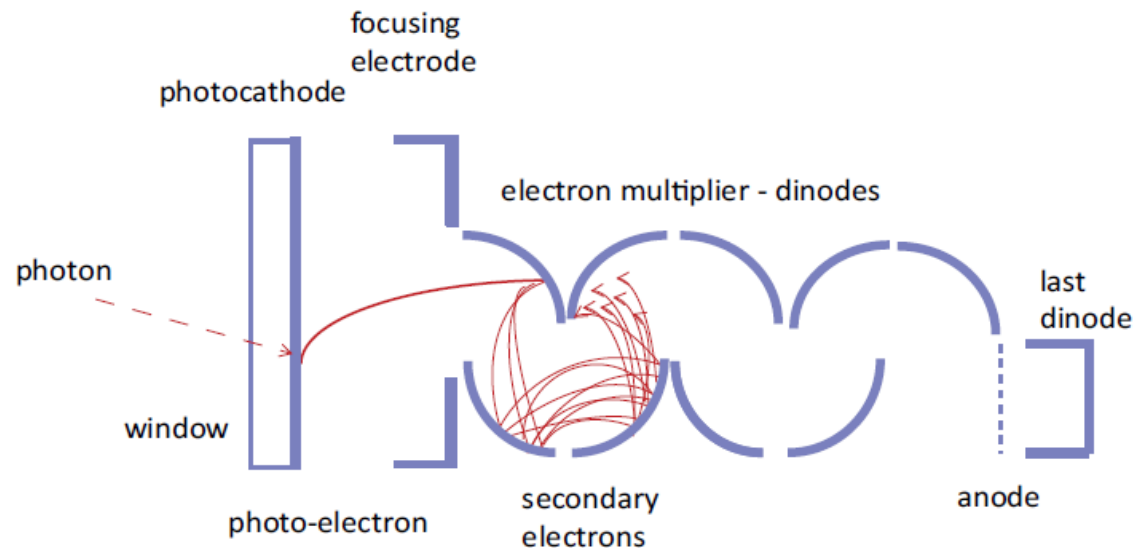
Time resolution (transient time spread – TTS)

Long term stability

Operation in magnetic field

Dark count rate

+ ...



Detection of light

Vacuum

- ◆ *Photomultiplier tubes (PMT)*
- ◆ *Microchannel plate photomultiplier tubes*

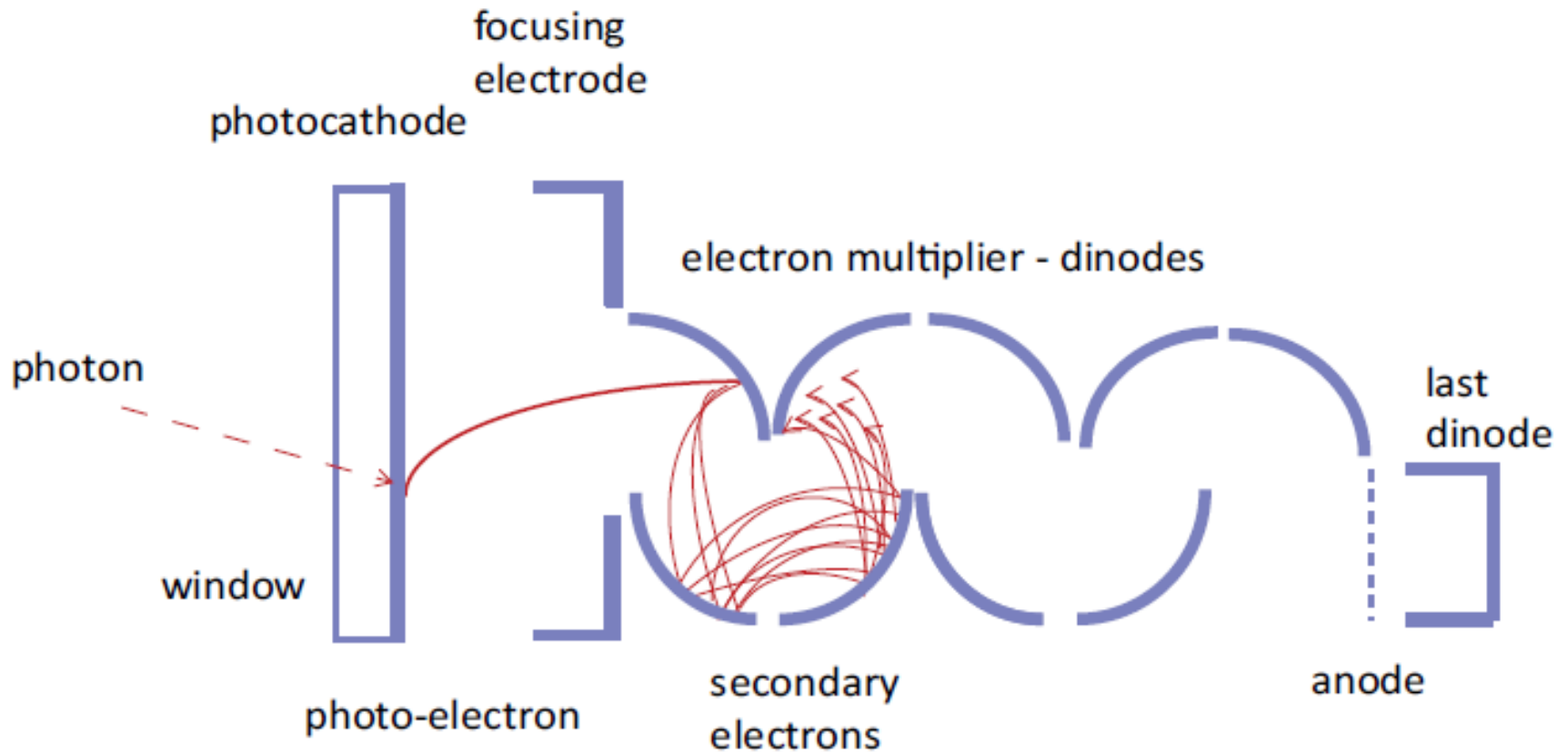
Solid-state photon detectors

Hybrid detectors

- ◆ *HPDs and HAPDs*
- ◆ *Other hybrid photosensors*

Gaseous photon detectors

Photomultiplier tube (PMT)



Photomultiplier tube

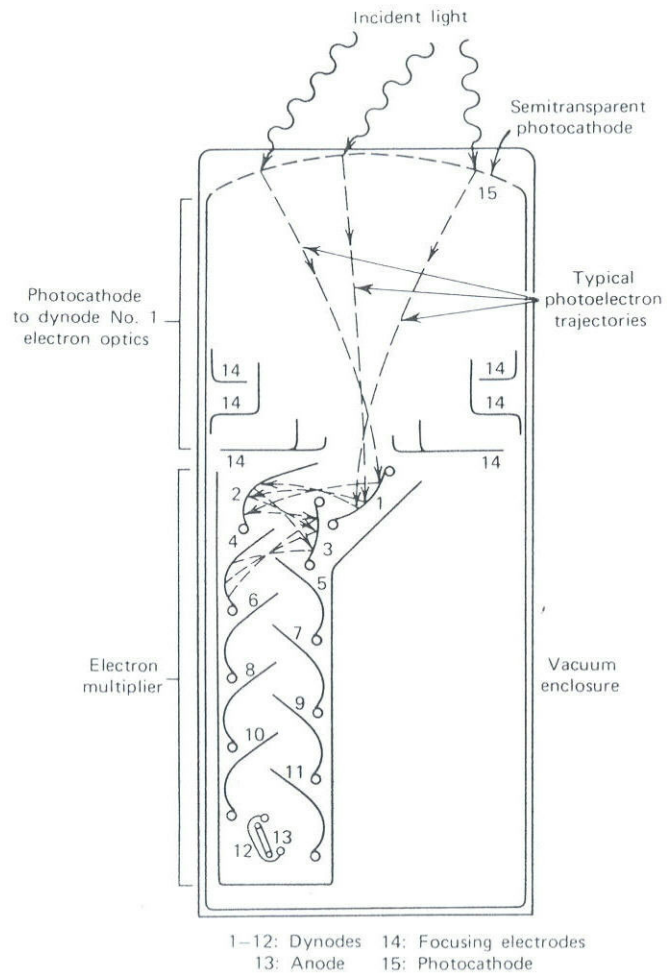
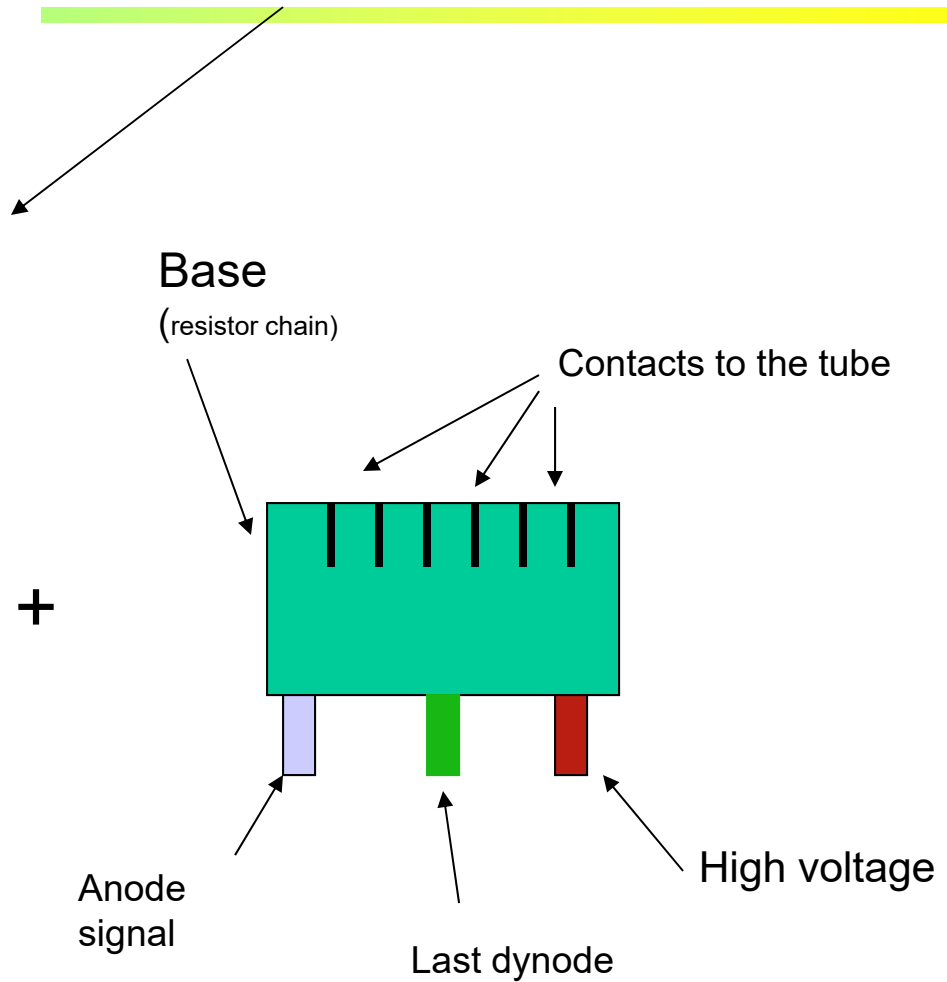


Figure 9-1 Basic elements of a PM tube. (From Ref. 1.)



- 1) Measure pulses
- 2) Measure current

Photocathode

◆ Photoeffect : $E_e = h\nu - \Phi$

Φ → Max kinetic energy of the photo-electron
 $h\nu$ → Energy of the photon
 Φ → Work function

◆ Quantum Efficiency

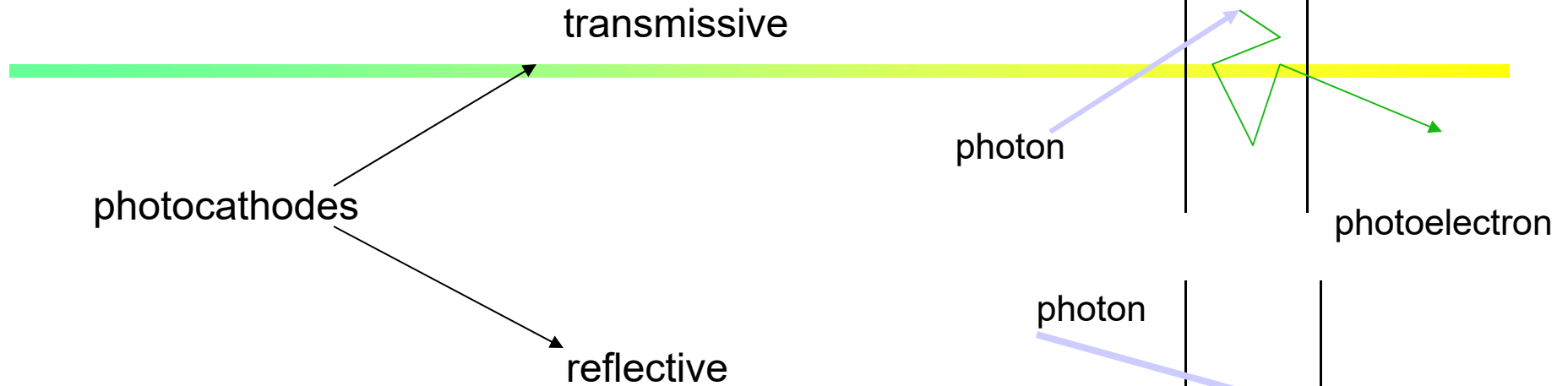
$$\eta(\lambda) = \frac{\text{Number of photoelectrons exiting the cathode}}{\text{Number of incoming photons}}$$

Spectral sensitivity

$$E(\lambda) = \frac{I_k}{P(\lambda)}$$

I_k → Photoelectron current (A)
 $P(\lambda)$ → Incoming light power (W)

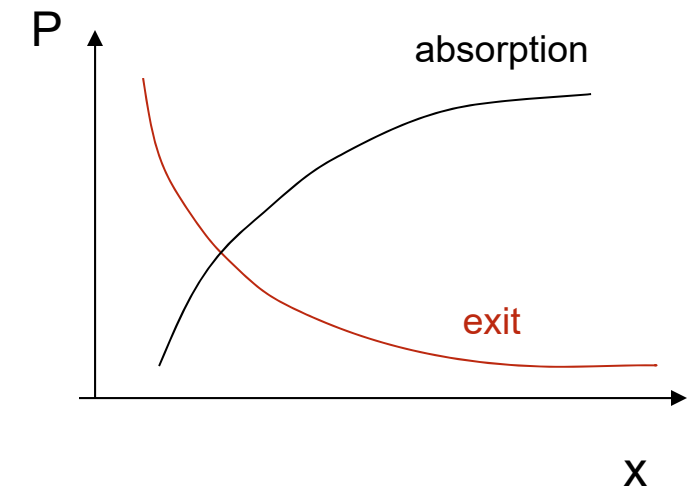
$$\eta(\lambda) = \frac{I_k/e_0}{P(\lambda)/h\nu} = \frac{hc}{\lambda e_0} E(\lambda)$$



Quantum efficiency is a product of:

- Transmission probability (window)
- Probability for absorption and photoeffect
- Probability for the electron to exit the photocathode

⇒ Optimal photocathode thickness



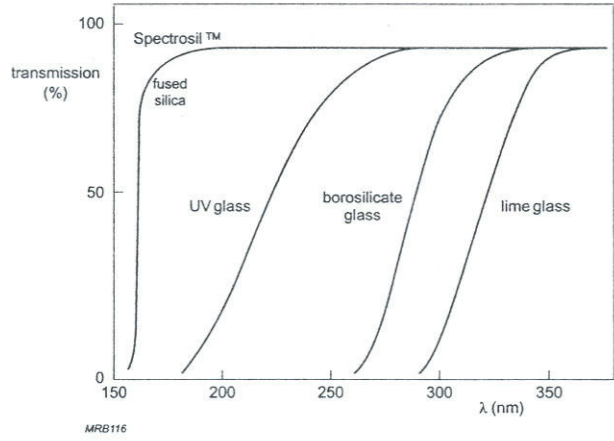


Fig.1.5 Transmission (%) as a function of wavelength λ for various glasses used in photomultiplier input windows (thickness 3 mm)

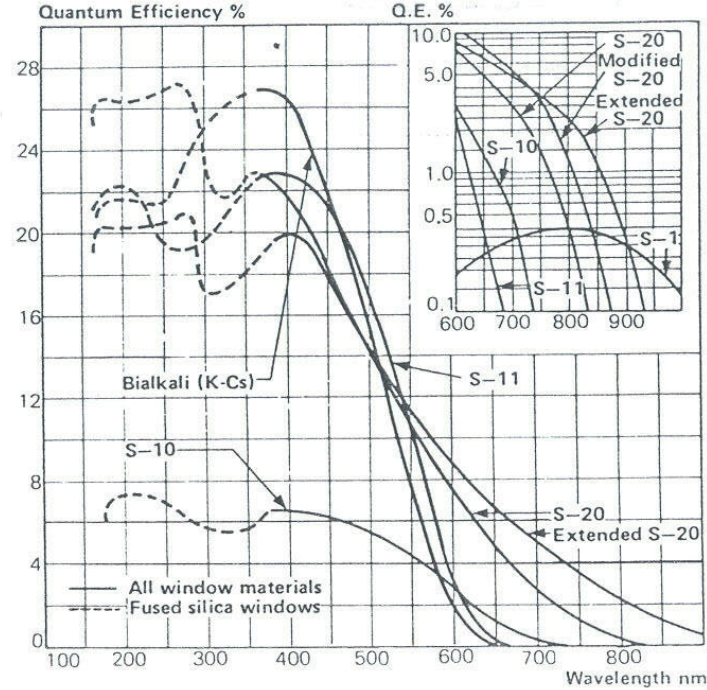


Fig. 8.2. Quantum efficiency of various photocathode materials (from EMI Catalog [8.2])

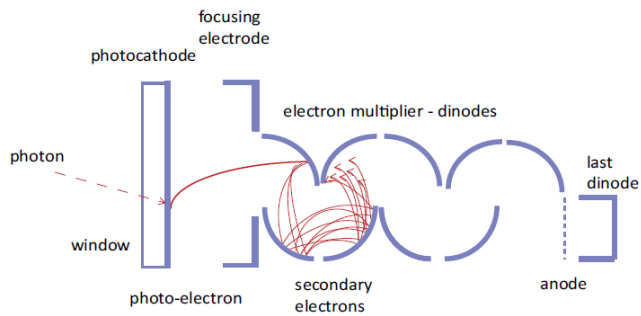


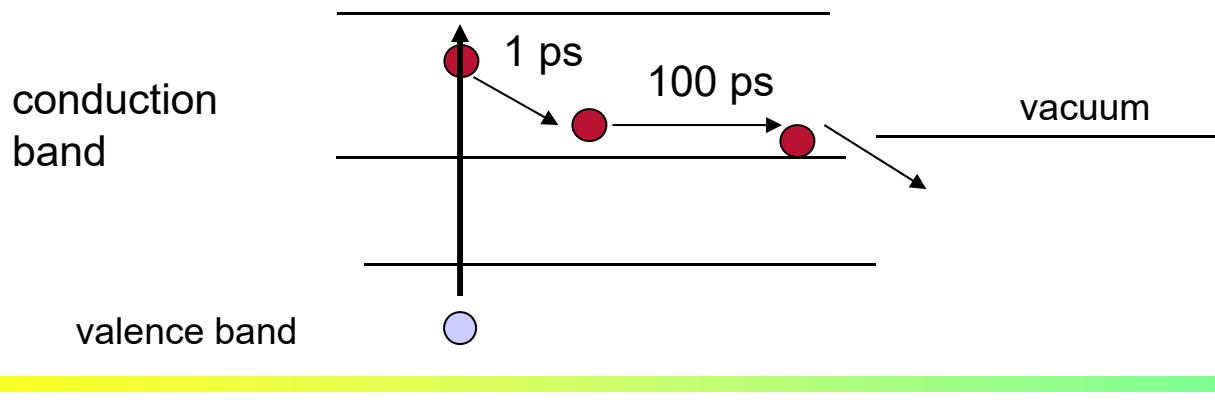
Table 8.1. Photocathode characteristics (from RTC catalog [8.3])

Cathode type	Composition	λ at peak response [nm]	Quantum efficiency at peak
S1 (C)	Ag - O - Cs	800	0.36
S4	SbCs	400	16
S11 (A)	SbCs	440	17
Super A	SbCs	440	22
S13 (U)	SbCs	440	17
S20 (T)	SbNa - KCs	420	20
S20R	SbNa - KCs	550	8
TU	SbNa - KCs	420	20
Bialkali	SbRb - Cs	420	26
Bialkali D	Sb - K - Cs	400	26
Bialkali DU	Sb - K - Cs	400	26
SB	Cs - Te	235	10

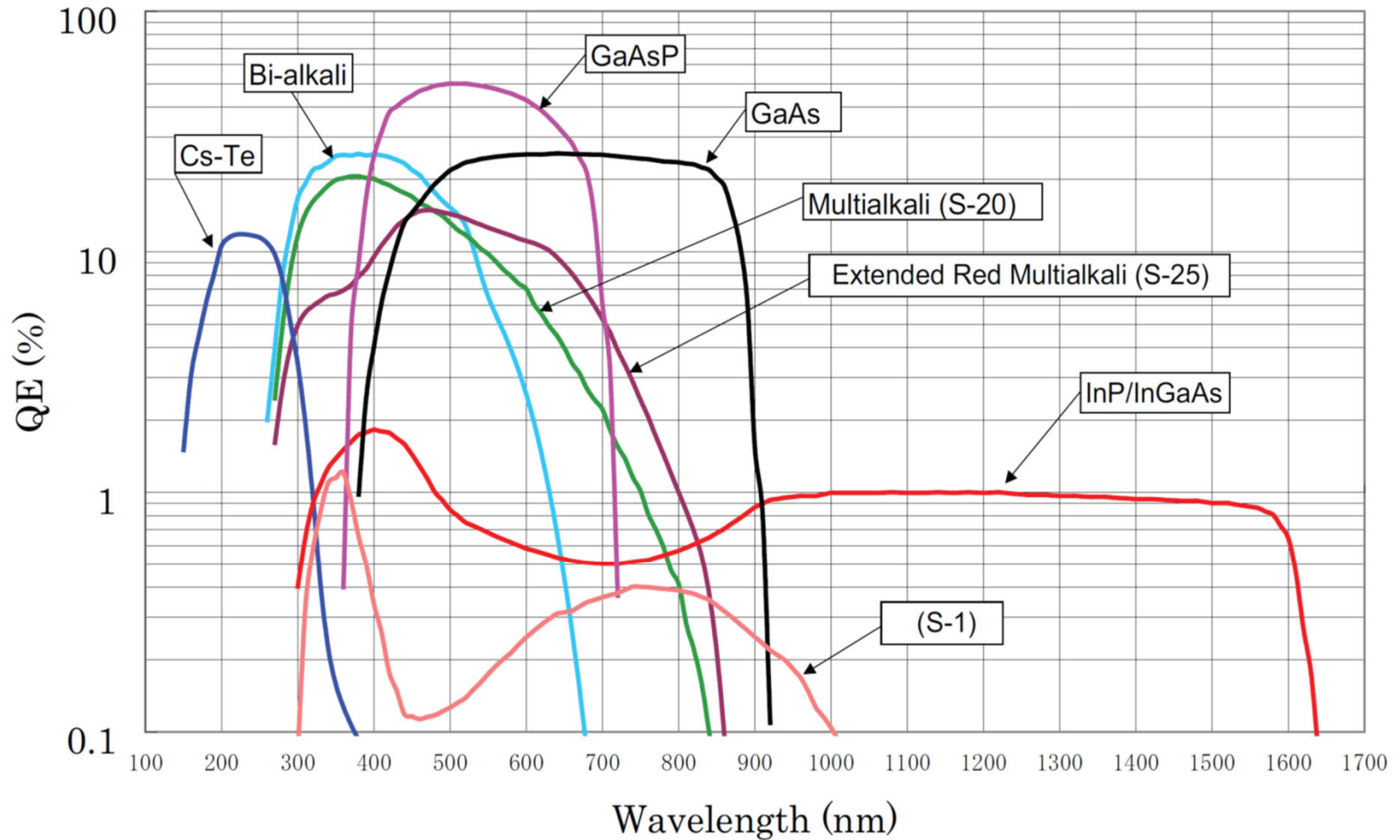
Photocathode material: usually semiconductors

e.g. antimony (Sb) + alkaline metals (K, Cs, Rb, Na ...)

- Photoelectron suffers energy losses in a metal because of many collisions with free electrons ($\eta \approx 0.1 \%$)
- Semiconductors: conduction band has only a few free electrons \rightarrow few collisions \rightarrow smaller energy loss before reaching the surface, $\eta = 10 - 30\%$.
- Material with negative electron affinity (like GaP doped with Zn+Cs) for electrons in the conduction band, $\eta \approx 80 \%$.

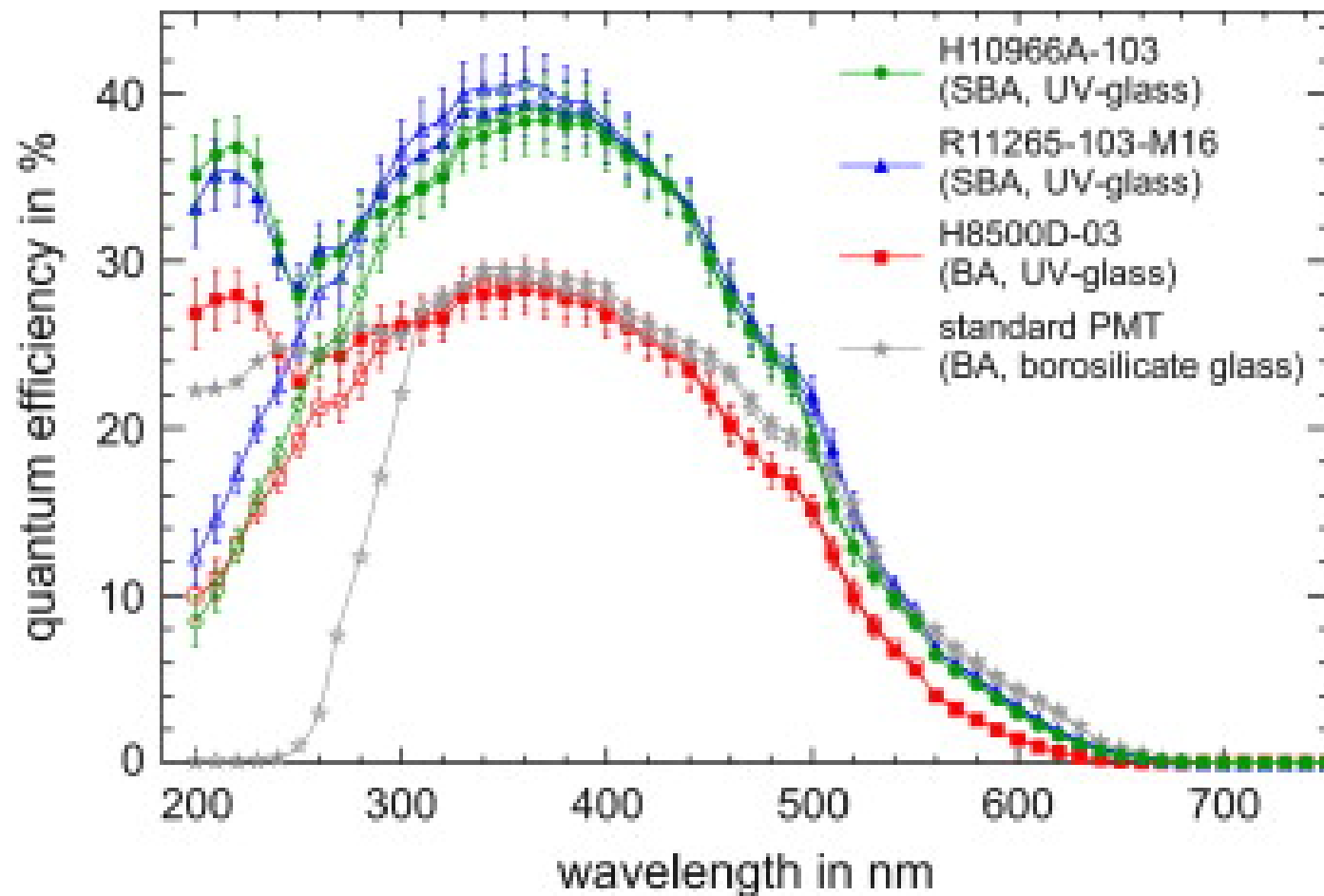


Quantum efficiency



Extending PMT sensitivity to lower wavelengths

CBM RICH R+D: **Wavelength-shifter coating** of the PMT window



→ NIM A766 (2014) 180

Collection of photoelectrons

Use a suitably formed electric field between the photocathode and the first dynode

Requirements:

- high efficiency for the photo-electron collection (for different paths, exit energies, directions).
- the collection efficiency should not depend on the photoelectron exit point
- the time of flight to the first dynode should also not depend on the photoelectron exit point (impact on time resolution)

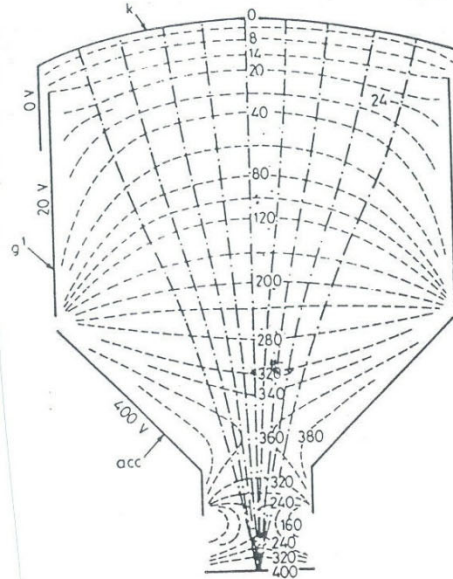


Fig. 8.15. Equipotential lines in the electron-optical input system of a fast photomultiplier (from Hull [8.9])

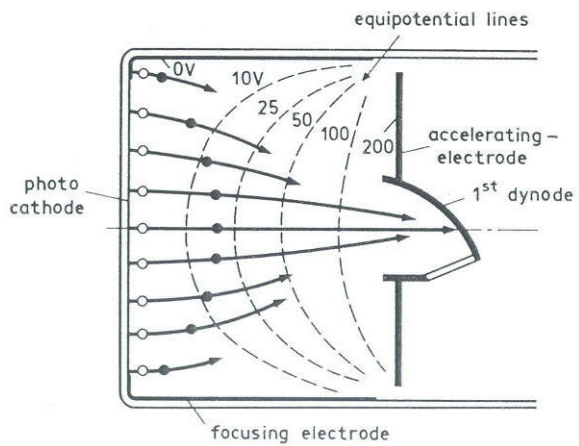


Fig. 8.14. Transit time difference (from Schonkeren [8.1])

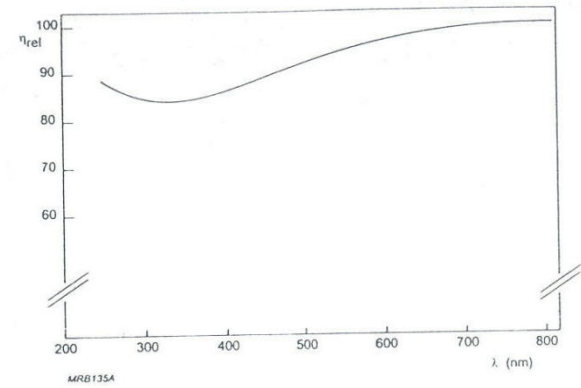
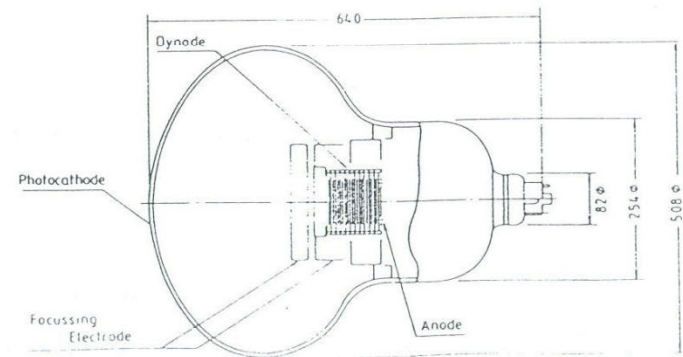


Fig. 2.2. Example of relative input system collection efficiency as a function of wavelength

Fig. 4.2. Section through photomultiplier tube R 1449 with a spherical photocathode of 508 mm diameter [KU 83].



Multiplication system (dynodes)

- secondary emission: number of secondary electrons per incoming electron $\delta \approx 3-5$
- dynode material: usually semiconductors or isolators (same reason as for the photocathode)
- semiconductor on a metal substrate (electric contact needed for E field for acceleration)

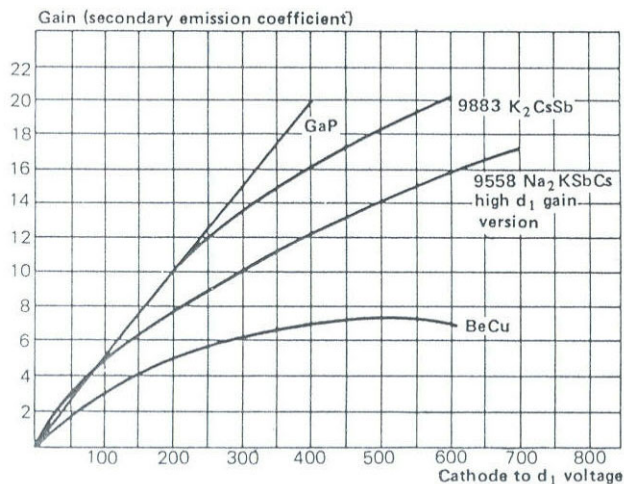


Fig. 8.9. Secondary emission factor for several dynode materials (from *EMI Catalog* [8.2])

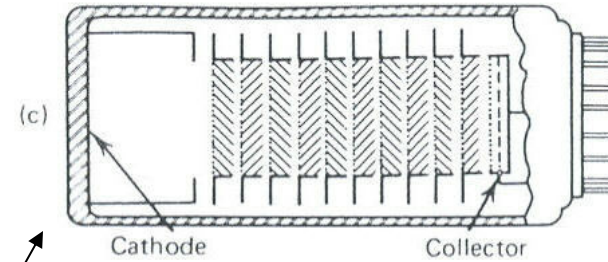
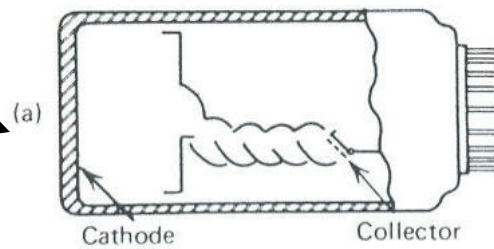
- 10-14 dynodes $\rightarrow G = 10^7-10^8$
- GaP dinode $\rightarrow 5$ dynodes \rightarrow same G

Dynode configuration

262

PHOTOMULTIPLIER TUBES AND PHOTODIODES

Linear focused



circular

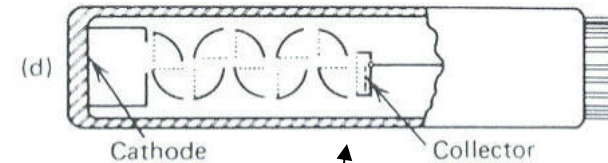
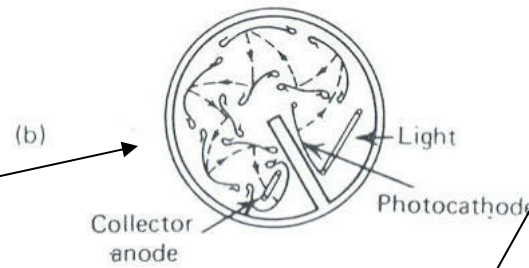


Figure 9-7 Configurations of some common types of PM tubes. (a) Focused linear structure. (b) Circular grid. (c) Venetian blind. (d) Box-and-grid. (Courtesy of EMI GENCOM Inc., Plainview, NY.)

“venetian blind”

“box grid”

Pulse height distributions for single photoelectrons

(multiple photons: convolution)

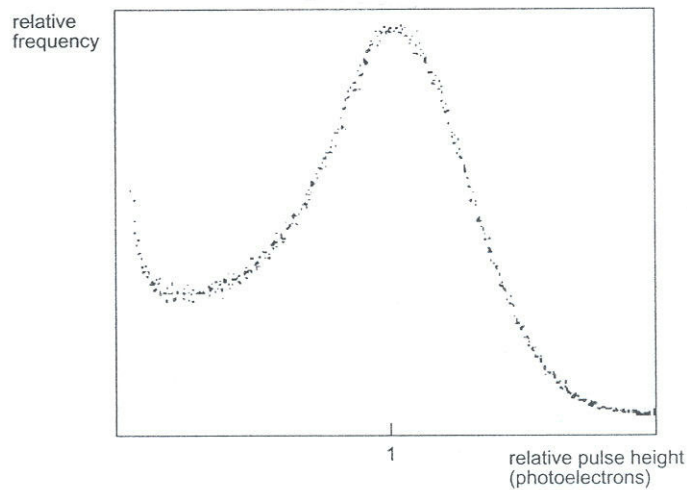


Fig.2.4 Typical single-electron spectrum. Resolution 67% FWHM. Peak-to-valley ratio 2.8:1

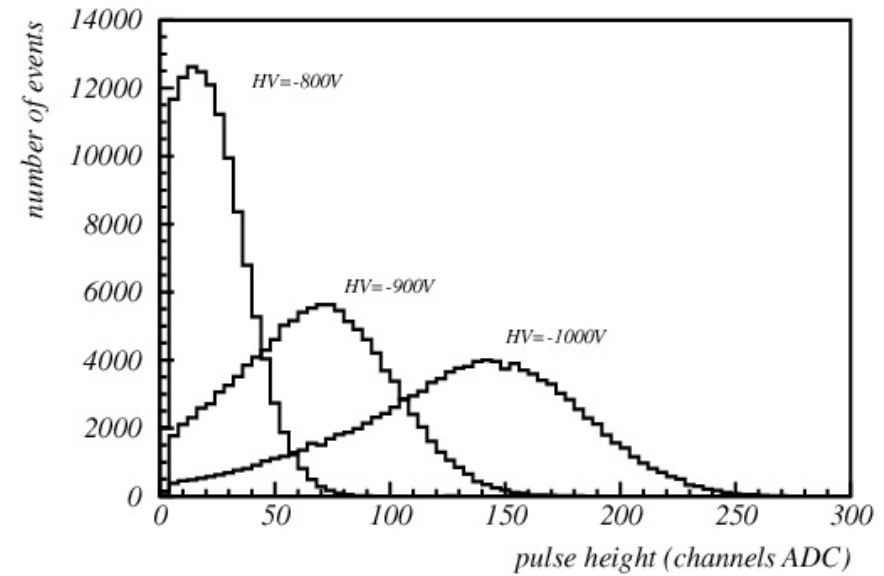


Figure 9-6 The measured pulse height spectrum for weak scintillation events obtained from a RCA 8850 photomultiplier tube. The high-gain first dynode results in distinguishable peaks in the spectrum corresponding to 1, 2, and 3 photoelectrons per pulse. (From Houtermans.¹²)

Noise in a photomultiplier tube

- 1) thermionic emission from the photocathode and from the dynodes (most important contribution)

$$I \propto T^2 \exp(-e\phi/kT), \quad \text{Richardson}$$

- 2) Current from the base contacts (“leakage”)
- 3) Contamination of PMT materials with radioactive isotopes

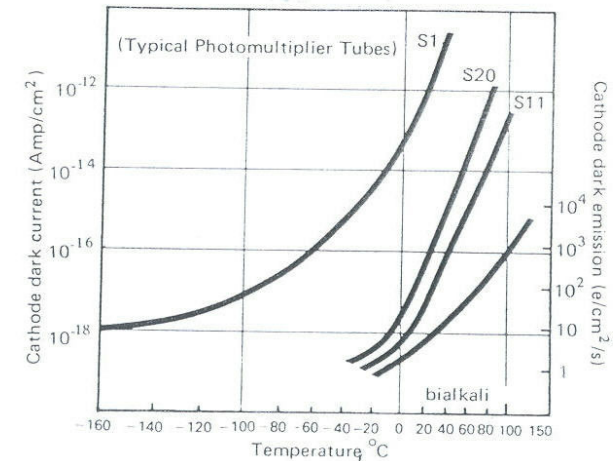


Fig. 8.19. Dark noise vs. temperature for various photocathodes (from Wardle [8.10])

“afterpulsing”

- Ionized molecules of the residual gas in the PMT volume hit the photocathode, kick out an electron → new pulse, $\Delta t \approx 100 \text{ ns} - 1 \mu\text{s}$
- “electrode glow”: the dynodes at the end of the dynode chain can emit light → hits the photocathode → new photoelectron; $\Delta t \approx 30\text{-}60 \text{ ns}$.

Enviromental effects

- 1) Exposure of the PMT to the ambient light
 - if PMT under HV, this can destroy the PMT, or at least increase the dark current / dark counts
 - no HV when exposed to ambient light: noise level will first increase (de-excitations in the PMT window), but will eventually decrease with time

- 2) B field (see next slide)
 - modifies the path of photoelectrons and of the secondary electrons
 - reduction of gain and of the photoelectron collection efficiency
 - most sensitive: path from the photocathode to the first dynode
 - partial mitigation with a μ -metal shield

- 3) Temperature
 - increase of the thermionic noise
 - QE depends on the T (typically $-0.5\%/K$)

PMT in a B field:
reduction of gain and of
the photoelectron
collection efficiency

partial mitigation with a
 μ -metal shield

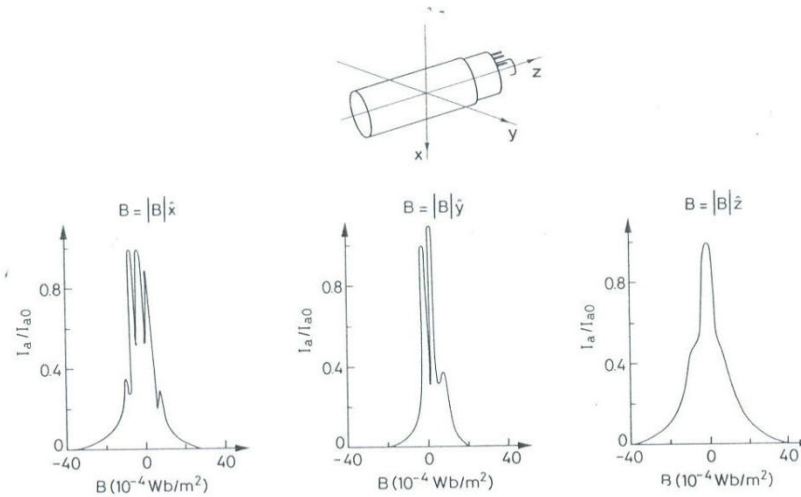


Fig. 8.17. Effect of magnetic fields on the anode current of an unscreened PM for different field orientations (from *Schonkeren* [8.1])

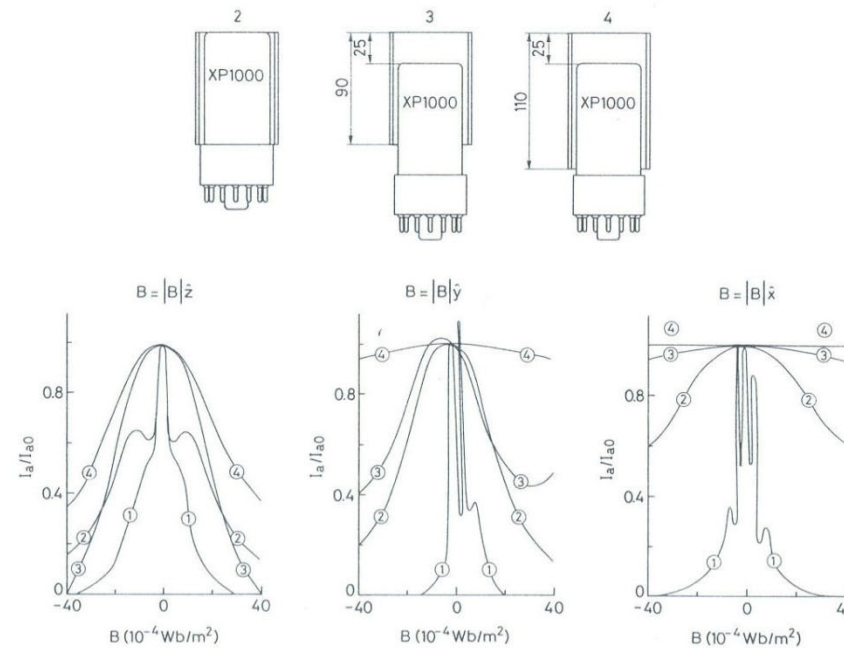


Fig. 8.18. Shielding effect of different μ -metal configurations (from *Schonkeren* [8.1])

2) Multianode PMTs

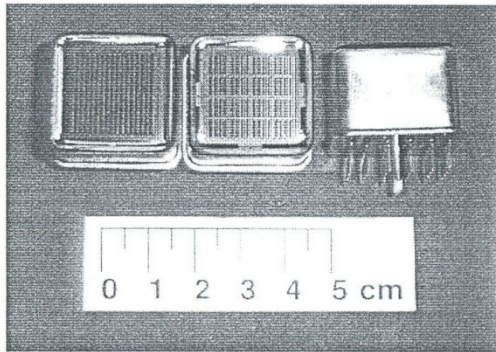


FIGURE 2. Hamamatsu multianode photomultipliers (L16, M16, M16 from left to right).

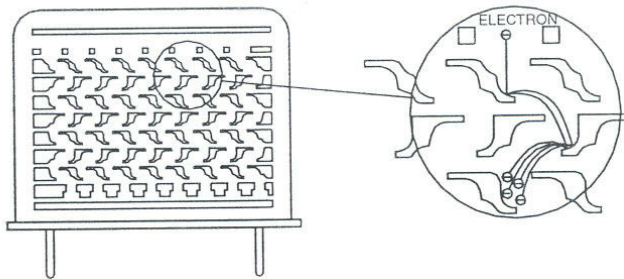
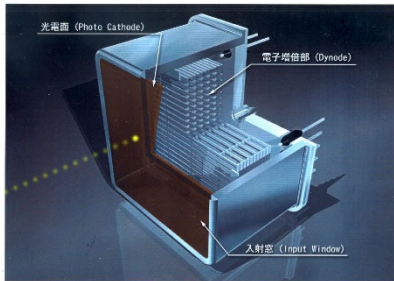
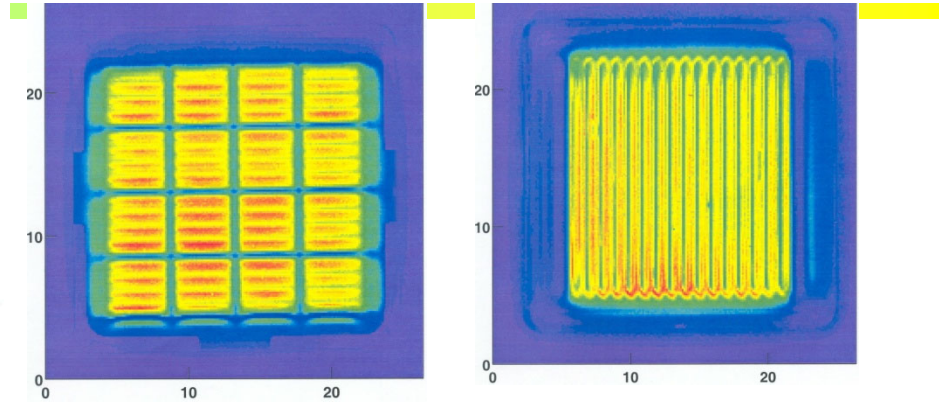
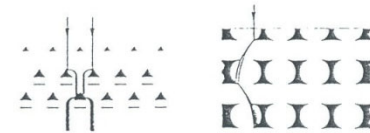


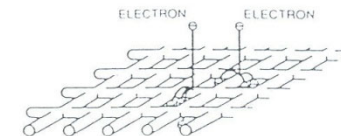
FIGURE 4. Metal channel type PMT [8].

POSITION SENSITIVE PMT'S - EXAMPLES

Philips mesh and foil types

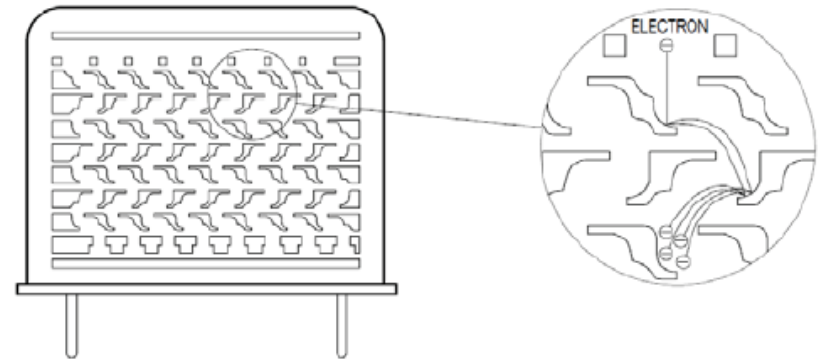
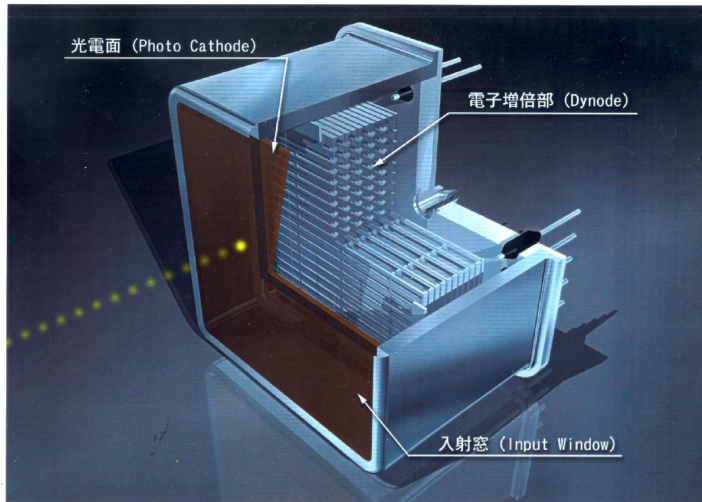


Hamamatsu fine mesh

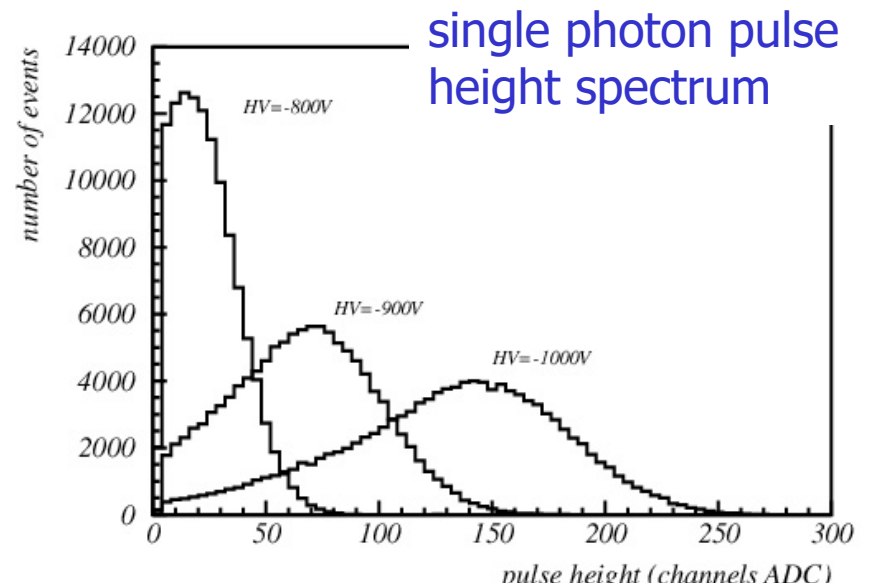


First fast multianode sensor for single photons: MA PMT

Multianode PMT Hamamatsu R5900 with metal foil dynodes



- Excellent single photon pulse height spectrum
- Low noise (few Hz/ch)
- Low cross-talk (<1%)



Light collection for a multianode PMT

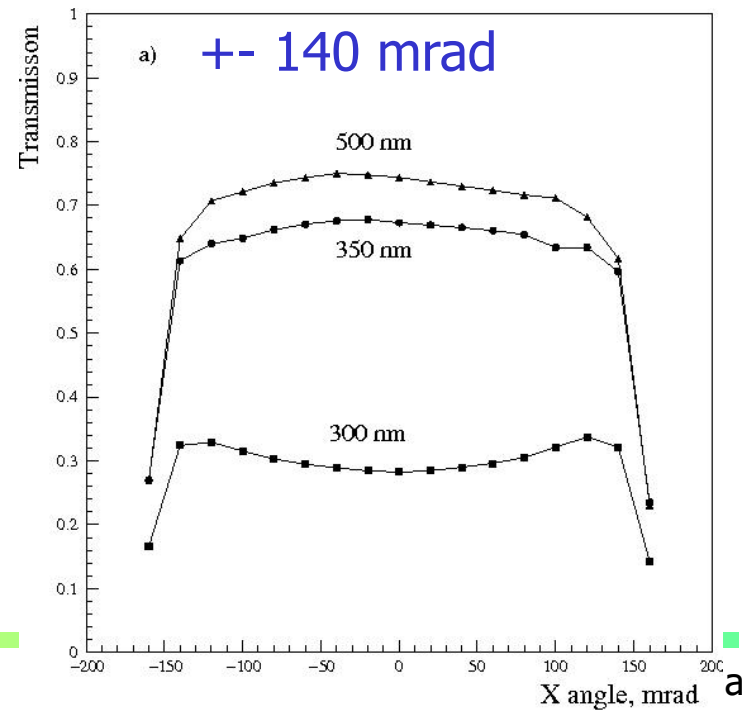
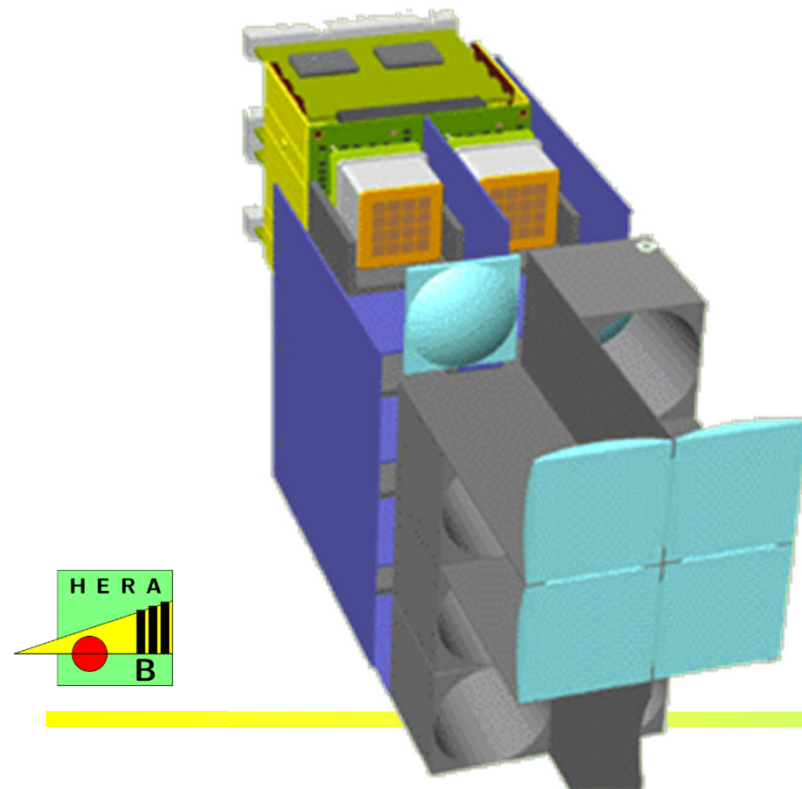
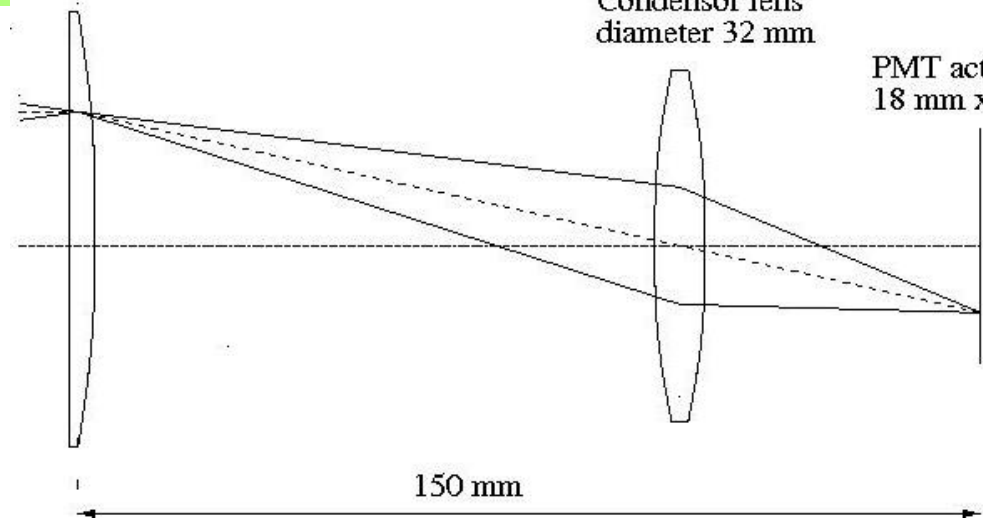
Light collection system (imaging!) to:

- Eliminate dead areas
- Adapt the pad size

Field lens, 35 mm x 35 mm

Condensor lens
diameter 32 mm

PMT active area
18 mm x 18 mm



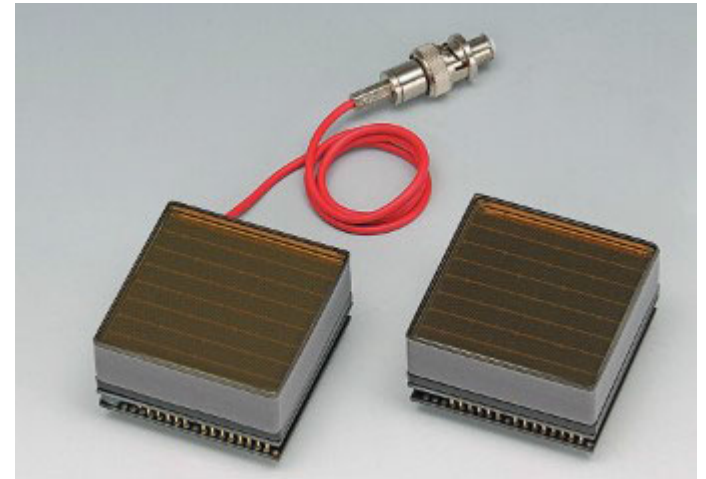
Flat pannel multianode PMTs

Problem of vacuum based sensors: active area fraction

One possible solution: make a larger sensor

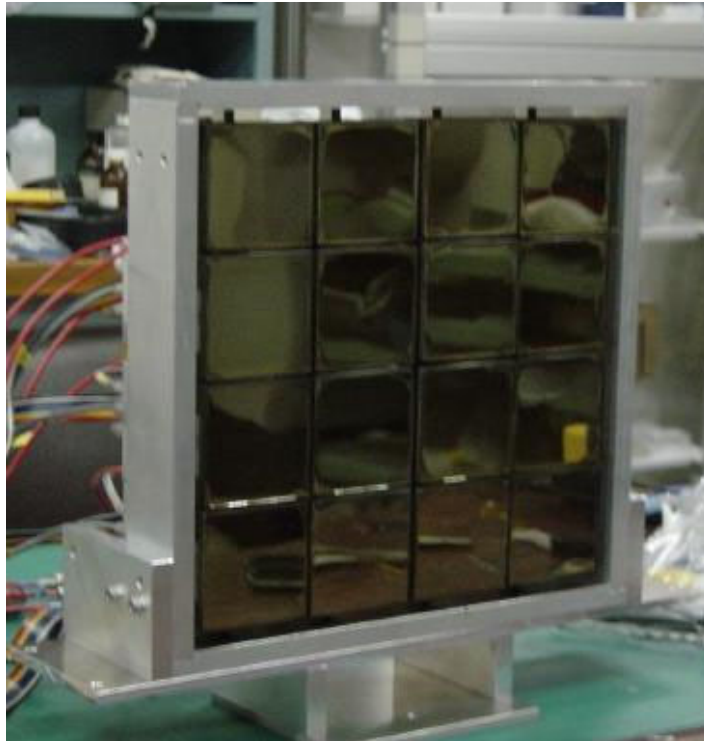
Hamamatsu: flat pannel PMT H8500

- 52 x 52mm², 89% effective coverage
- 64 channels, pixel size 5.8 x 5.8 mm²
- 12 dynodes, metal foil type
- Bialkali cathode, max 25% quantum efficiency
- single photon pulse height distribution not as good as in the smaller R5900 (and related tubes like 7600)

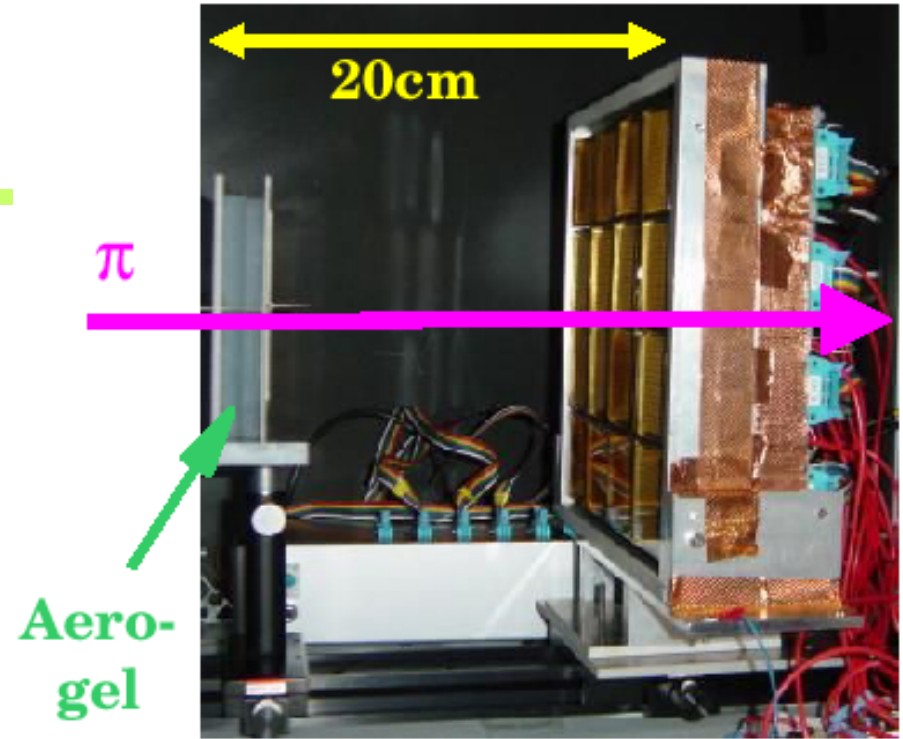


Flat pannel MA PMTs

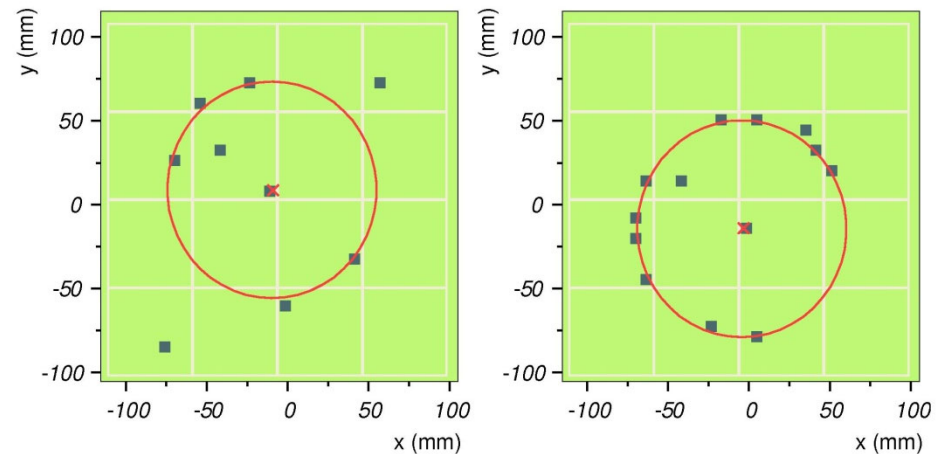
First used in a prototype RICH for Belle II, with aerogel radiator.



array of 16 H8500 PMTs

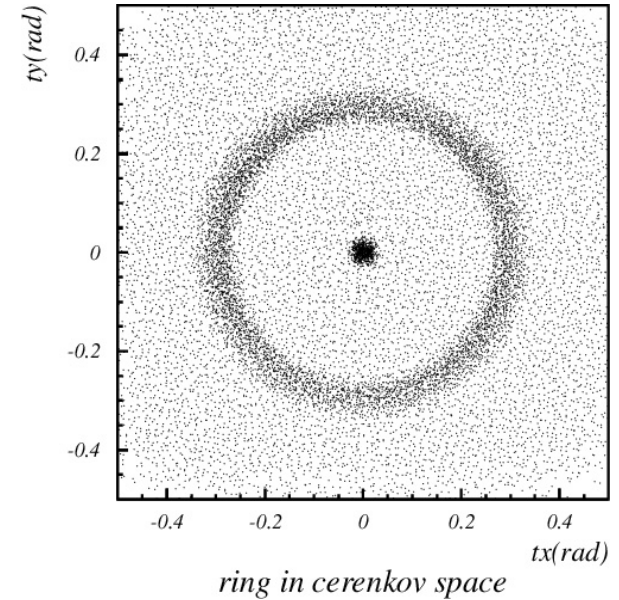
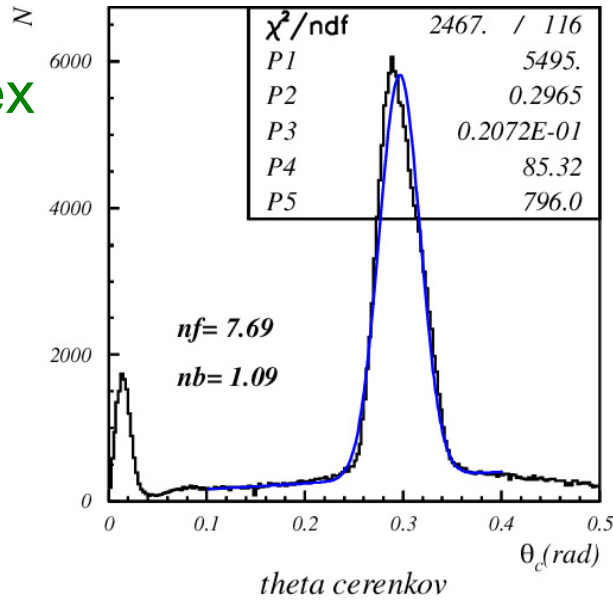
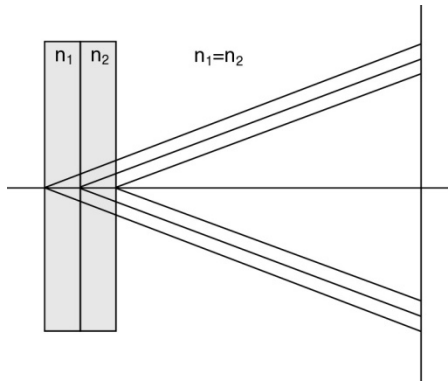


Clear rings, little background

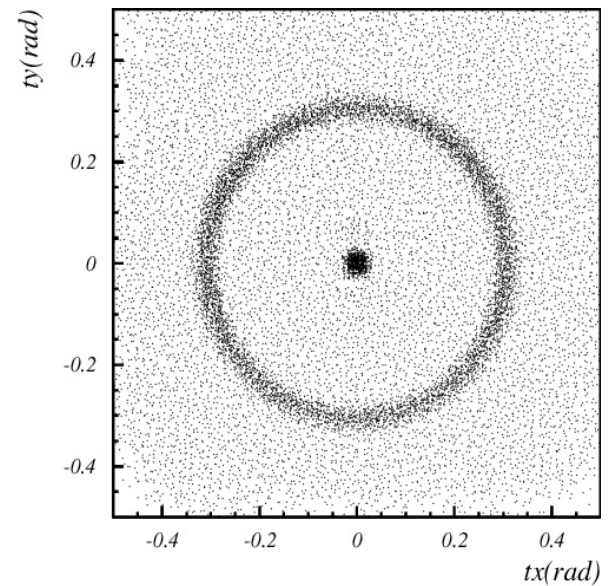
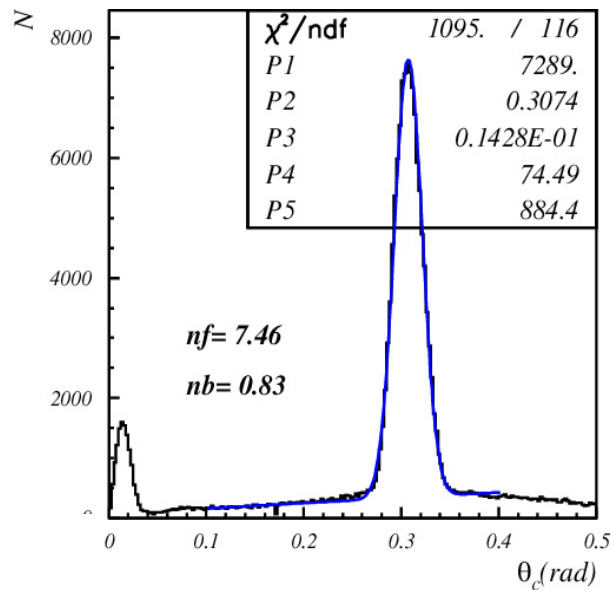
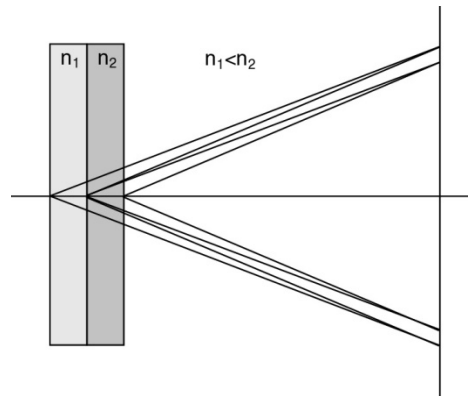


Used for the proof-of-principle test of the focusing radiator configuration

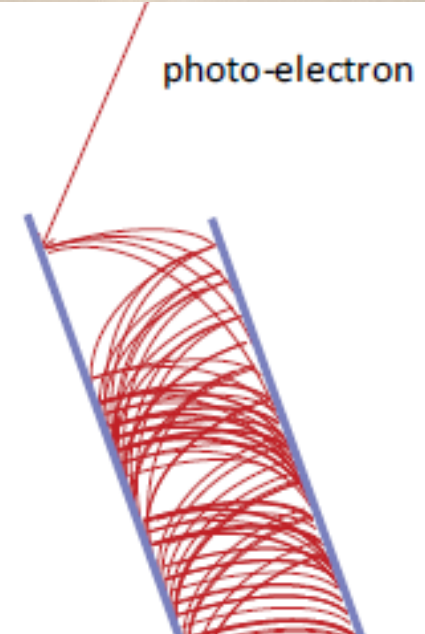
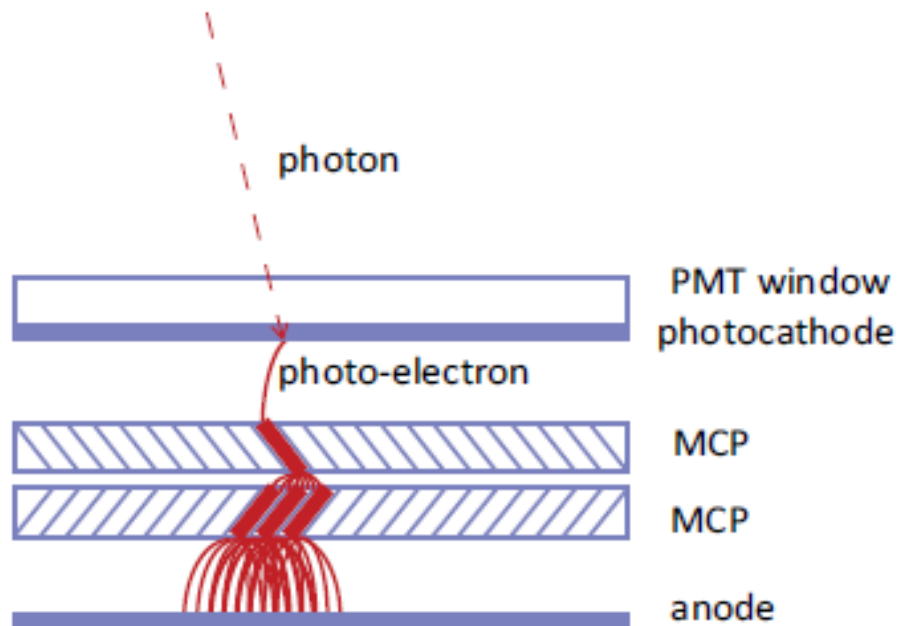
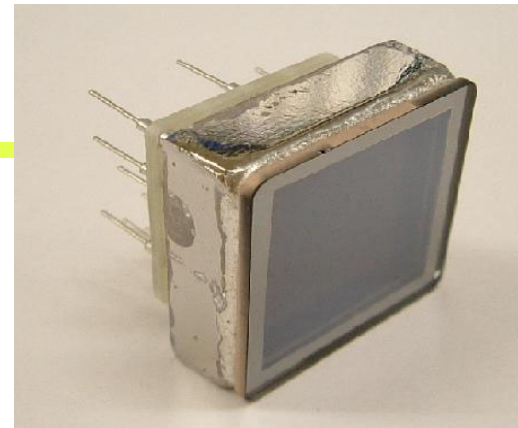
4cm aerogel single index



2+2cm aerogel



Micro-channel plate PMTs



- Fast
- Immune to an axial magnetic field

Mikrokanalne plošče

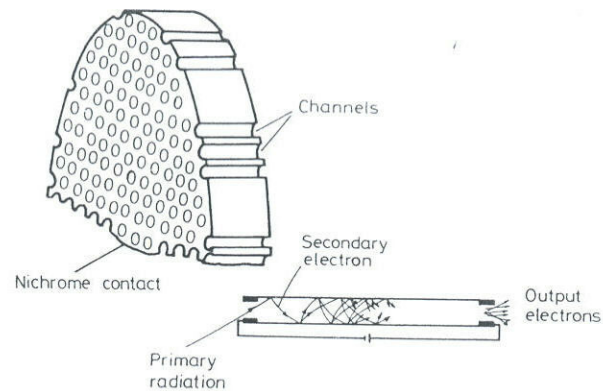


Fig. 8.6. Schematic diagram of a microchannel plate. The many channels act as continuous dynodes (from *Dhawan* [8.4]; picture © 1975 IEEE)

- pore diameter 10-100 μm
- channel length $\approx 1\text{mm}$
- multiplication $G \approx 10^5\text{-}10^7$ (“chevron”)
- time resolution $< 100\text{ ps}$
- spatial sensitivity
- 25 μm pores: up to $B \approx 0.8\text{T}$
- 10 μm : up to $B \approx 1.5\text{T}$

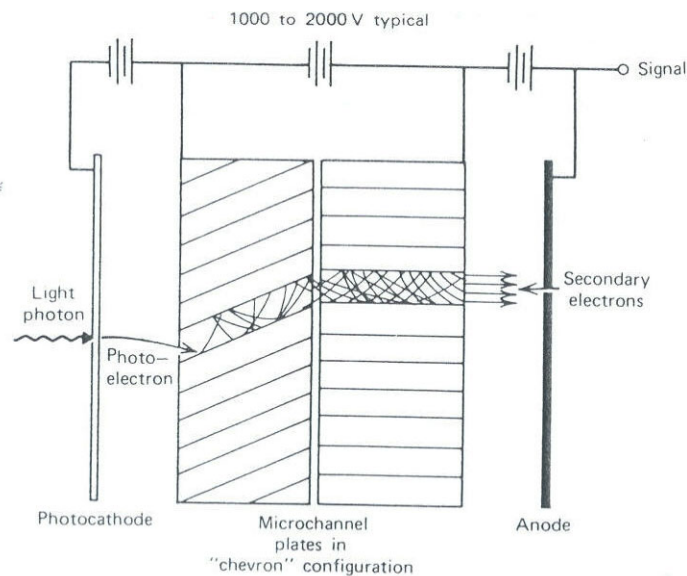
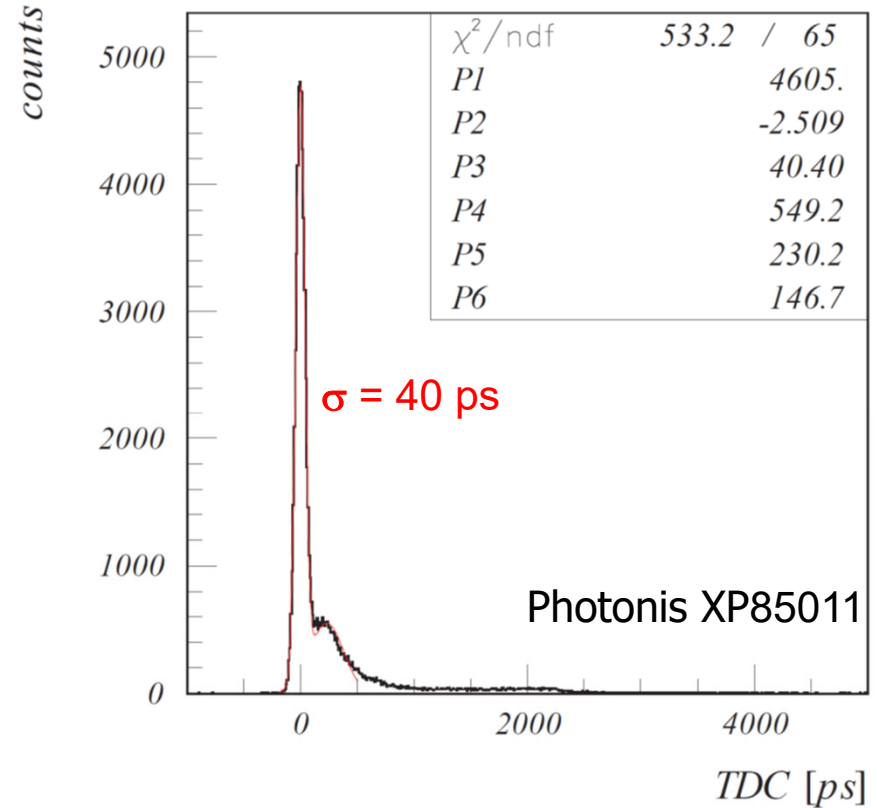
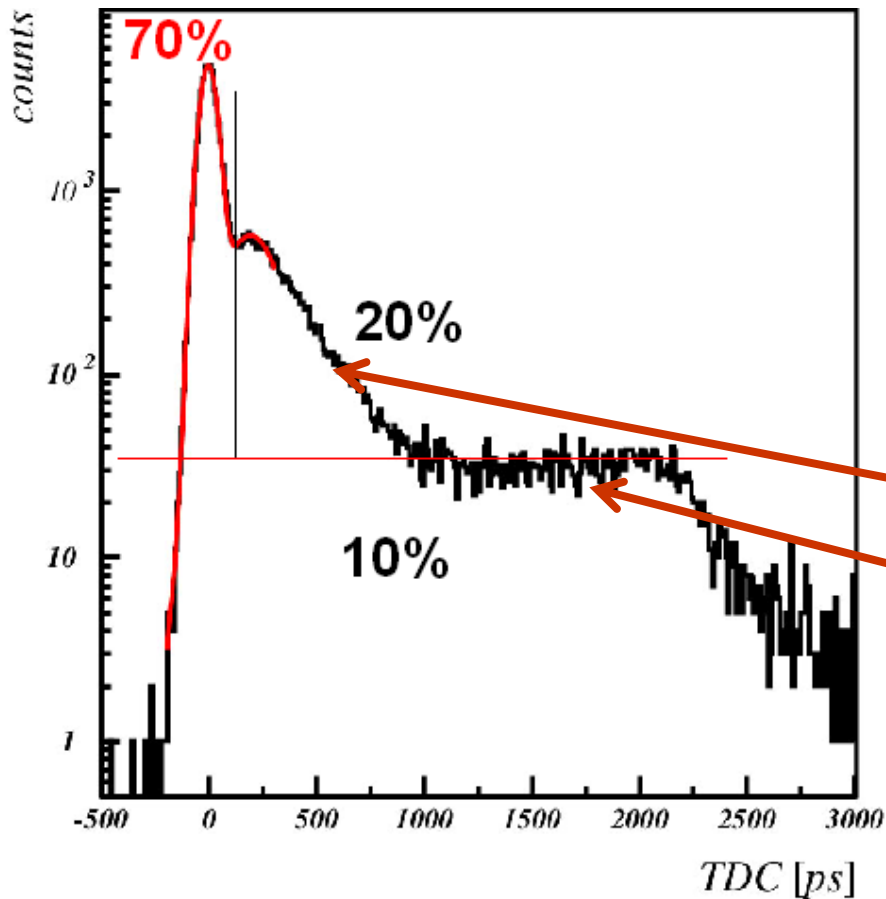


Figure 9-9 Elements of a PM tube based on microchannel plate electron multiplication.

MCP PMT timing

MCP PMTs: main peak with excellent timing accompanied with a tail



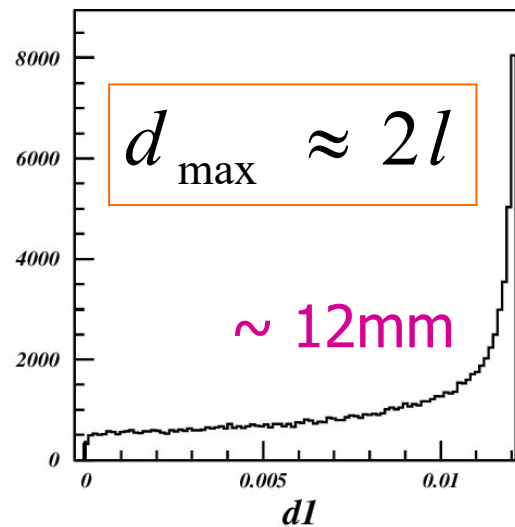
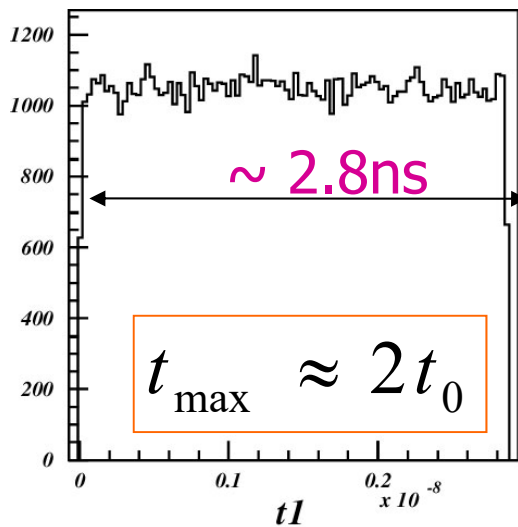
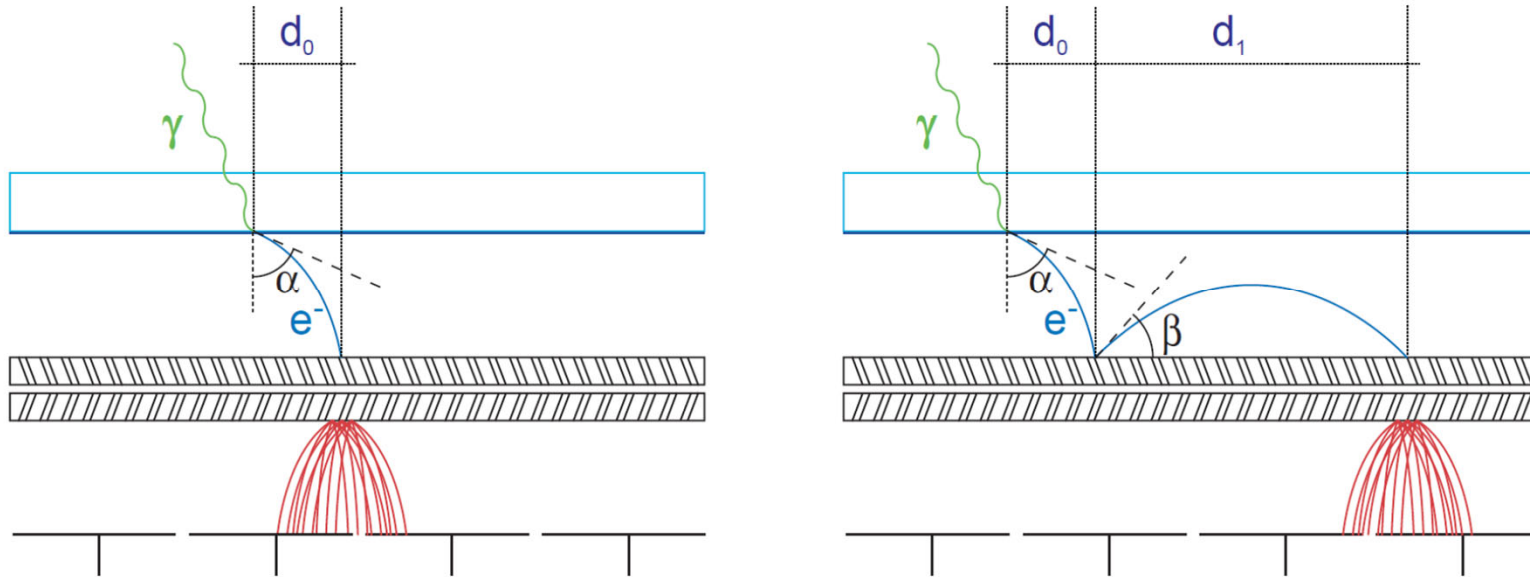
- Inelastic back-scattering
- Elastic back-scattering

→ good agreement with a simple model →

→ NIMA 595 (2008) 169

→ JINST 4 (2009) P11017

Elastically backscattered photoelectrons



Results of a simple modeling: we assume that the photoelectron backscattering by the angle β is uniform over the solid angle.

→ NIMA 595 (2008) 169
JINST 4 (2009) P11017

MCP PMT: processes involved in photon detection

MCP PMT parameters
used: Photonis XP85011

Parameters used:

- $U = 200 \text{ V}$
- $l = 6 \text{ mm}$ (K-MCP)
- $E_0 = 1 \text{ eV}$
- $m_e = 511 \text{ keV}/c^2$
- $e_0 = 1.6 \cdot 10^{-19} \text{ As}$

$$t_{\max} \approx 2t_0$$

$$d_{\max} \approx 2l$$

Tails can be significantly reduced by:

- decreased photocathode-MCP distance and
- increased voltage difference

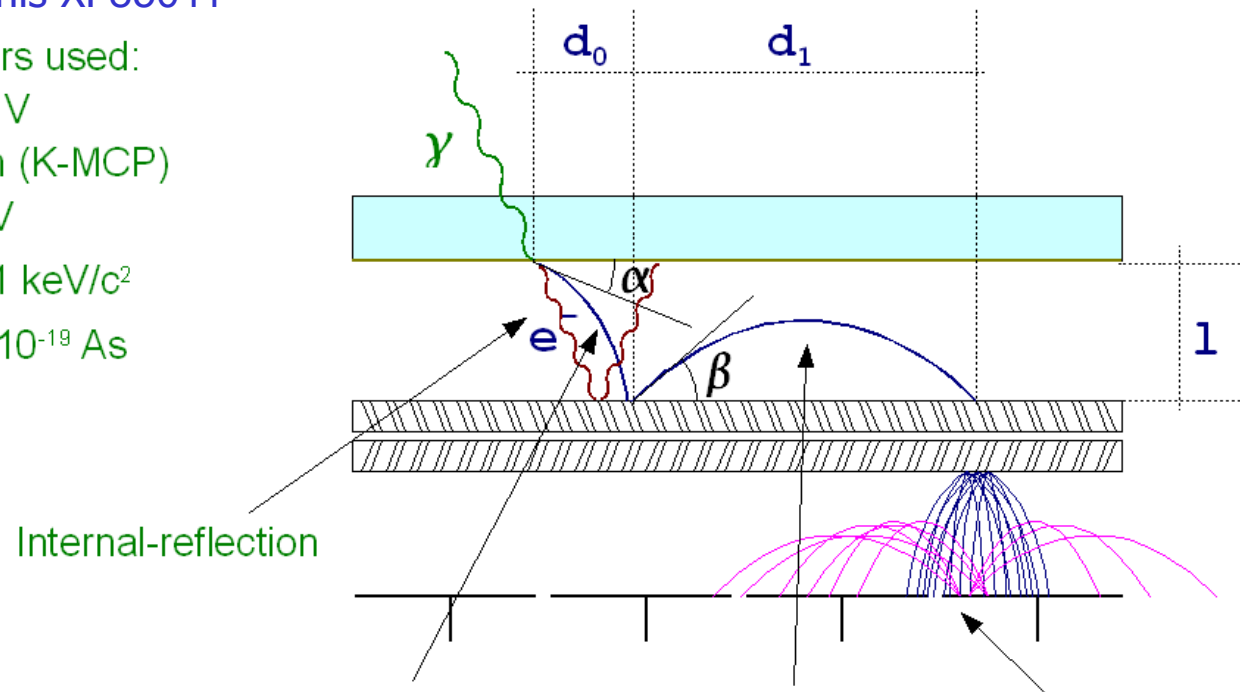


Photo-electron:

- $d_{0,\max} \sim 0.8 \text{ mm}$
- $t_0 \sim 1.4 \text{ ns}$
- $\Delta t_0 \sim 100 \text{ ps}$

Backscattering:

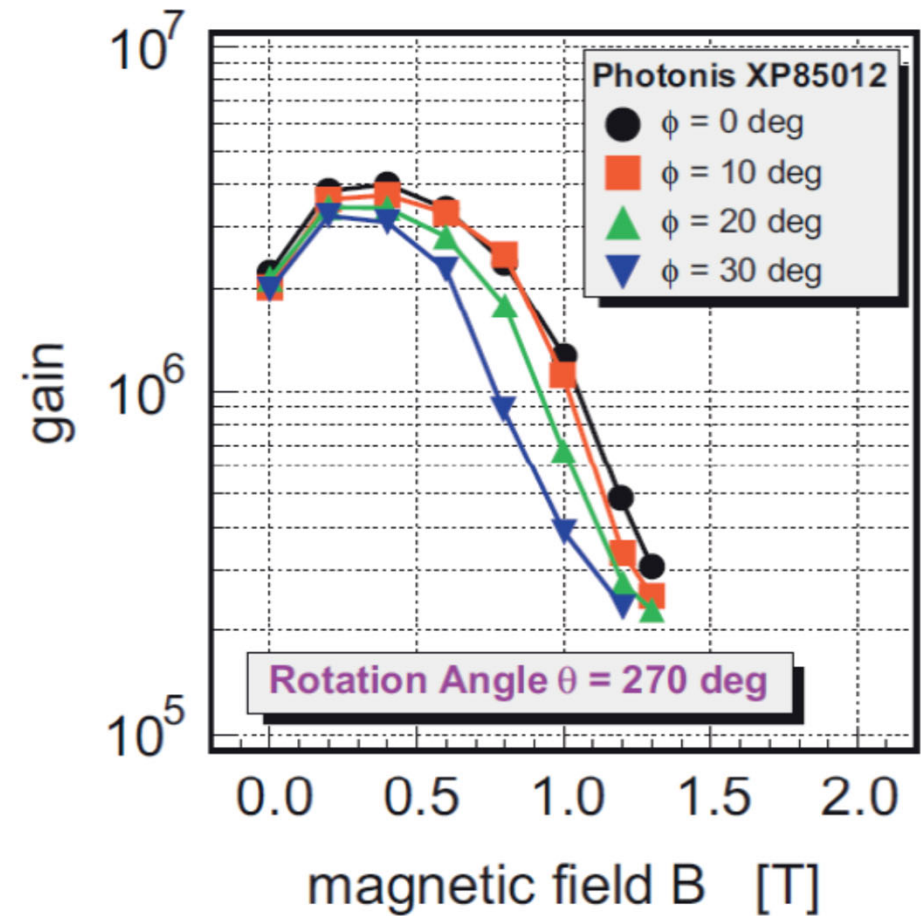
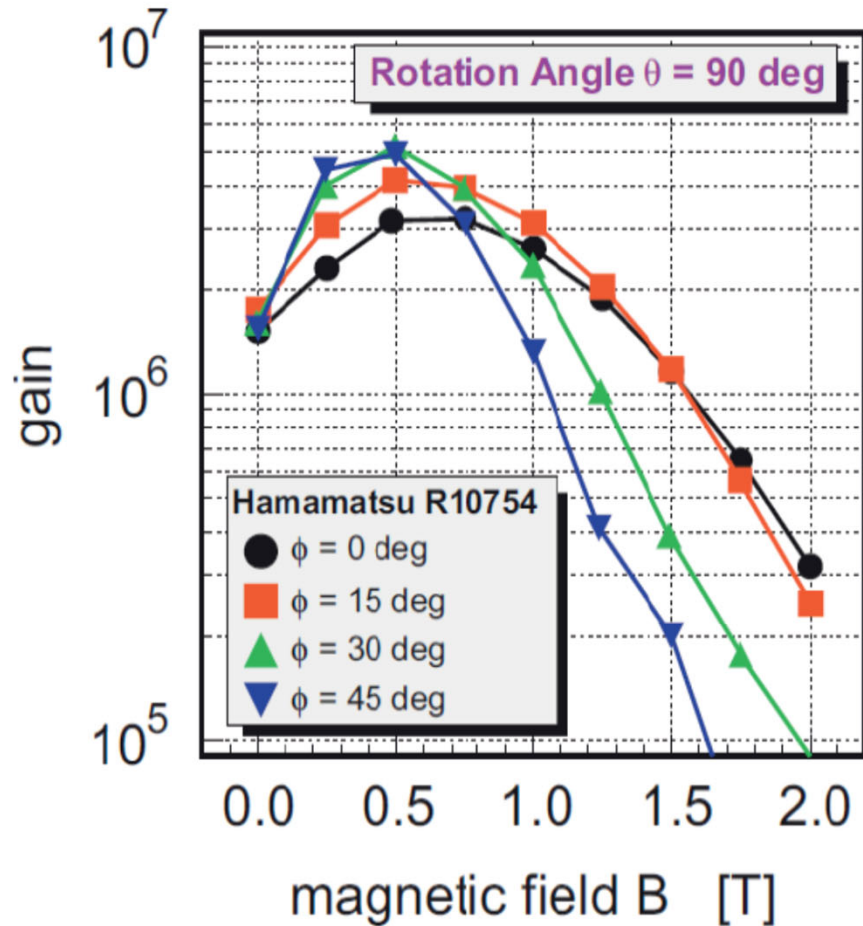
- $d_{1,\max} \sim 12 \text{ mm}$
- $t_{1,\max} \sim 2.8 \text{ ns}$

Charge sharing

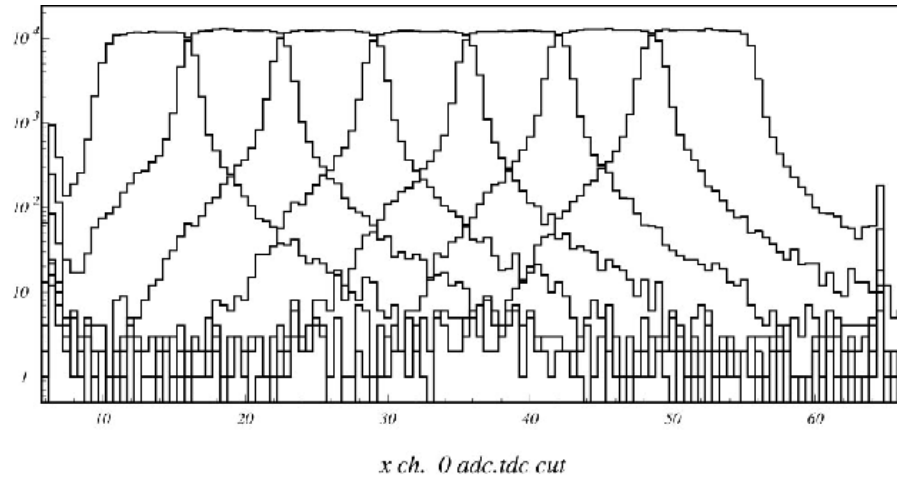
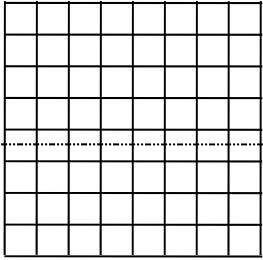
→ NIMA 595 (2008) 169
JINST 4 (2009) P11017

MCP PMTs in magnetic field

Gain vs B field for different tilt angles

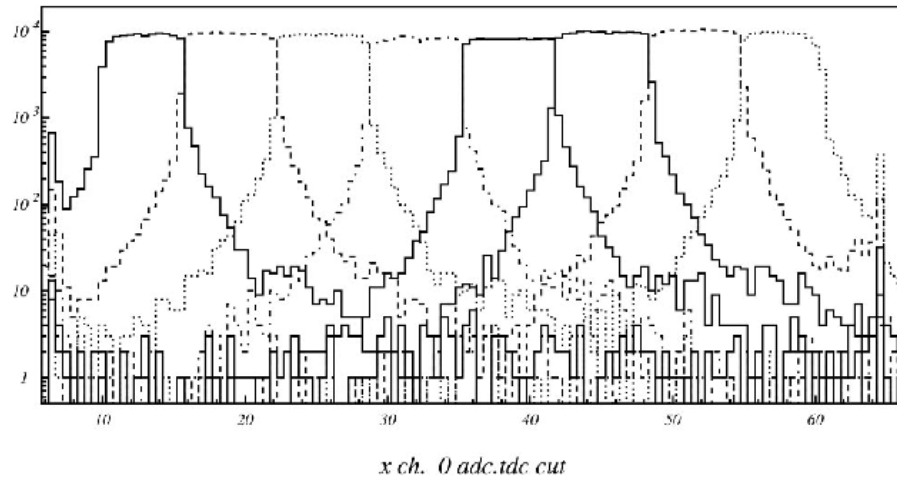


MCP PMT: improved performance in magnetic field



Number of detected hits on individual channels as a function of light spot position.

$B = 0 \text{ T}$,
 $HV = 2400 \text{ V}$



$B = 1.5 \text{ T}$,
 $HV = 2500 \text{ V}$

Backscattered photoelectrons get "locked" to the B field lines

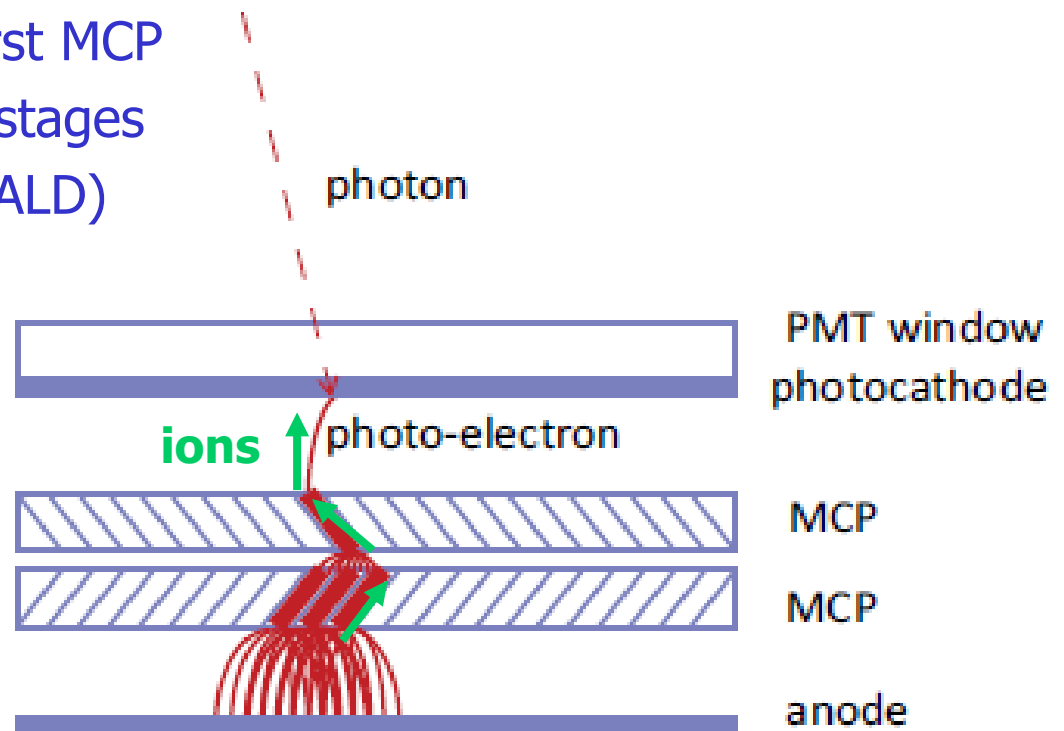
In the presence of magnetic field, charge sharing and cross talk due to long range photoelectron back-scattering are considerably reduced.

MCP PMTs ageing

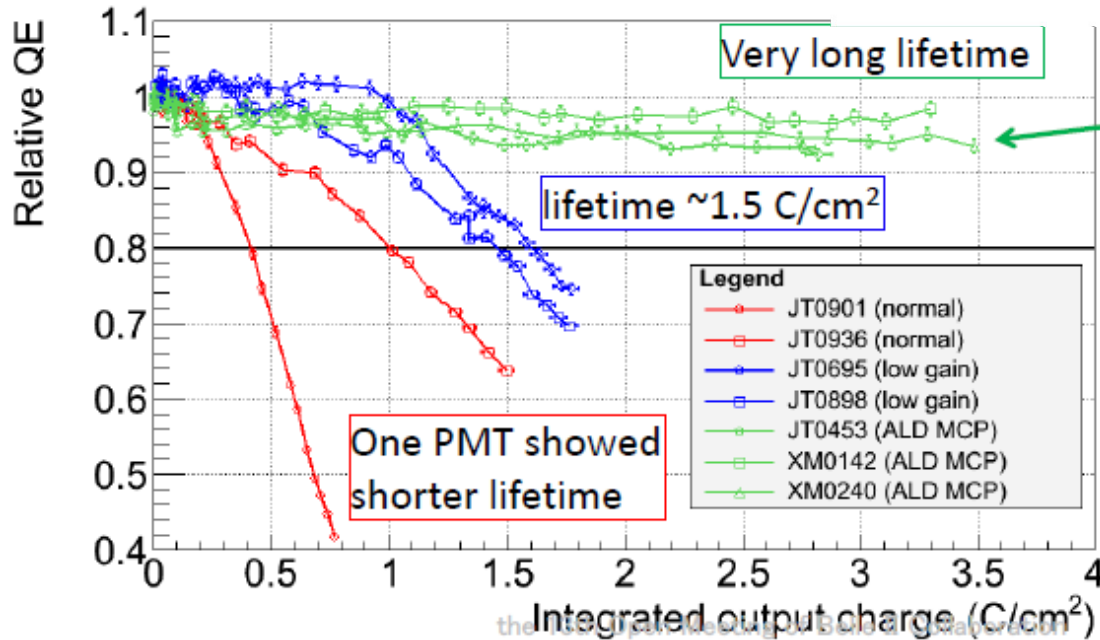
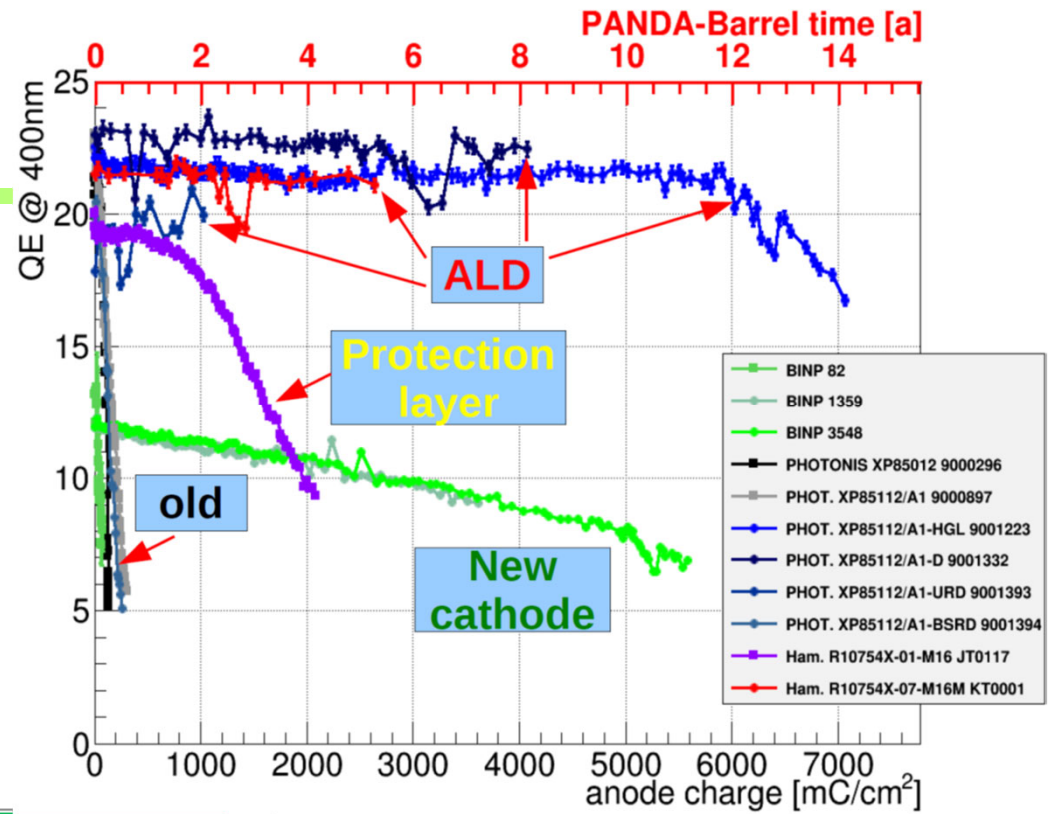
MCP PMT ageing: a serious problem in most of the planned applications.

Cures:

- Better cleaning of the MCPs, better vacuum
- Al foil between PC and first MCP
- Al foil between two MCP stages
- Atomic layer deposition (ALD)



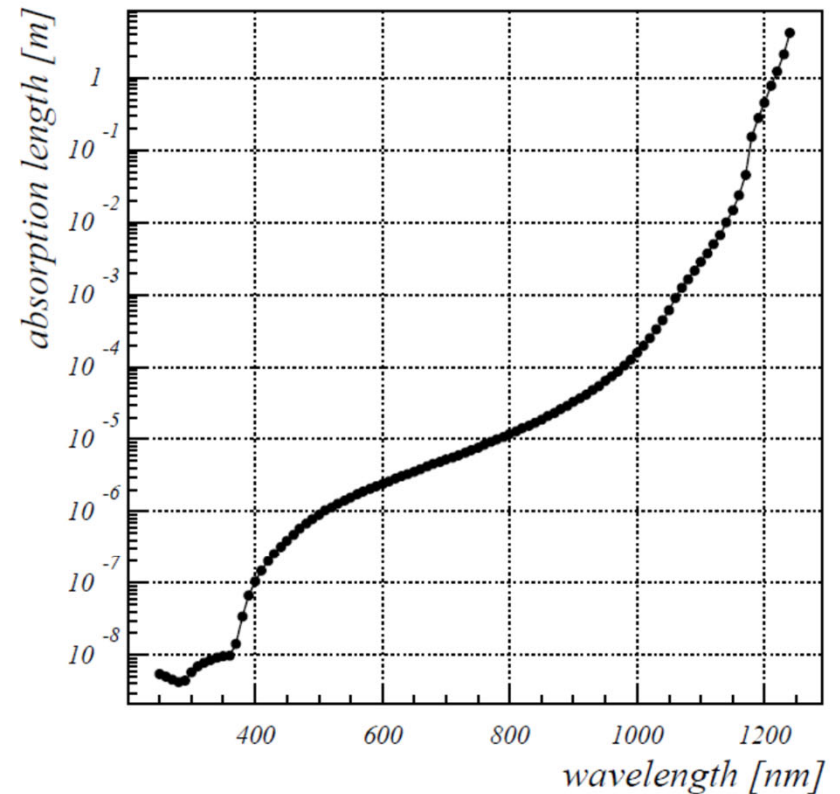
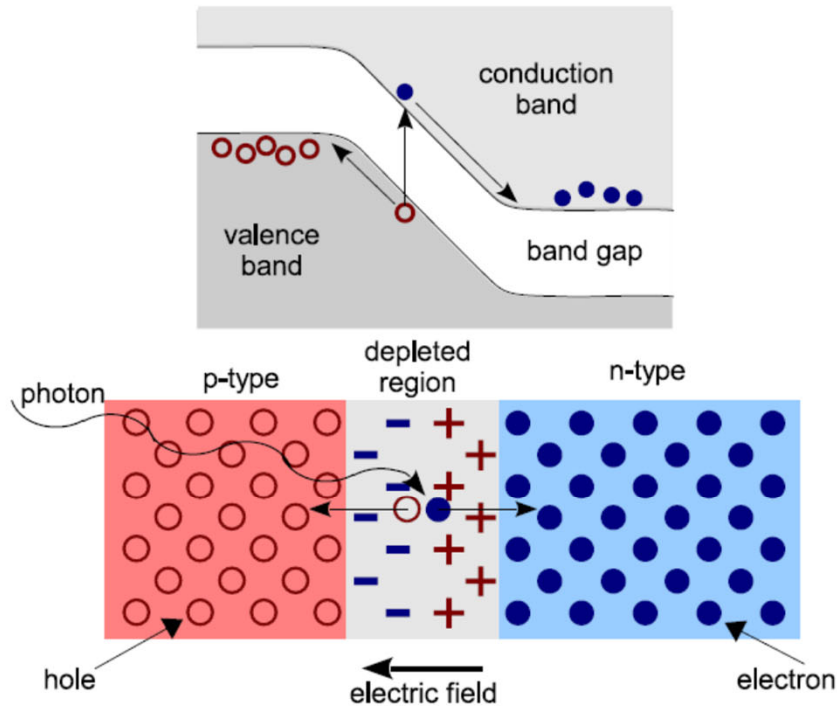
MCP PMTs ageing, cure



7.4 C/cm² in total
(4.1 C/cm² at HPK)

Hamamatsu, ALD deposition

Semiconductor light sensor: photodiode



Semiconductor light sensor: CCD

- In cameras and phones - but not useful for single (or few) photons...

Semiconductor light sensors

Photodiodes (PD)

- High QE (also in the IR region),
- No multiplication
- Can be used in cases with large light yields (calorimeters)

Avalanche photodiodes APD

- region with high E field -> multiplication in an avalanche, $G \approx 10^2$ - 10^3 .
- signal/noise still poor compared to a PMT
- used for calorimeters

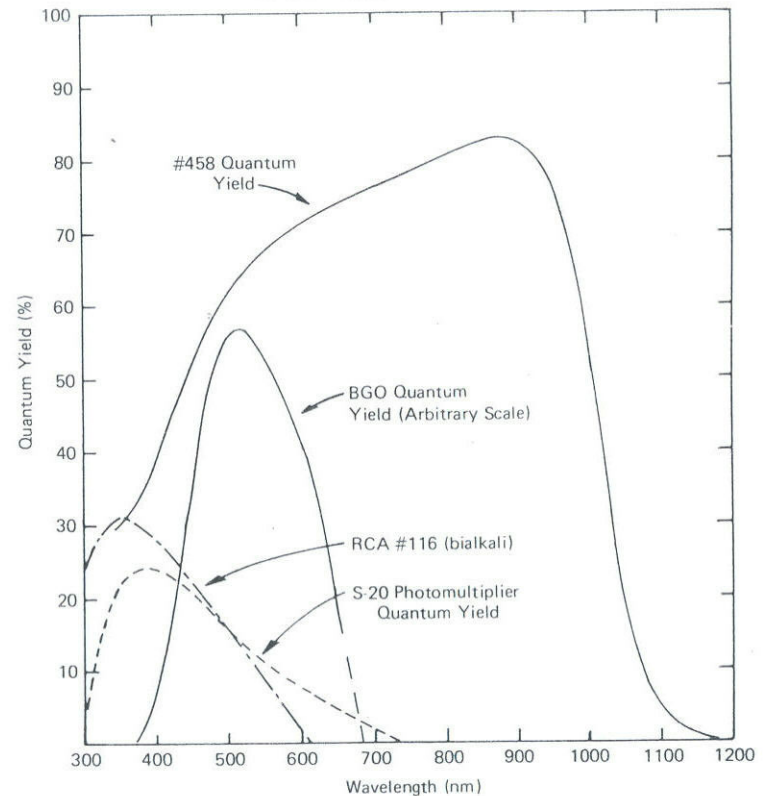


Figure 9-14 A comparison of the quantum efficiency of a silicon photodiode (labeled #458) with representative bialkali and S-20 photocathode quantum efficiencies. The emission spectrum from a BGO scintillator is shown for reference. (From Groom.⁵³)

Semiconductor light sensor: SiPM

Geiger mode avalanche photo-diode (G-APD), also known as SiPM – Silicon Photomultiplier

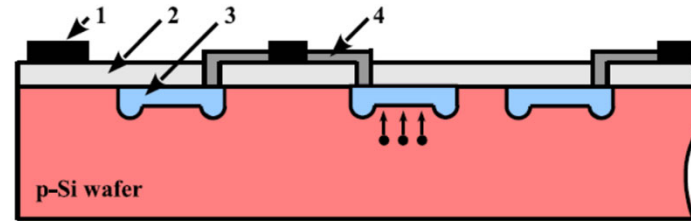
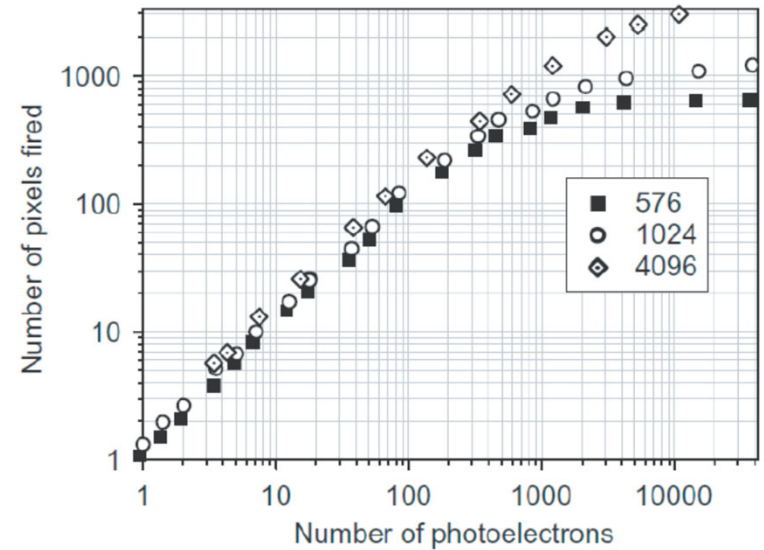
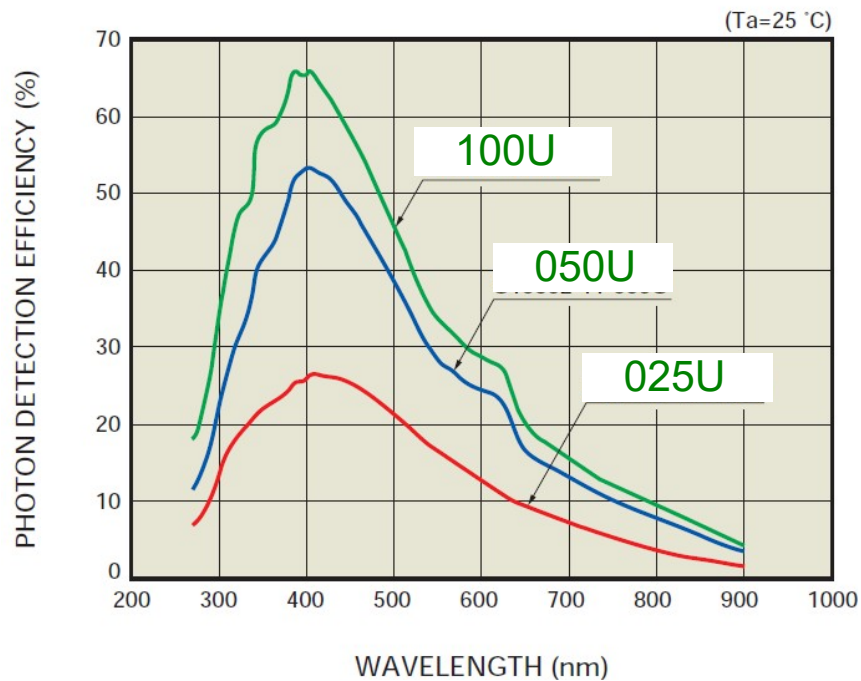
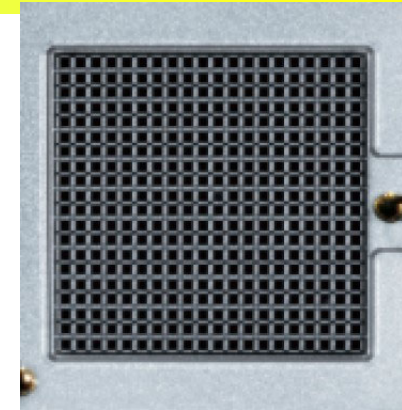
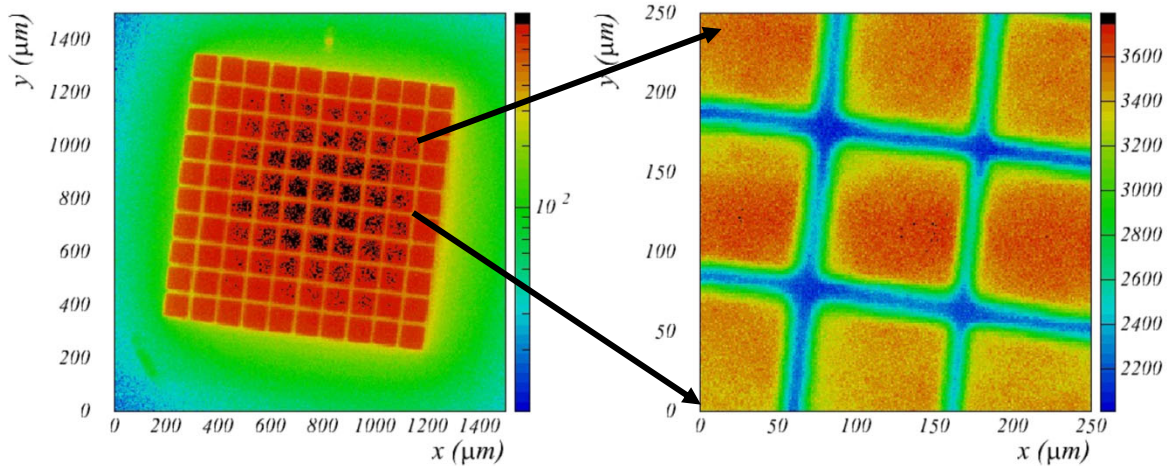


Figure 9: Schematic drawing of a cross-section of a SiPM: metal electrode (1), silicon oxide layer (2), p-n junctions/micro-cell (3) and individual quenching resistor (4) (23).

SiPM is an array of APDs operating in the Geiger mode. Characteristics:

- low operation voltage $\sim 10\text{-}100\text{ V}$
- gain $\sim 10^6$
- peak PDE up to 65%(@400nm)
 $\text{PDE} = \text{QE} \times \epsilon_{\text{geiger}} \times \epsilon_{\text{geo}}$ (up to 5x PMT!)
- ϵ_{geo} – dead space between the cells
- time resolution $\sim 100\text{ ps}$
- works in high magnetic field
- dark counts $\sim \text{few } 100\text{ kHz/mm}^2$
- radiation damage (p,n)

SiPMs as photon detectors



SiPM as photon detector?

Can we use SiPM (Geiger mode APD) as the photon detector in a RICH counter?

+immune to magnetic field

+high photon detection efficiency, single photon sensitivity

+easy to handle (thin, can be mounted on a PCB)

+potentially cheap (not yet...) silicon technology

+no high voltage

-very high dark count rate (100kHz – 1MHz) with single photon pulse height

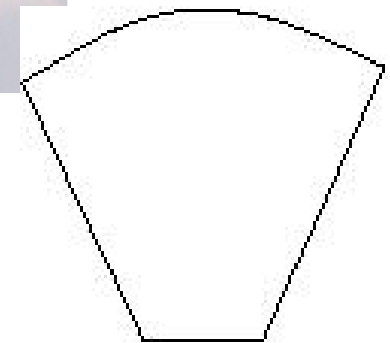
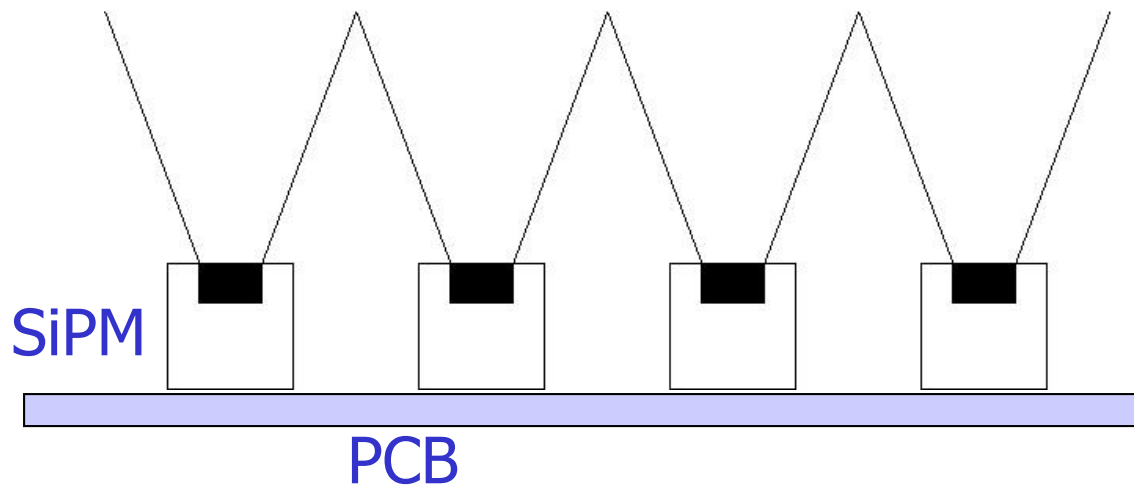
-radiation hardness

Can such a detector work?

Improve the signal to noise ratio:

- Reduce the noise by a narrow ($<10\text{ns}$) time window
- Increase the number of signal hits per single sensor by using light collectors and by adjusting the pad size to the ring thickness

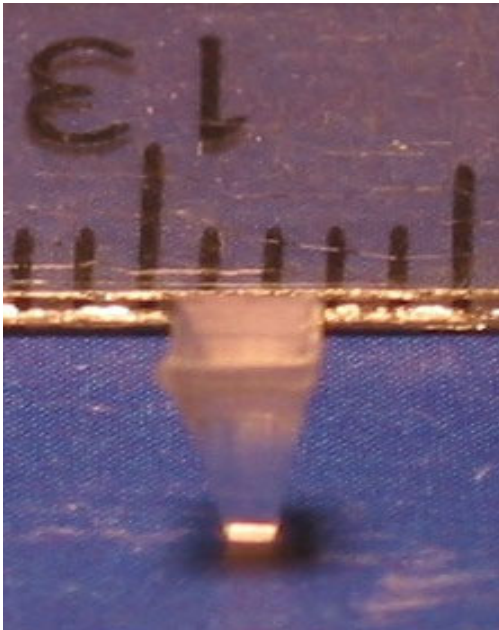
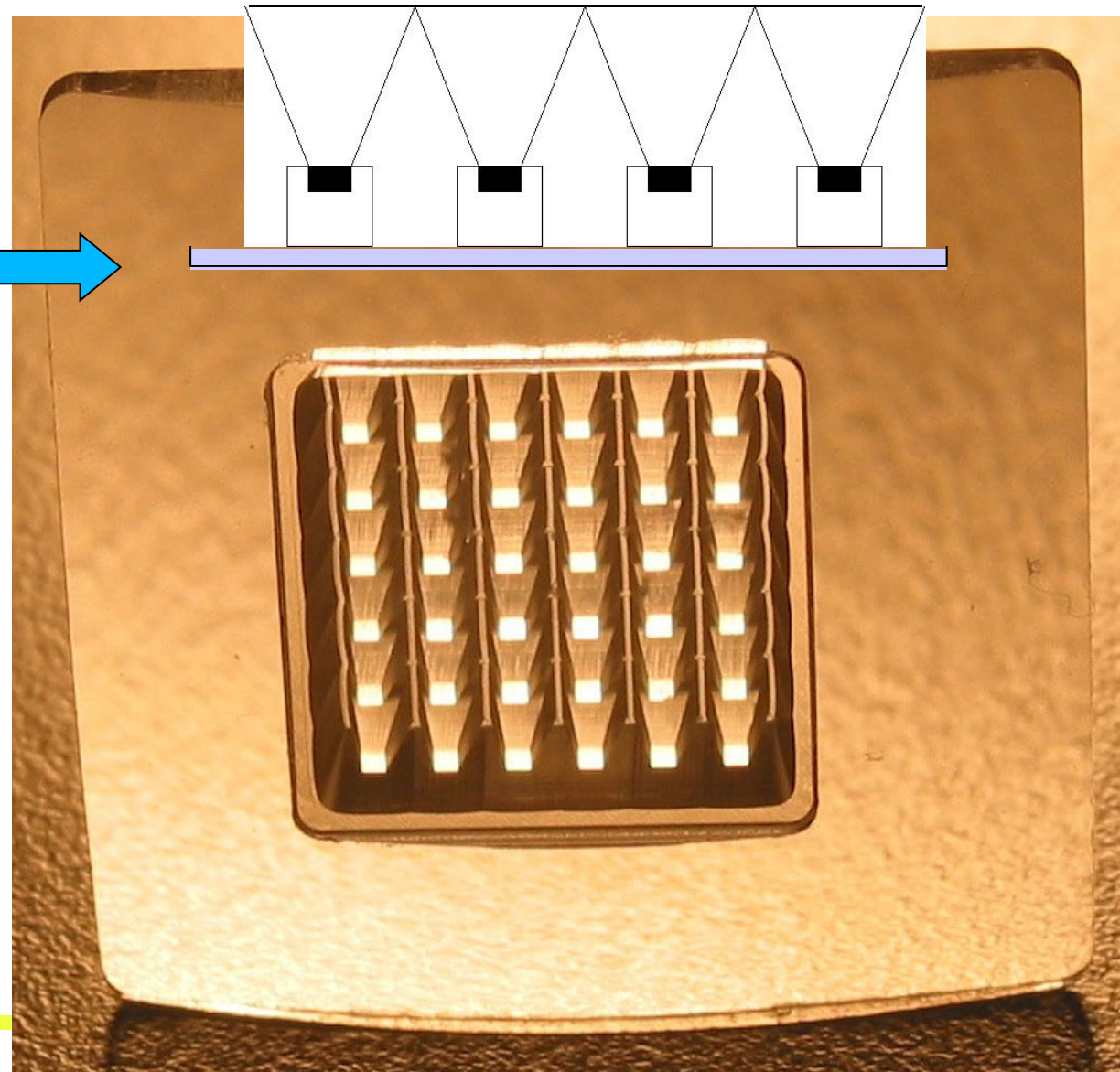
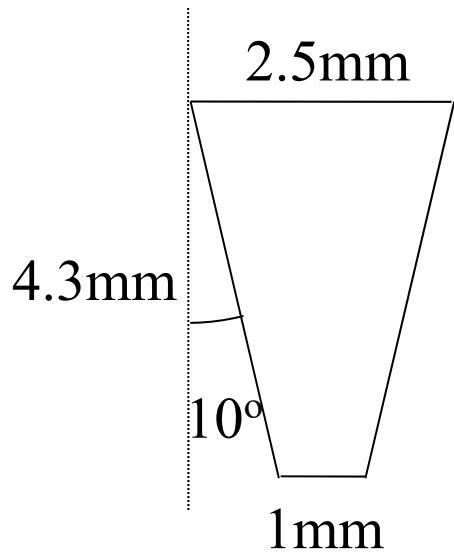
E.g. light collector with reflective walls



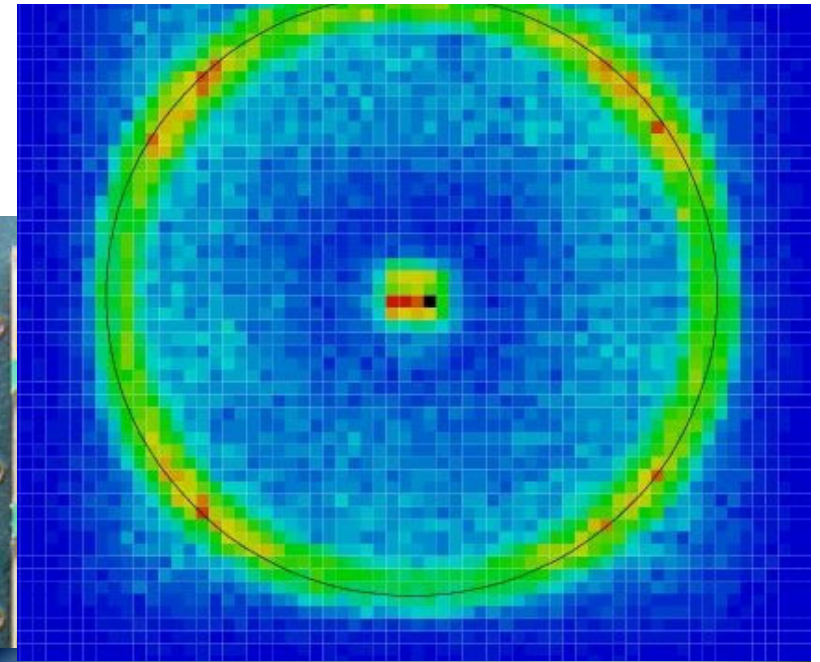
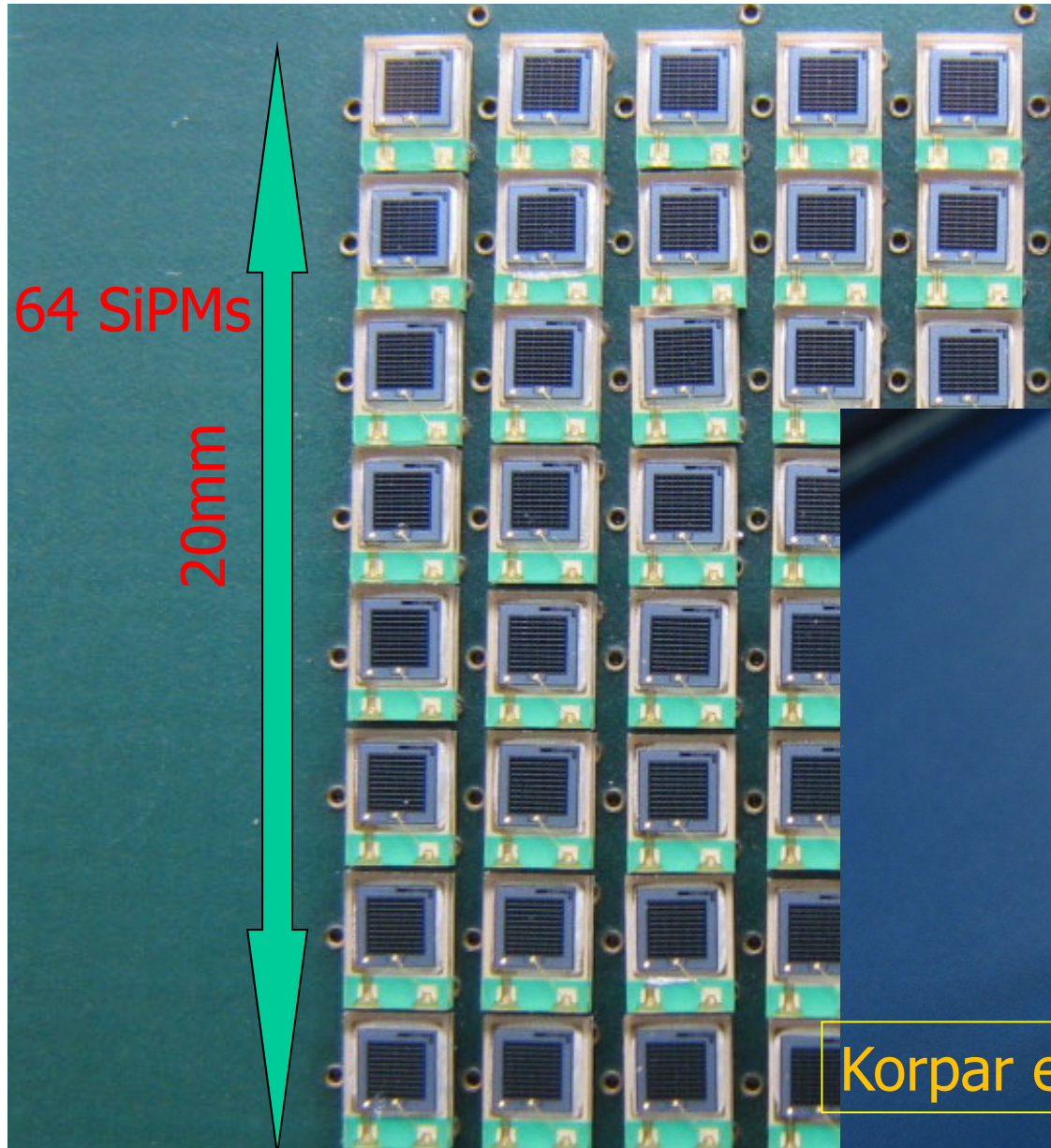
or combine a lens
and mirror walls

Detector module design

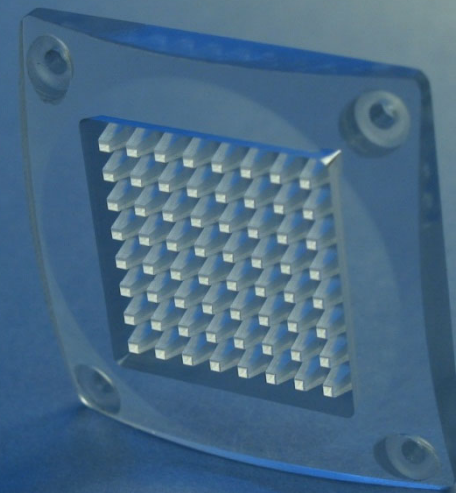
SiPM array with light guides



Photon detector with SiPMs and light guides



Full ring in a pion beam

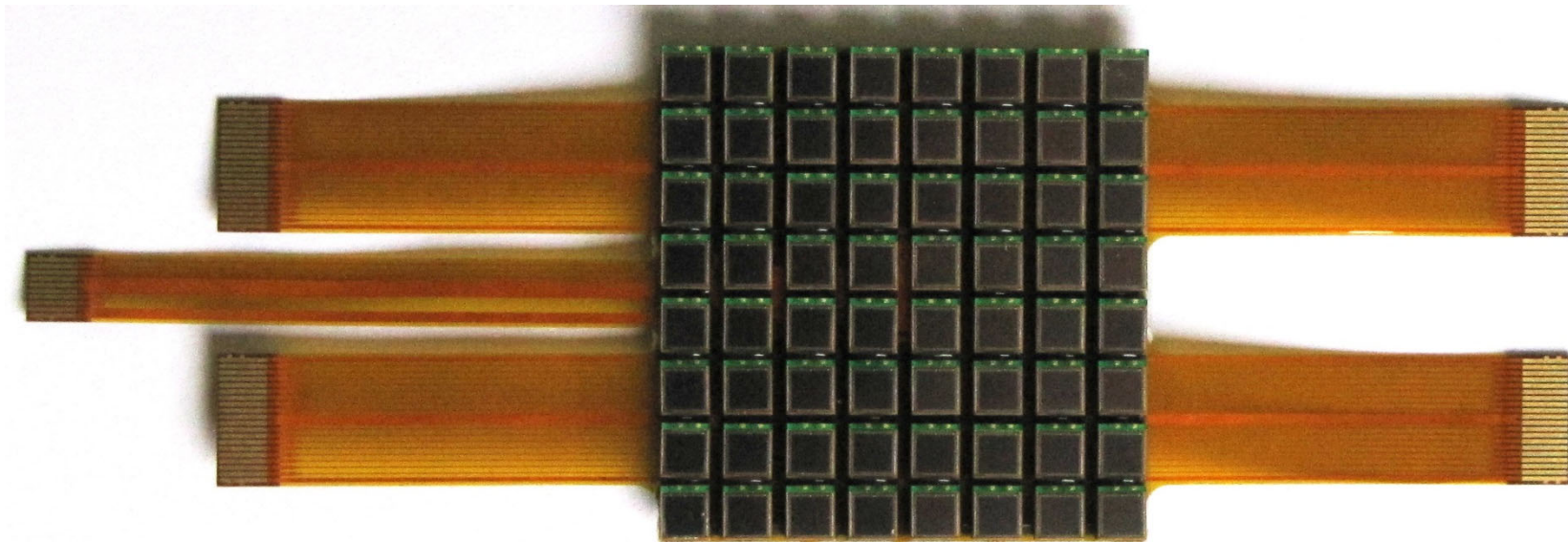


Korpar et al., NIM A613 (2010) 195

A new SiPM device

Array of SiPMs: Hamamatsu MPPC S11834-3388DF

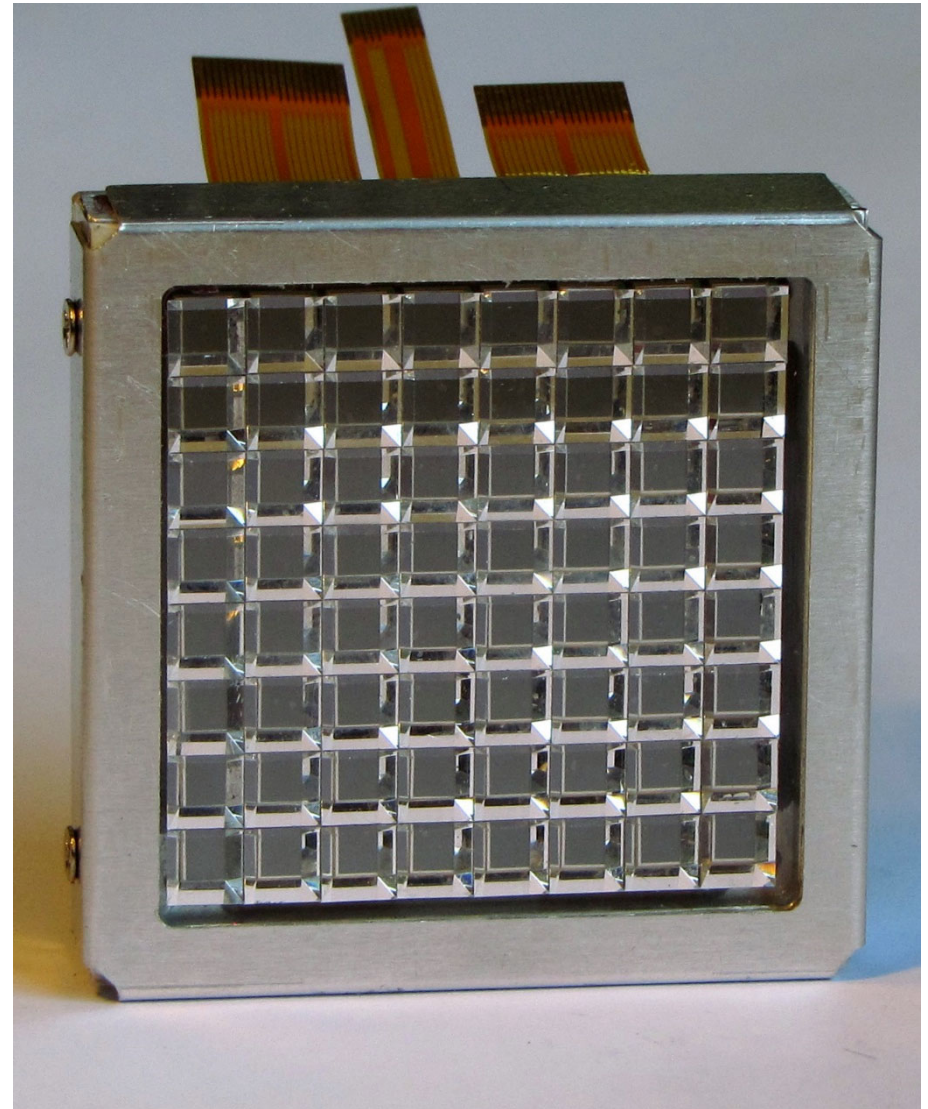
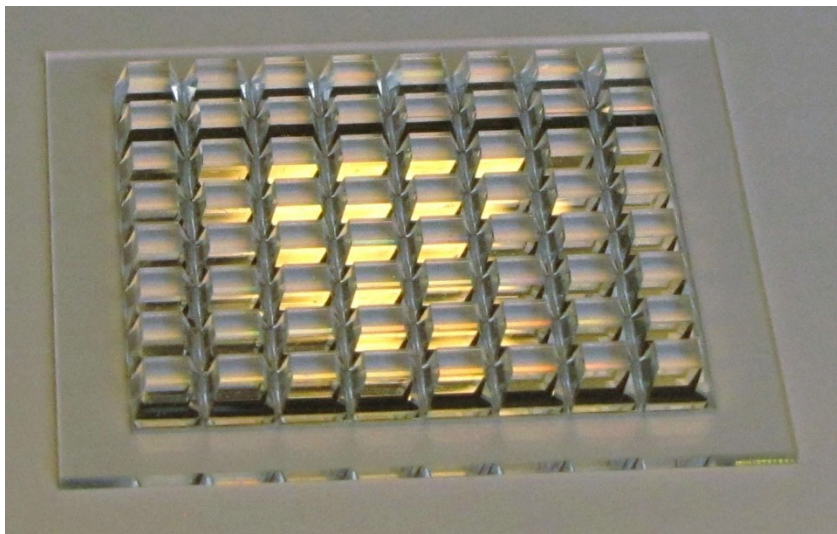
- A novel type of a multi-pixel Photon Counter (MPPC)
- 8x8 SiPM array, with 5x5 mm² SiPM channels
- Active area 3x3 mm²
- Cell size: 50 μm
- Rather low dark count rate (~ 100 kHz/mm²)
- Operating voltage: (70 ± 10) V



Detector module

Consists of the MPPC, light concentrator and support

Measured gain: $\sim 3.5 \times 10^5$ @ 72.8 V



Pulse height distribution for low light levels

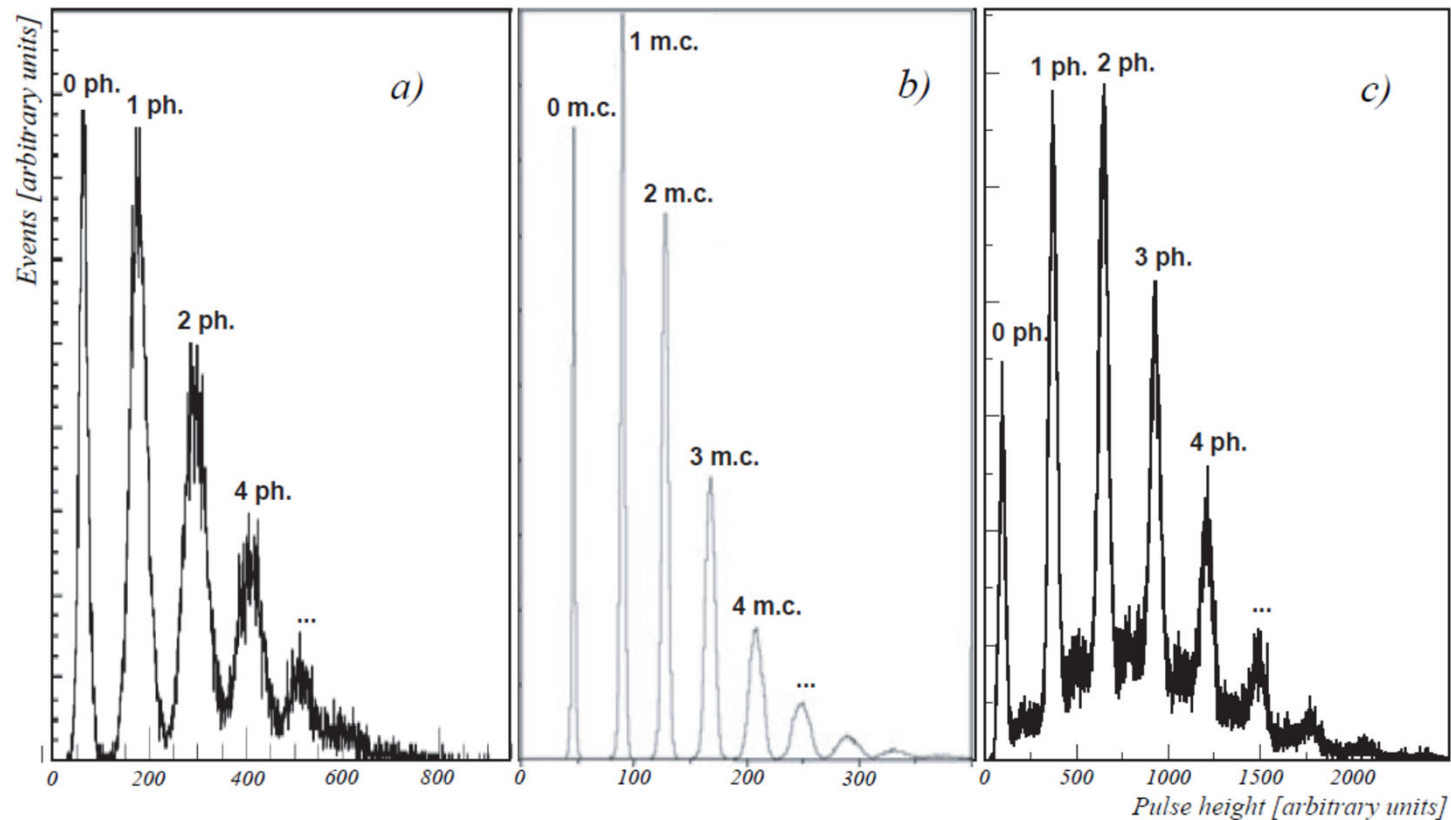
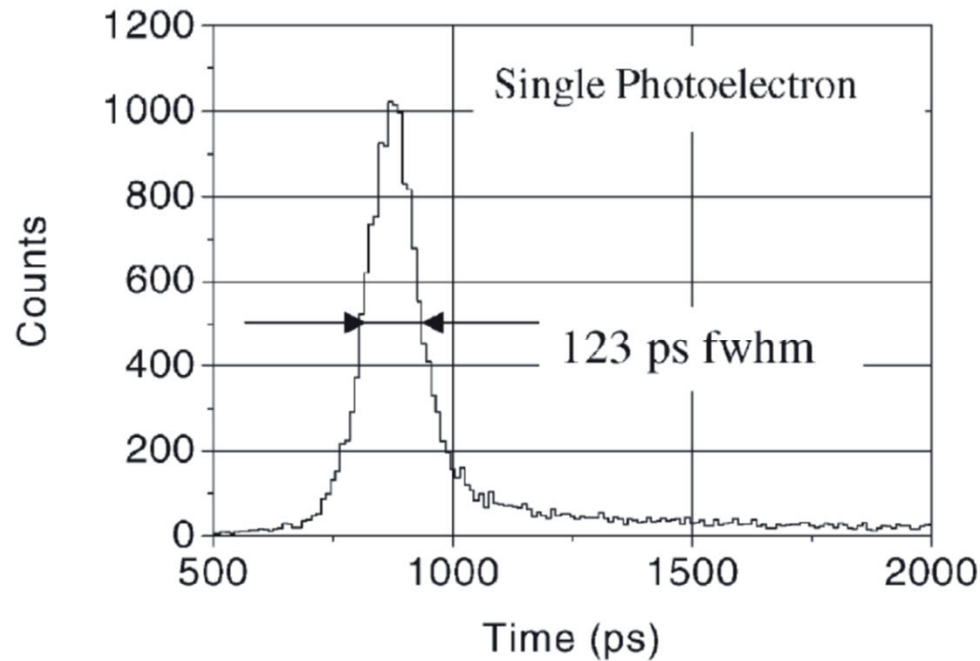


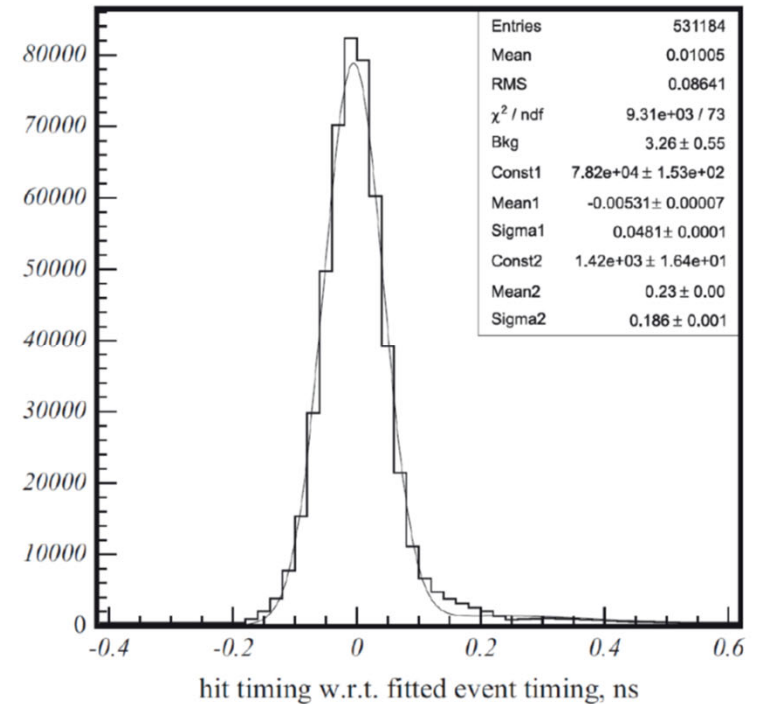
Figure 8: Pulse height spectrum of low intensity light pulses recorded with a VLPC (left, adopted from (20)), SiPM (middle, adopted from (21)) and HAPD (right)

SiPM: time resolution for single photons

Very fast analog SiPM



Digital SiPM



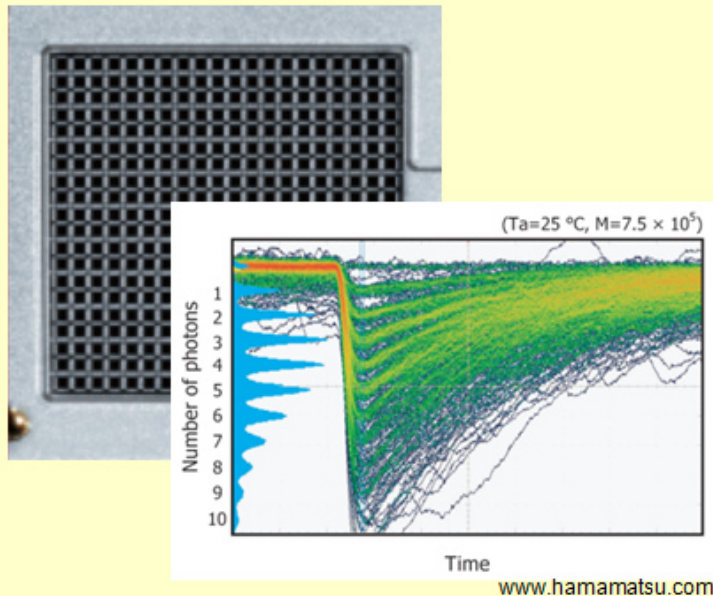
Analog SiPMs: typically 80 ps (sigma), 200 ps FWHM

Digital SiPMs: main peak 48 ps (sigma)!

New player: digital dSiPM

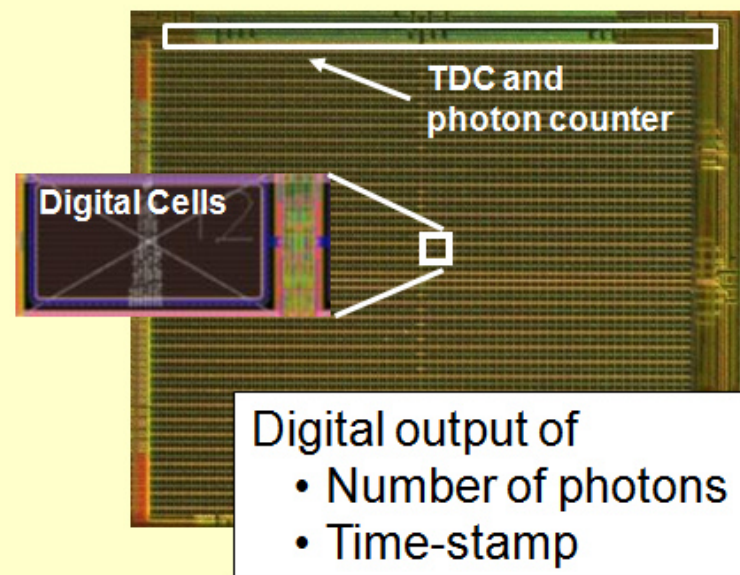
DPC: Front-end Digitization by Integration of SPAD & CMOS Electronics

analog SiPM



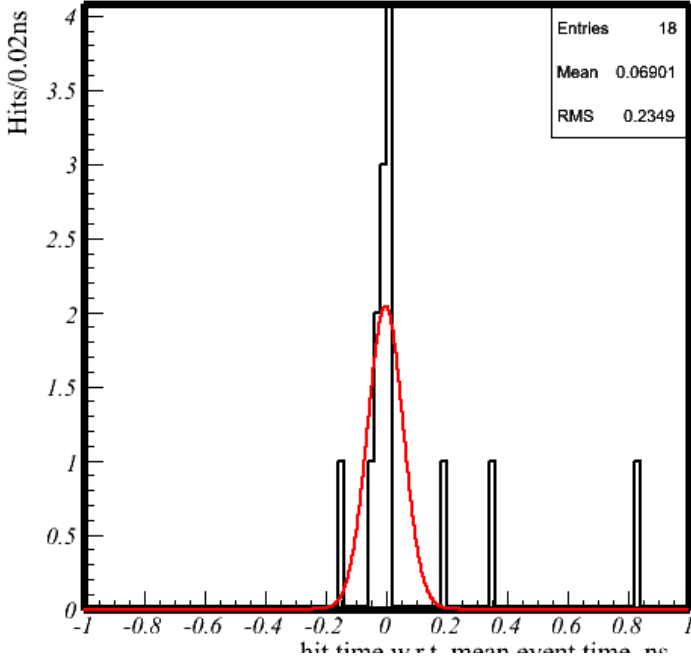
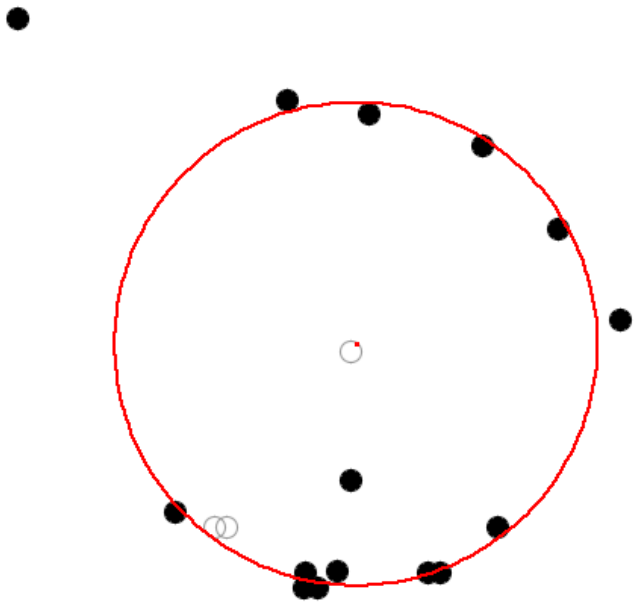
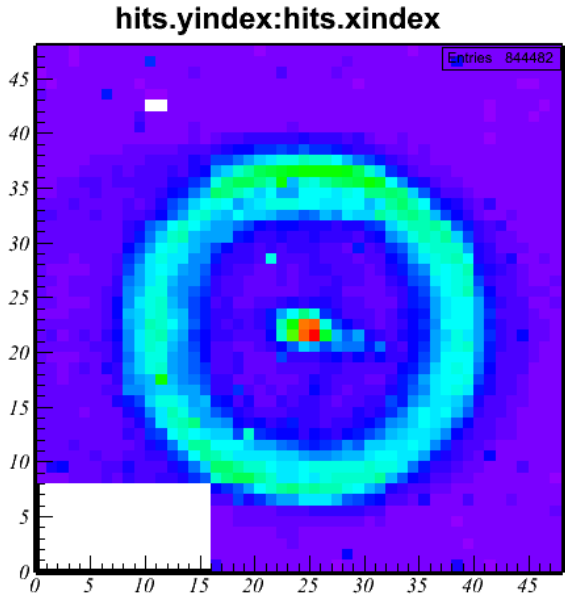
Summing all cell outputs leads to an analog output signal and limited performance

digital SiPM (dSiPM)



Integrated readout electronics is the key element to superior detector performance

dSiPM in beam tests



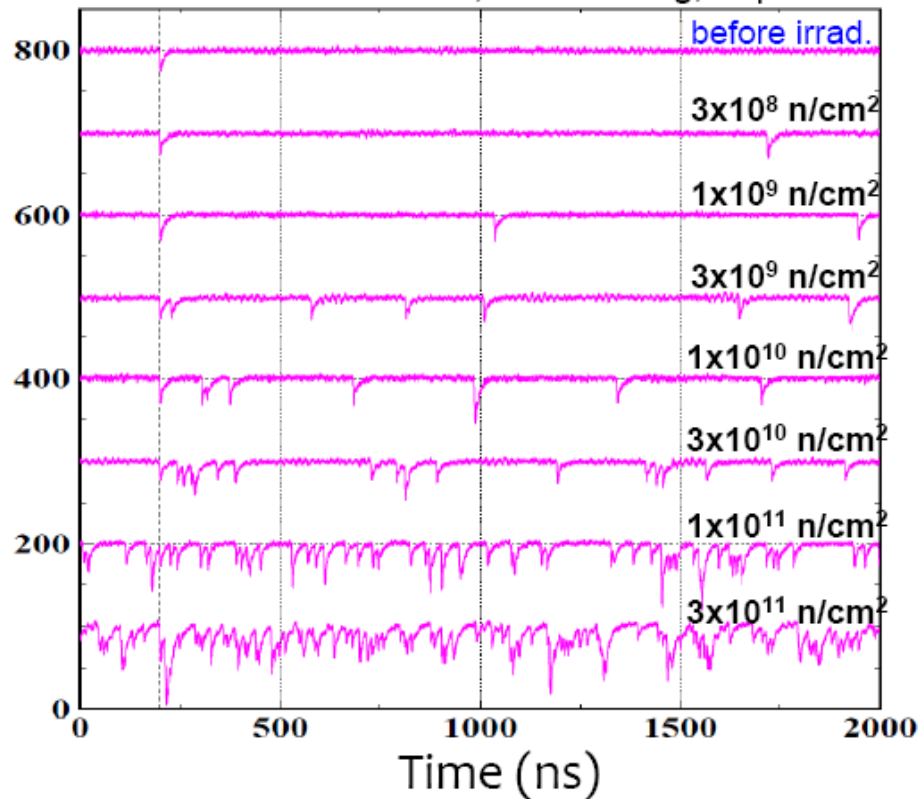
Sergey Kononov

VCI 2013

ana

Radiation damage

I.Nakamura, JPS meeting, Sep. 2008

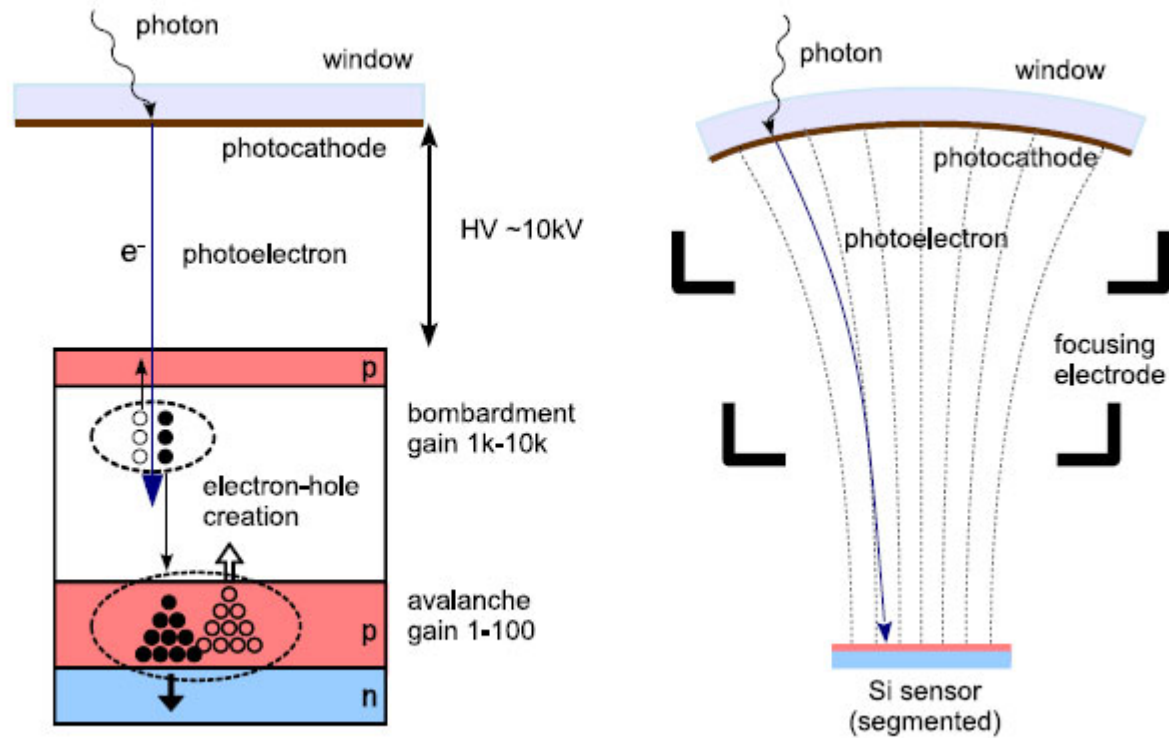


Expected fluence at 50/ab at
Belle II: $2-20 \cdot 10^{11} \text{ n cm}^{-2}$
→ Worst than the lowest line

→ Very hard to use present SiPMs as single photon detectors in many applications (including Belle II) because of radiation damage by neutrons

→ Also: could only be used with a sophisticated electronics – wave-form sampling

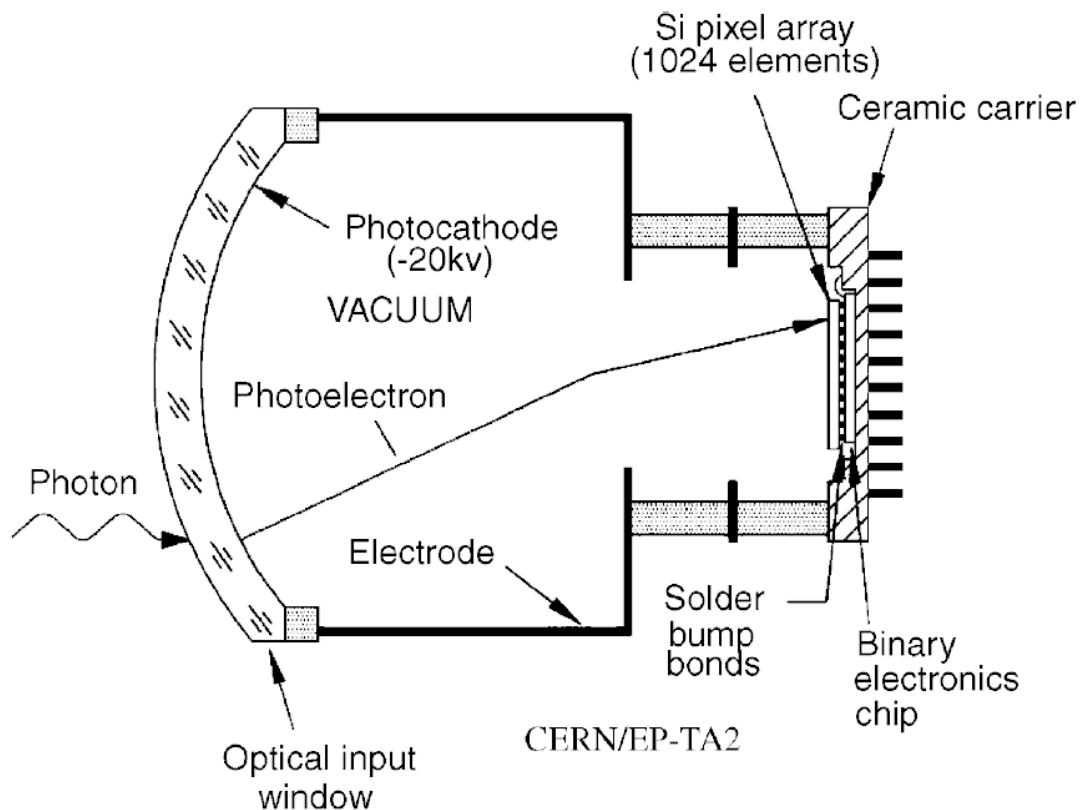
Hybrid photodetectors



Hybrid photodetector: LHCb RICHes

Photon detector: hybrid PMT (R+D with DEP) with 5x demagnification (electrostatic focusing).

Hybrid PMT: accelerate photoelectrons in electric field ($\sim 20\text{kV}$), detect it in a pixelated silicon detector.



NIM A553 (2005) 333

Aerogel RICH

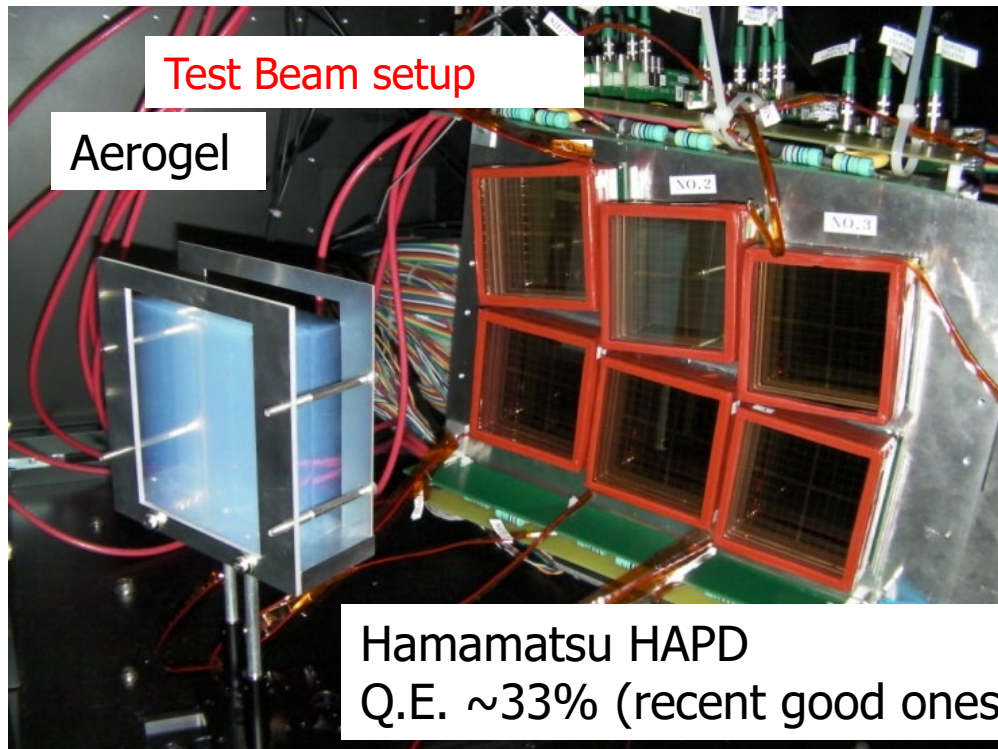
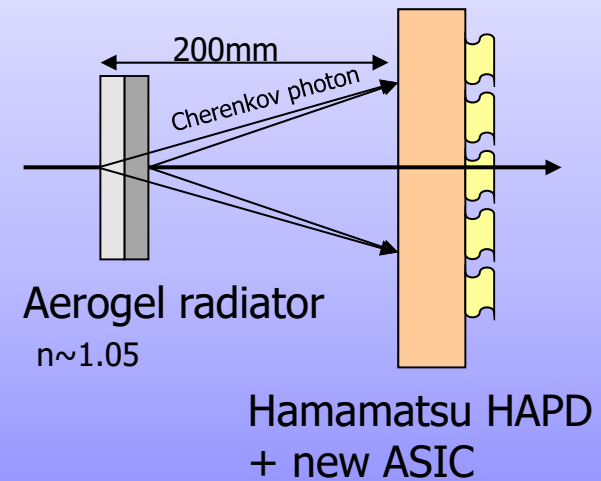
Need:

Operation in 1.5 T magnetic field

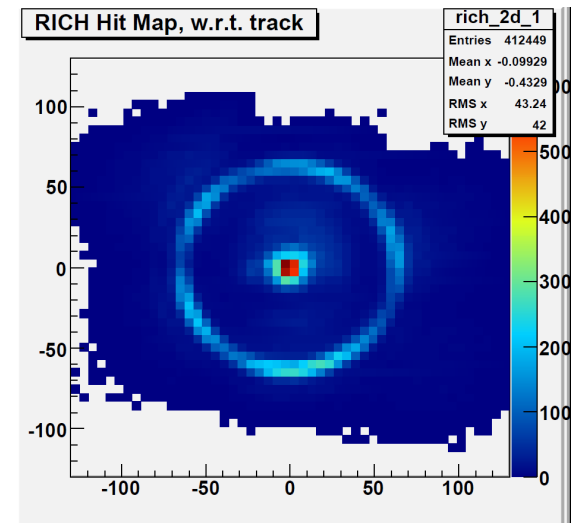
Pad size $\sim 5\text{-}6\text{mm}$

Photosensor: large active area HAPD of the proximity focusing type

Endcap PID: Aerogel RICH (ARICH)



Clear Cherenkov image observed



6.6 σ p/K at 4GeV/c!

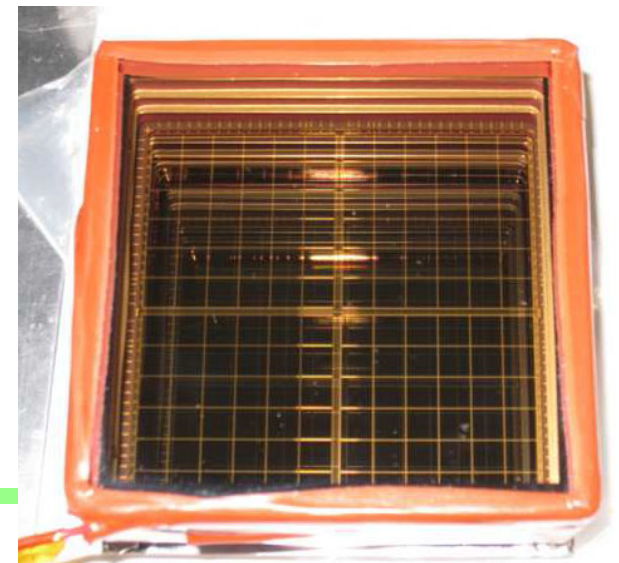
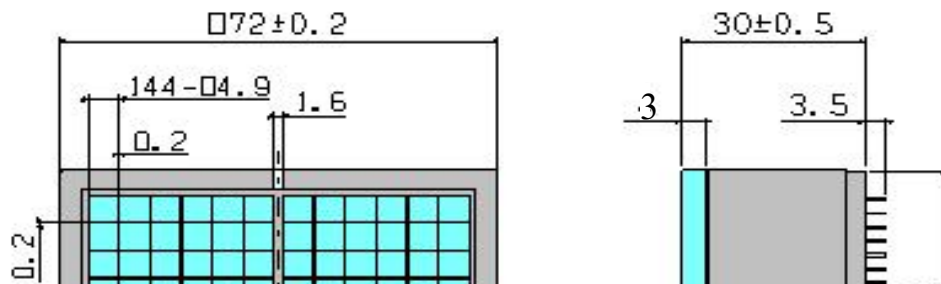
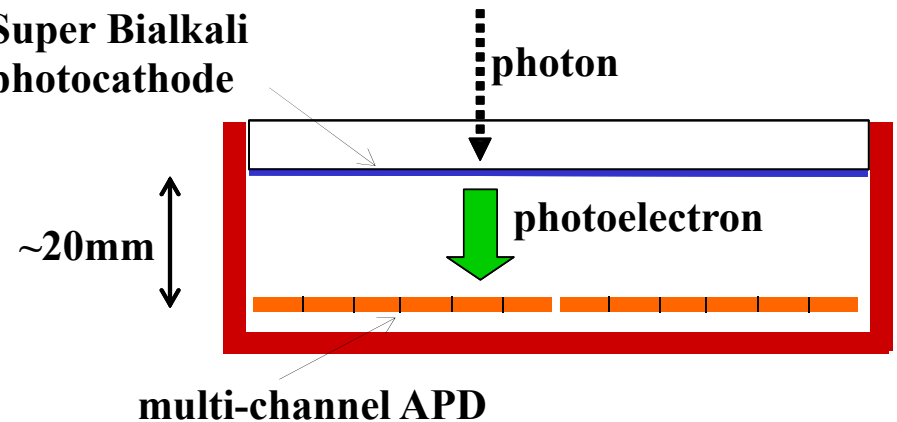
\rightarrow NIM A595 (2008) 180

ARICH photon detector: HAPD

Hybrid avalanche photo-detector developed in cooperation with Hamamatsu Photonics K.K. (proximity focusing configuration):

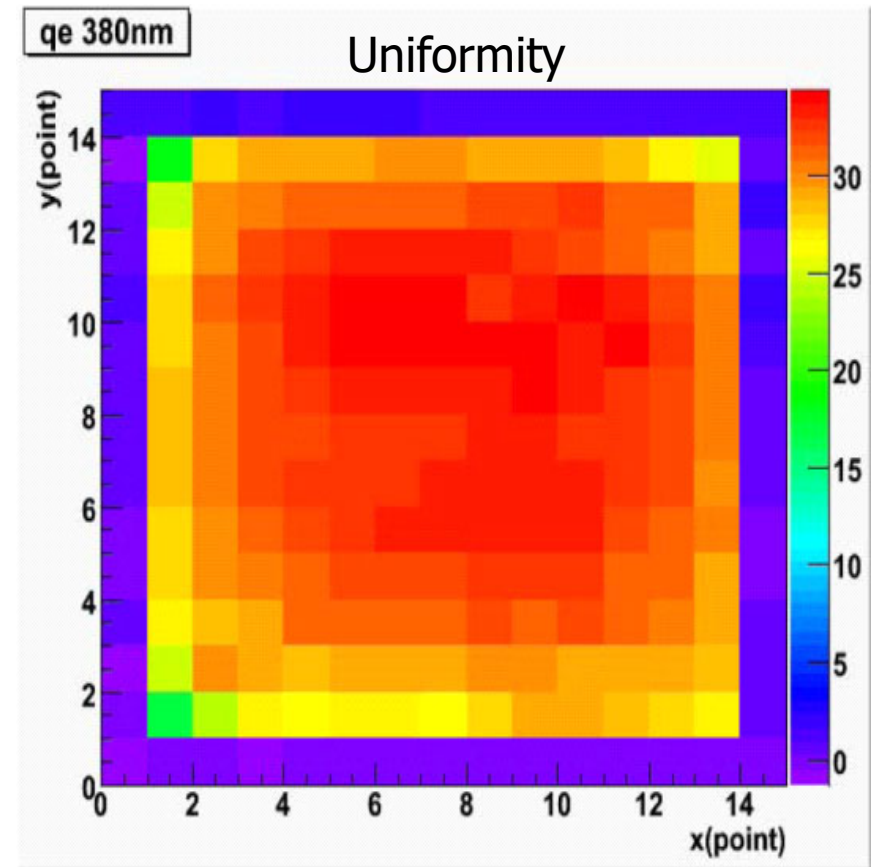
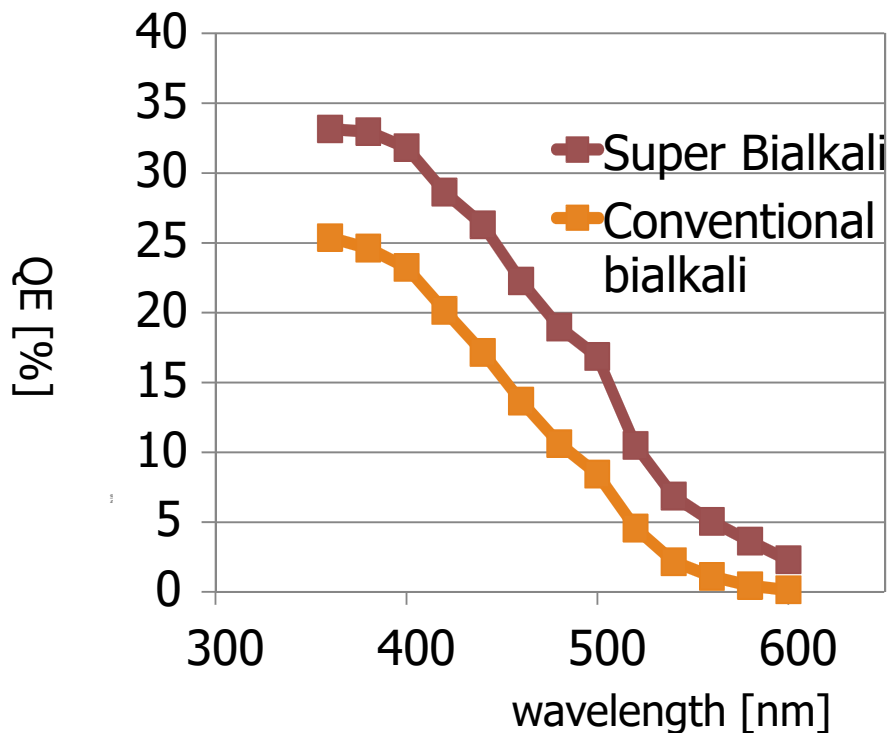
- 12 x12 channels ($\sim 5 \times 5 \text{ mm}^2$)
- size $\sim 72 \text{ mm} \times 72 \text{ mm}$
- $\sim 65\%$ effective area
- total gain $> 4.5 \times 10^4$ (two steps: bombardment > 1500 , avalanche > 30)
- detector capacitance $\sim 80 \text{ pF/ch.}$
- super bialkali photocatode, typical peak QE $\sim 28\%$ ($> 24\%$)
- works in mag. field (\sim perpendicular to the entrance window)

Super Bialkali photocathode



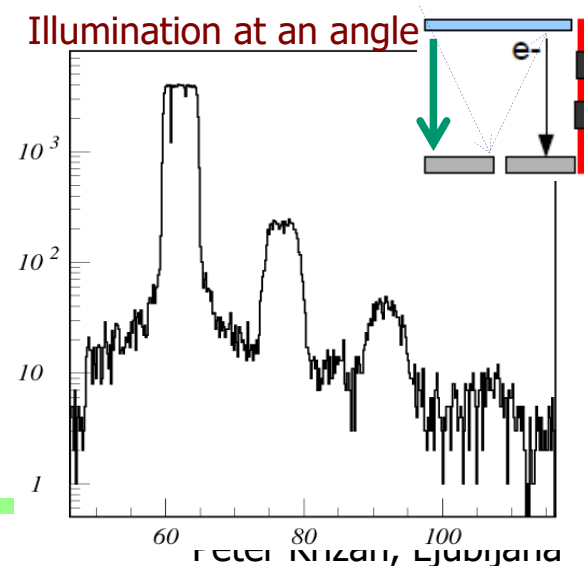
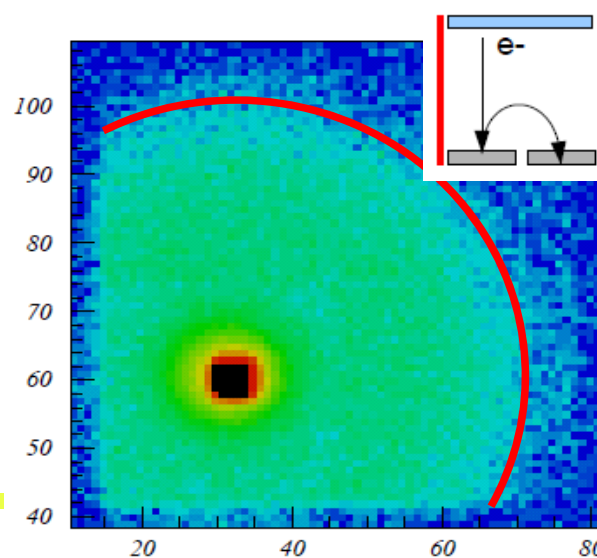
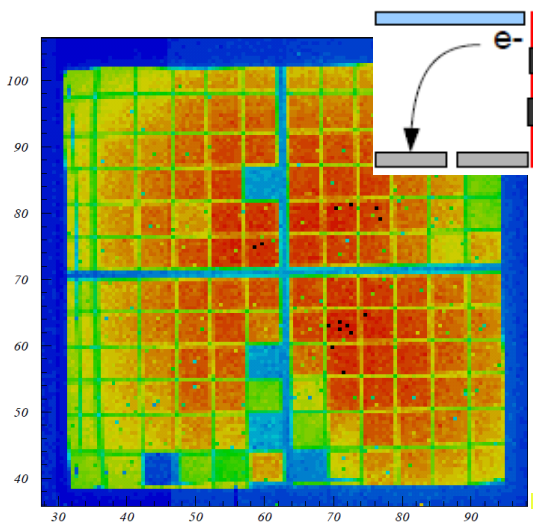
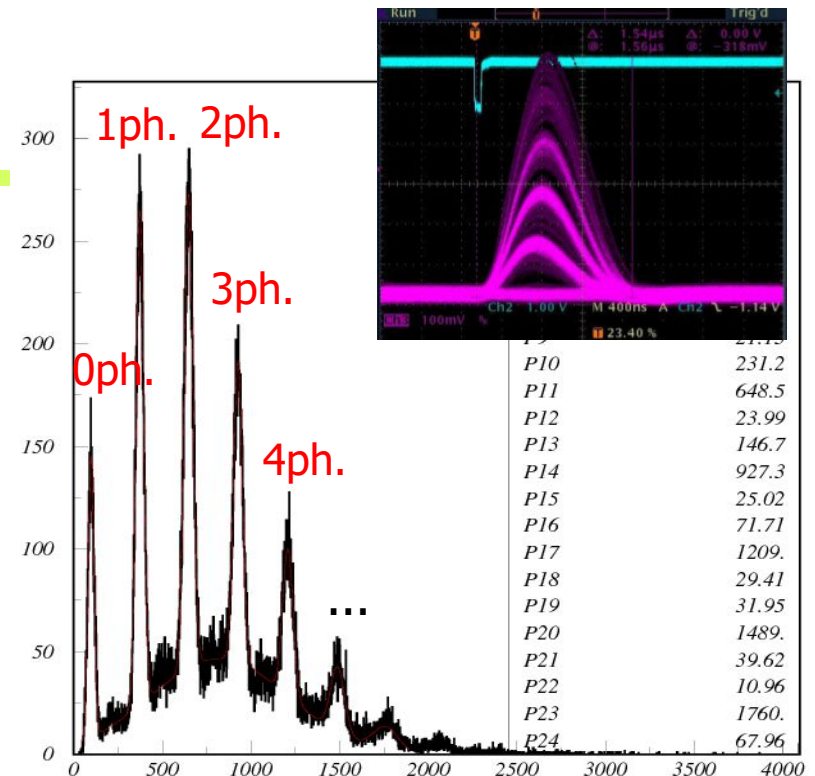
HAPD QE

- peak QE improved by Hamamatsu with super bialkali photocathode:
25% → >30%
- typically QE is somewhat lower at the edges of the HAPD



HAPD performance @ B=0T

- excellent photon counting affected only by photo-electron back-scattering → high single photon counting efficiency
- sharp transition between channels
- image distortion due to a non-uniform electric field at the edges
- back-scattering induced cross-talk
- optical cross-talk by reflection from APD surface → weak echo ring



Another hybrid photo-detector: add a fast scintillator

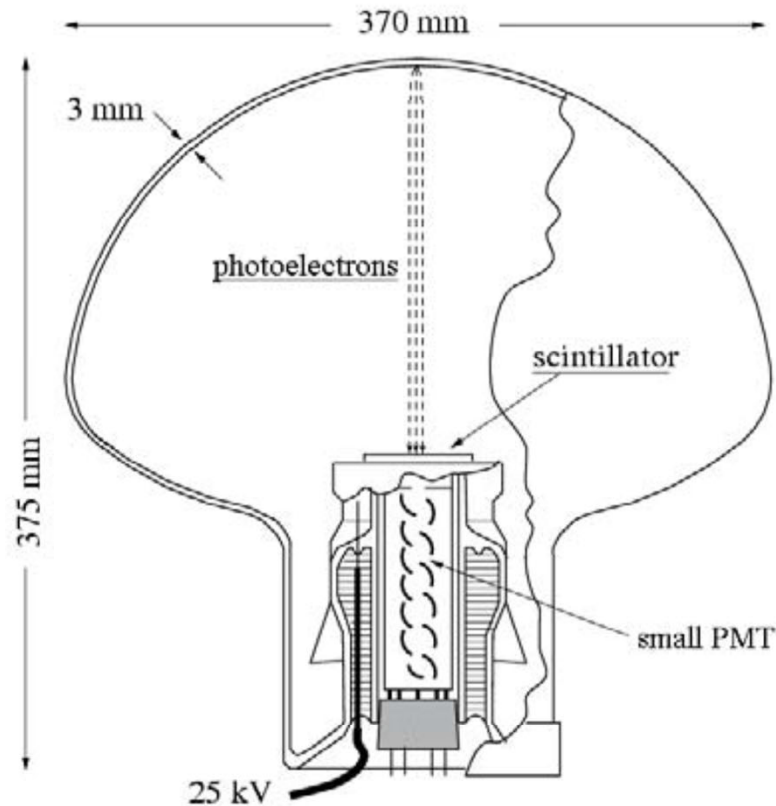


Figure 14: Hybrid photon detector with a scintillating crystal QUASAR-370 (31).

4) Gas chamber based photosensors

=MWPC + (TMAE, TEA or Csl)

gas additive to the MWPC gas

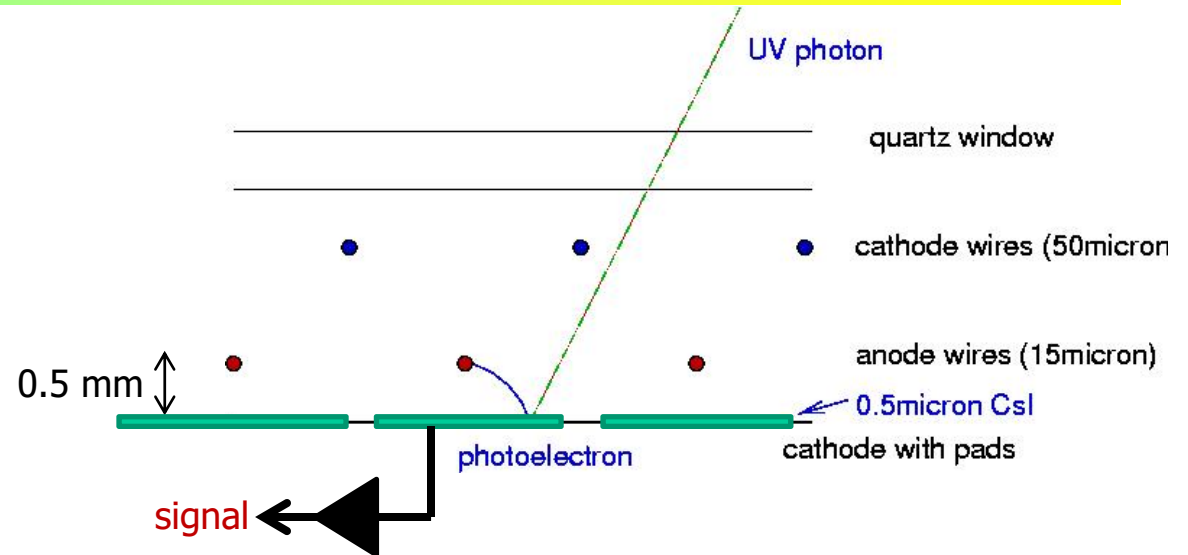
- -TEA ; $E_{\text{ion}} = 7.5 \text{ eV}$, $p_n = 5 \text{ tor}$, $\lambda \approx 0.6 \text{ mm pri } 20^\circ\text{C}$
- TMAE; $E_{\text{ion}} = 5.4 \text{ eV}$, $p_n = 0.35 \text{ tor}$, $\lambda \approx 23 \text{ mm pri } 20^\circ\text{C}$

Csl

- evaporate $\approx 500 \text{ nm}$ onto the chamber cathode plane

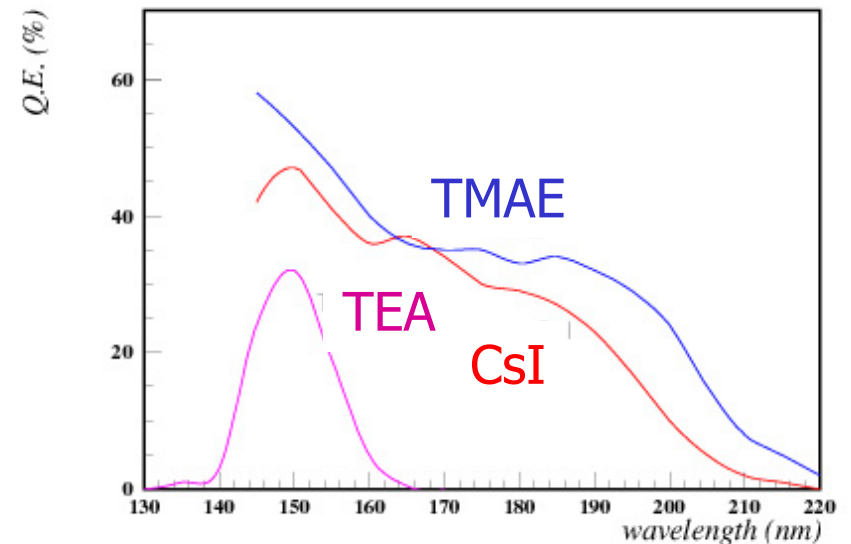
Gas chamber based photosensors

Multiwire chamber with
cathode pad read-out:
→ short drift distances,
fast detector



Photosensitive component:

- in the gas mixture (**TEA**):
CLEOIII RICH
- or a layer on one of the cathodes
(**CsI** on the printed circuit cathode
with pads) →



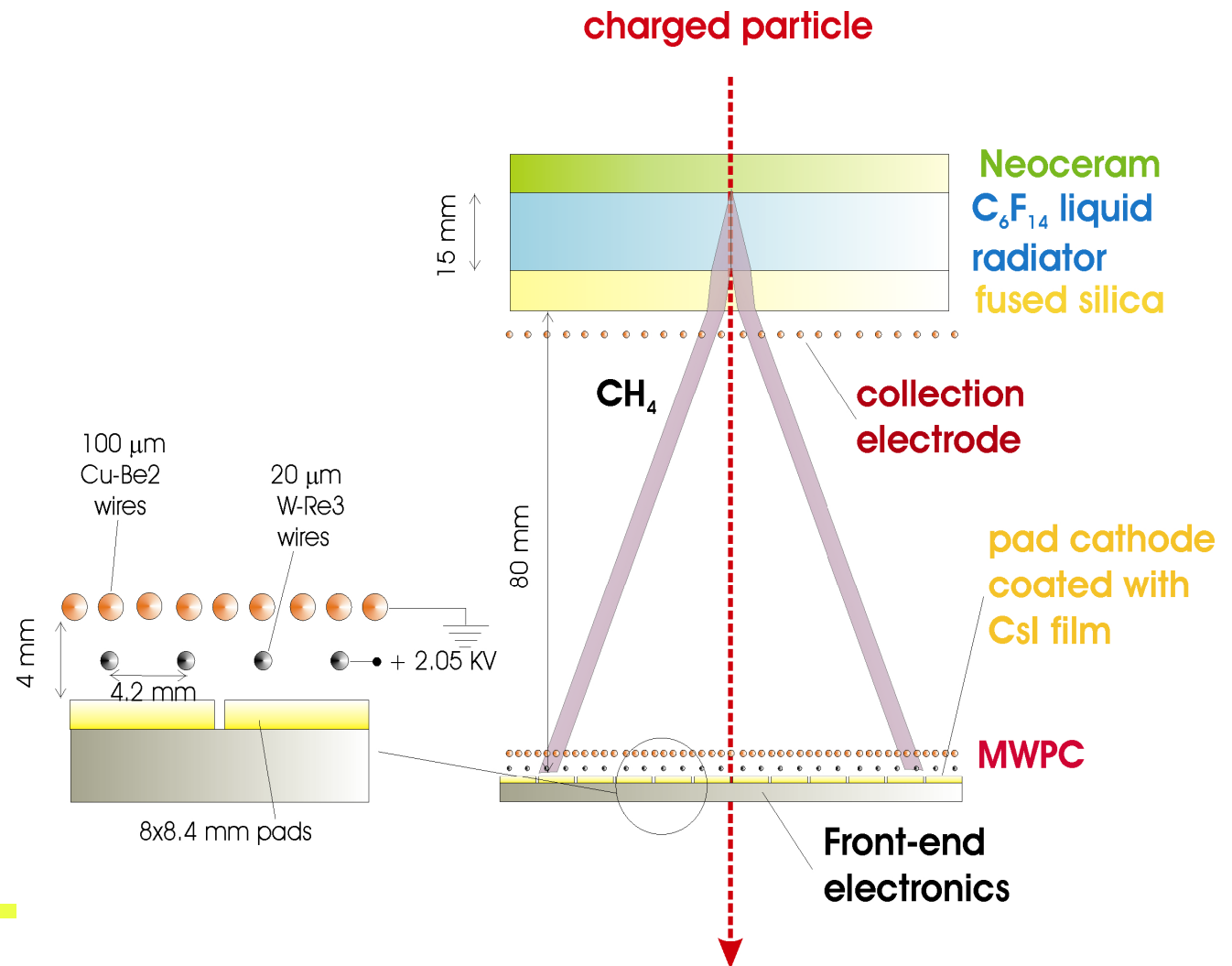
Works in high magnetic field!

CsI based RICH counters: HADES, COMPASS, ALICE

HADES and COMPASS RICH: gas radiator + CsI photocathode – long term experience in operation

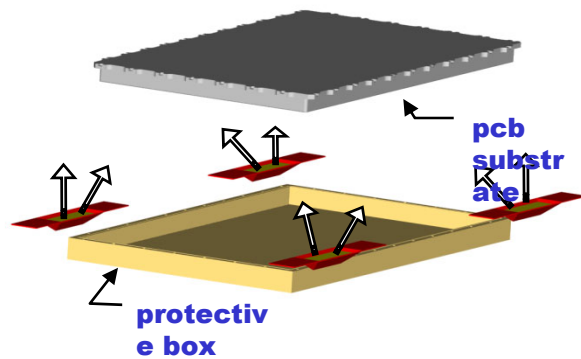
ALICE:

- liquid radiator
- proximity focusing



CERN CsI deposition plant

Photocathode produced with a well defined, several step procedure, with CsI vacuum deposition and subsequent heat conditioning

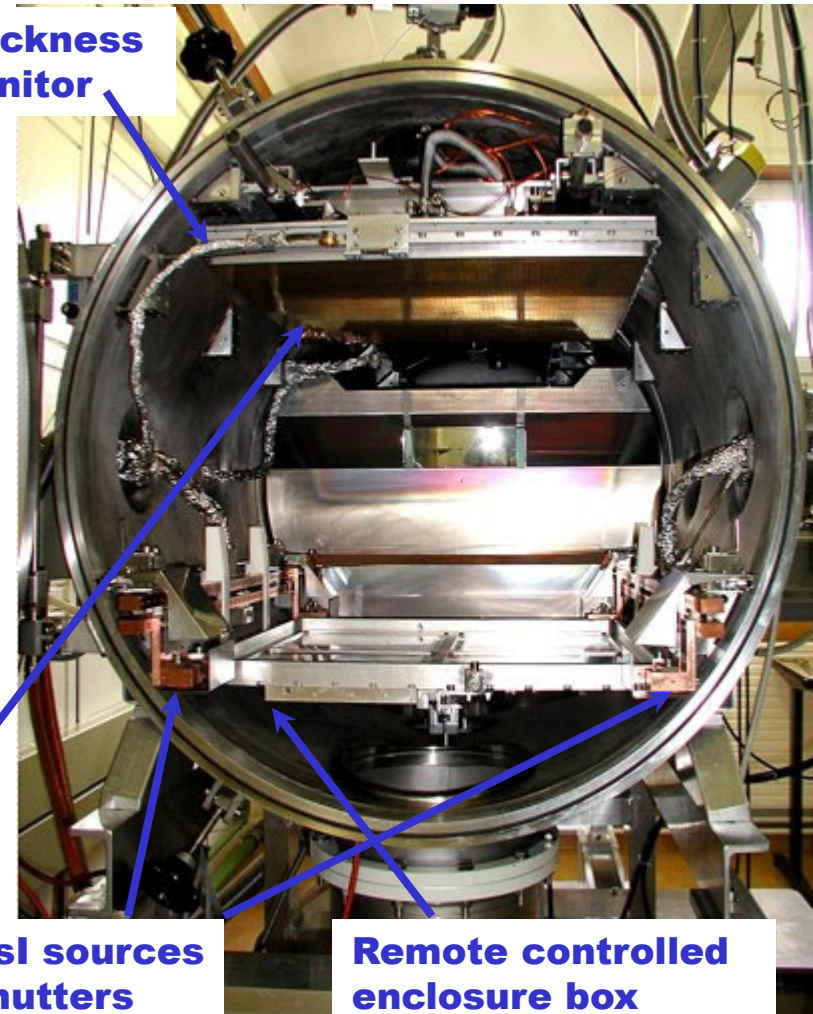


Thickness monitor

PC

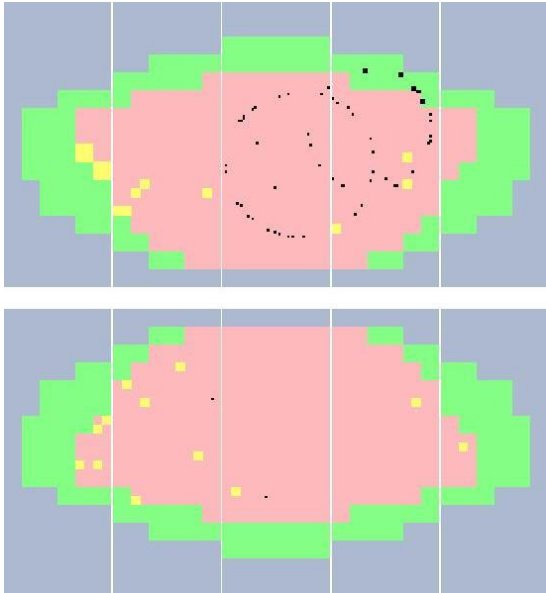
4 CsI sources + shutters

Remote controlled enclosure box



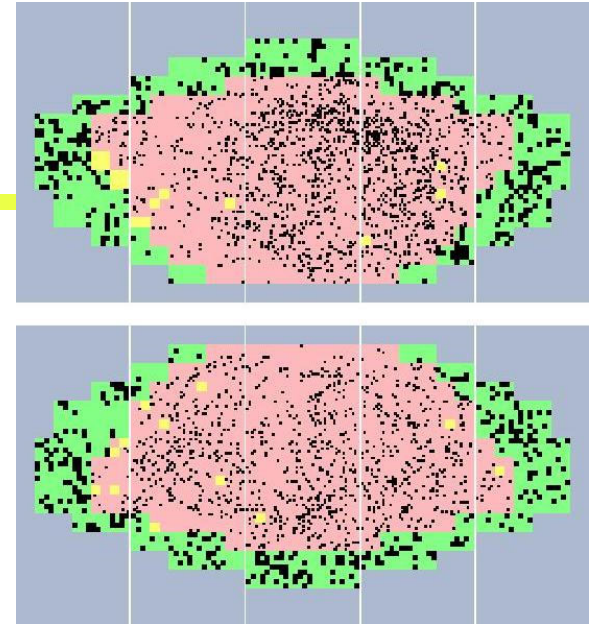
Examples of applications

HERA-B RICH

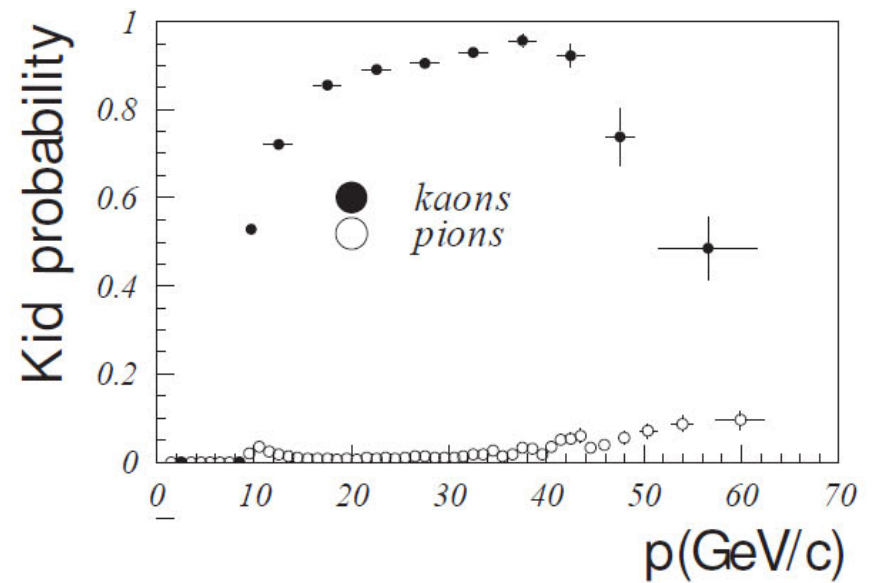
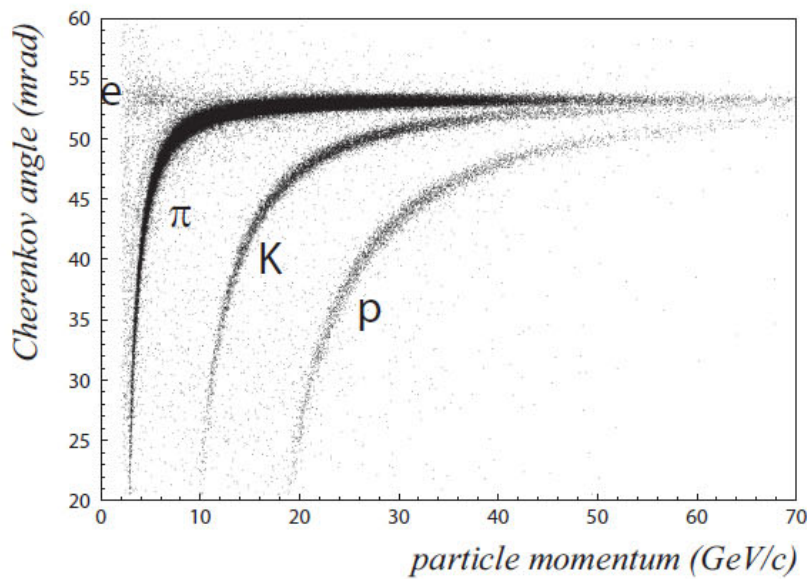


← Little noise, ~ 30 photons per ring

Typical event →



Very good performance:

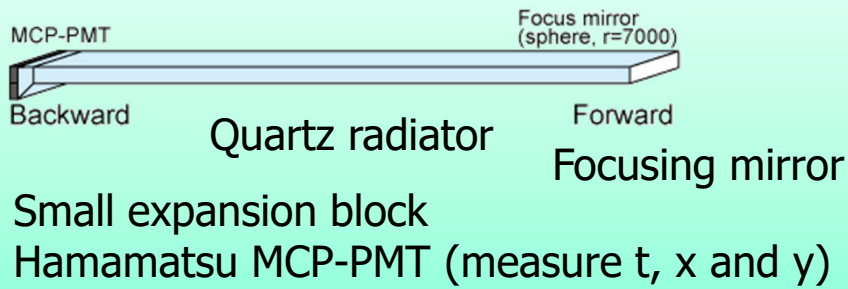


Kaon efficiency and pion fake probability

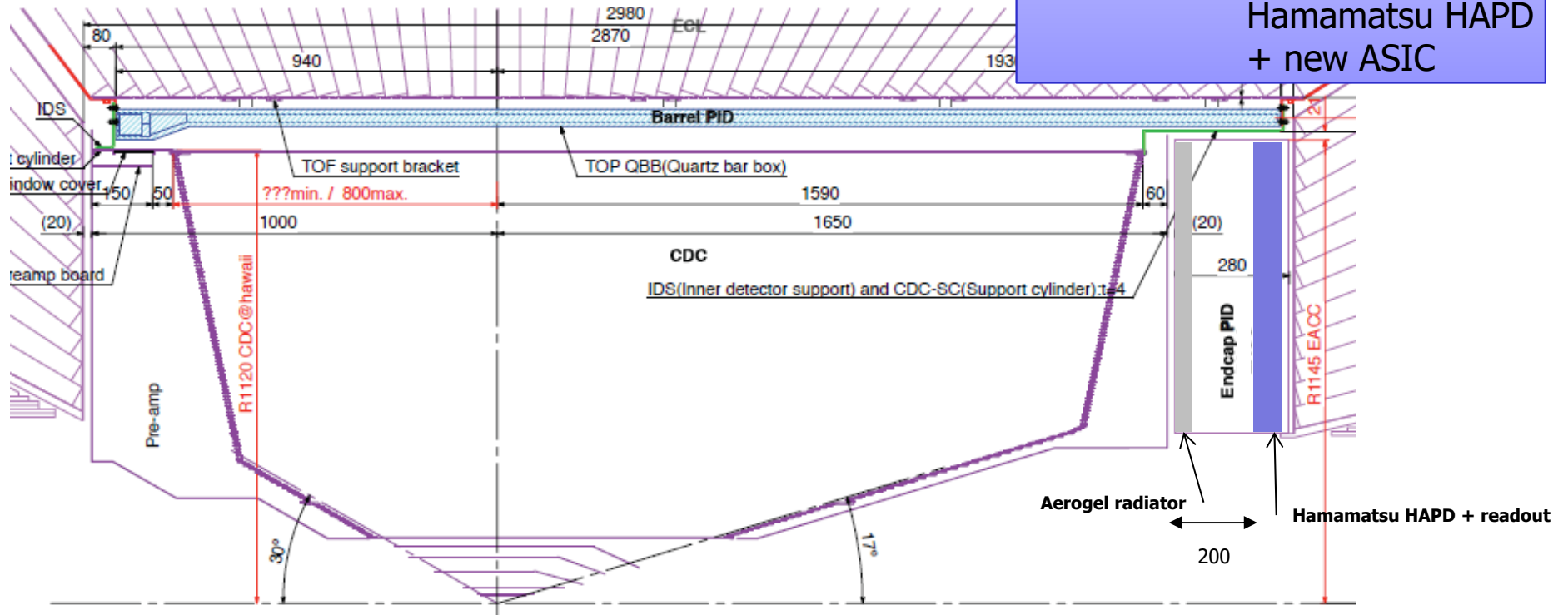
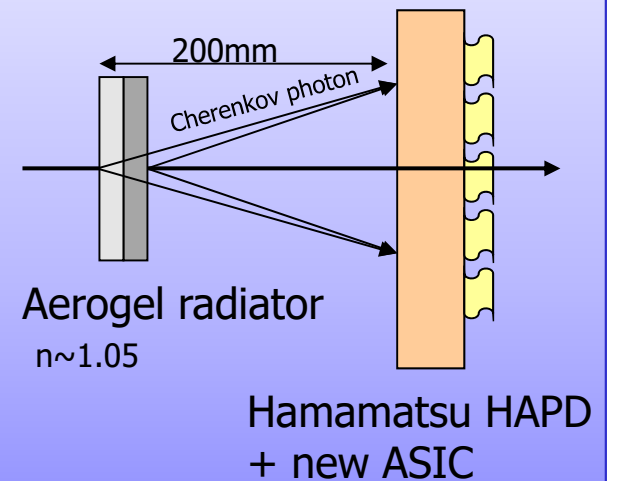


Belle II Cherenkov detectors

Barrel PID: Time of Propagation Counter (TOP)



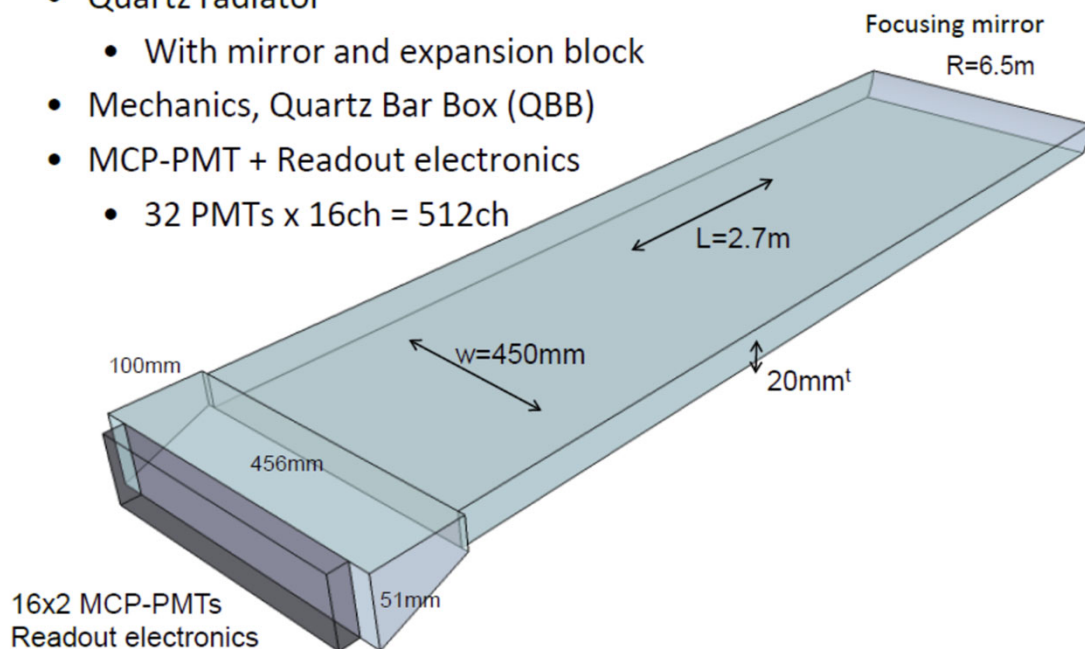
Endcap PID: Aerogel RICH (ARICH)



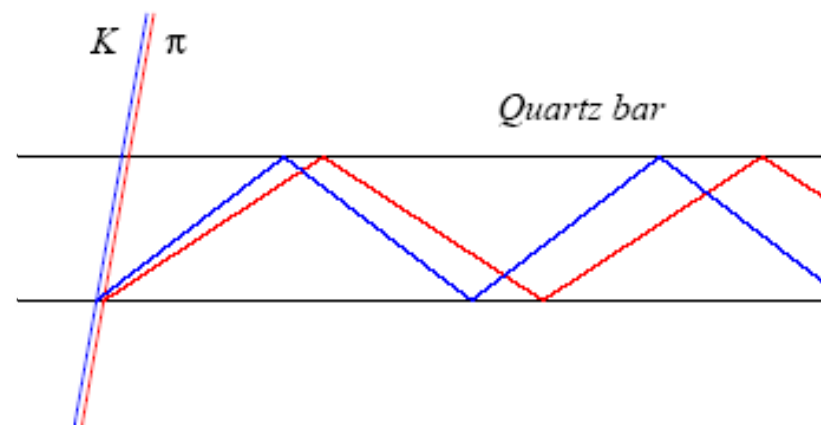
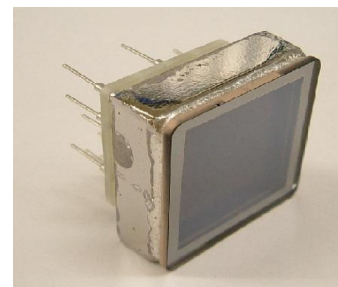


Time-Of-Propagation (TOP) counter

- Quartz radiator
 - With mirror and expansion block
- Mechanics, Quartz Bar Box (QBB)
- MCP-PMT + Readout electronics
 - 32 PMTs x 16ch = 512ch



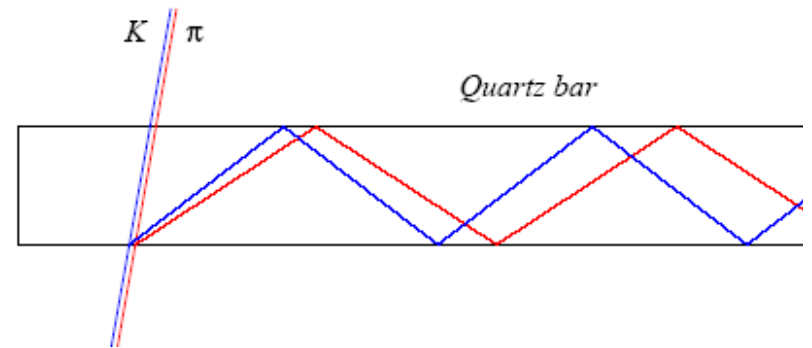
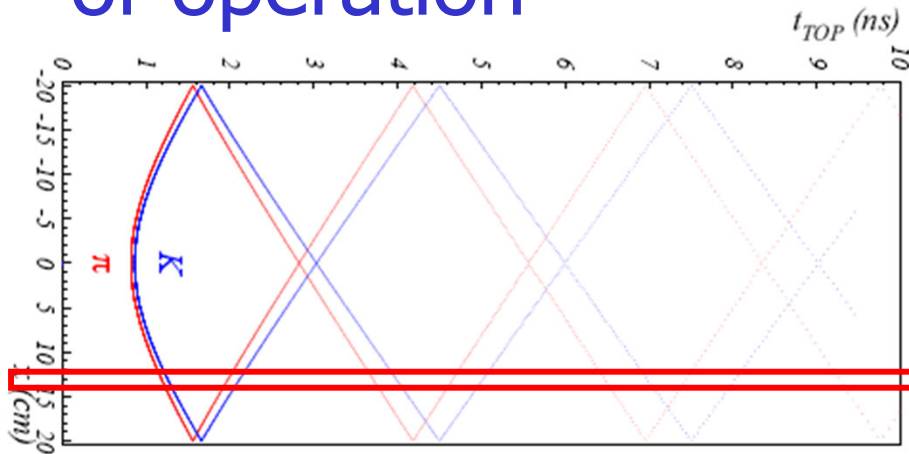
Hamamatsu
SL10 MCP-PMT



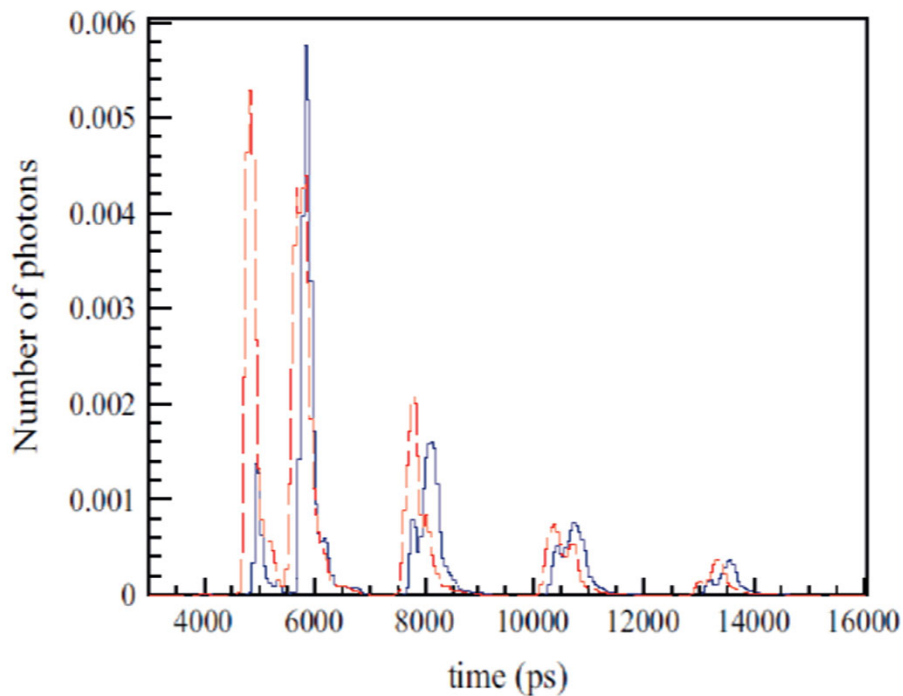
Instead of a 2D image in two coordinates ('ring') measure:

- One (or two coordinates) with a few mm precision
- **Time-of-arrival**
- Excellent time resolution $< 100\text{ps}$ (incl. read-out)
required for single photons in 1.5T B field

TOP counter: principle of operation



Pattern in the coordinate-time space ('ring') of a pion and a kaon hitting a quartz bar



Time distribution of signals recorded by one of the PMT channels: different for π and K (\sim shifted in time)

Fast photon detection

New generation of Cherenkov counters: precise time information needed to further improve performance:

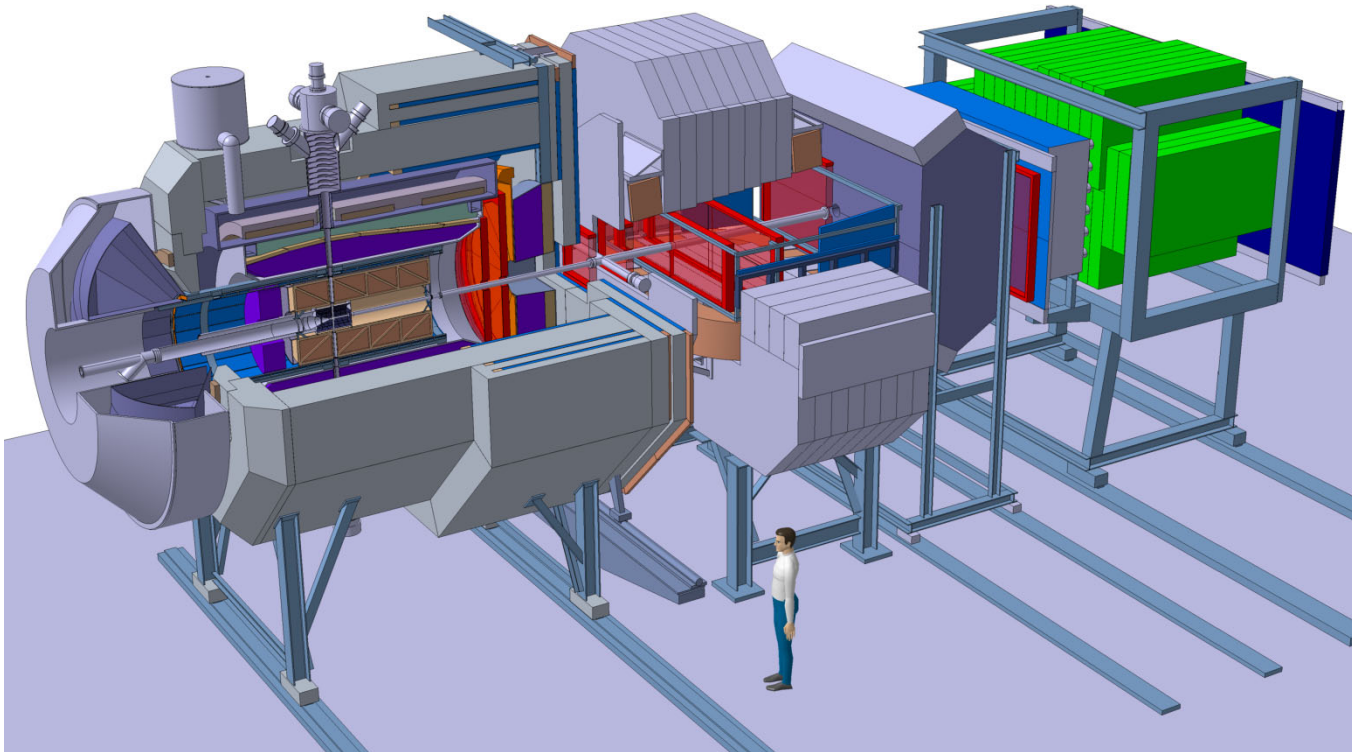
- Reduce chromatic aberration in a RICH detector (measure group velocity): Focusing DIRC
- Combine TOF and RICH techniques: TOP (Time-of-propagation counter), TORCH
- Dedicated TOF

New possibilities in medical imaging: TOFPET with Cherenkov light

→ Need photo sensors with excellent timing

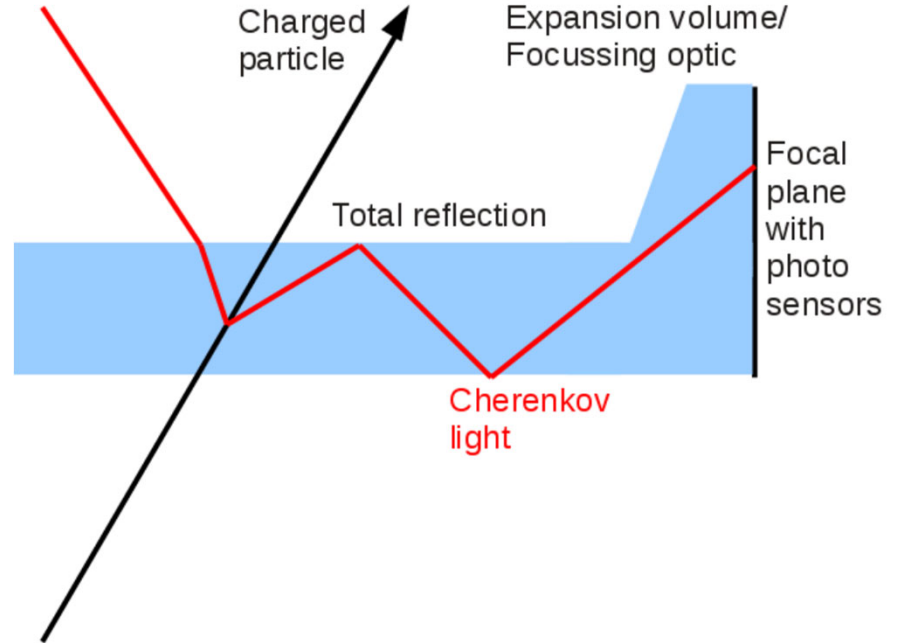
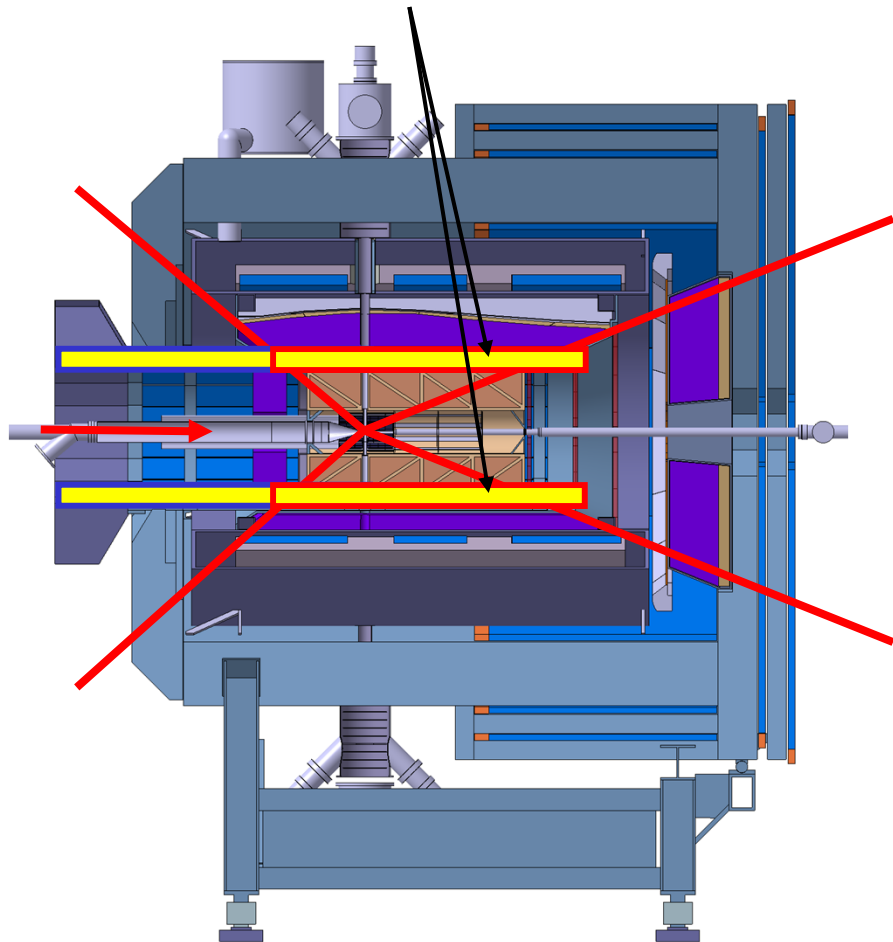
DIRC counters for PANDA (FAIR, GSI)

Two DIRC-like counters are under preparation for the PANDA experiment

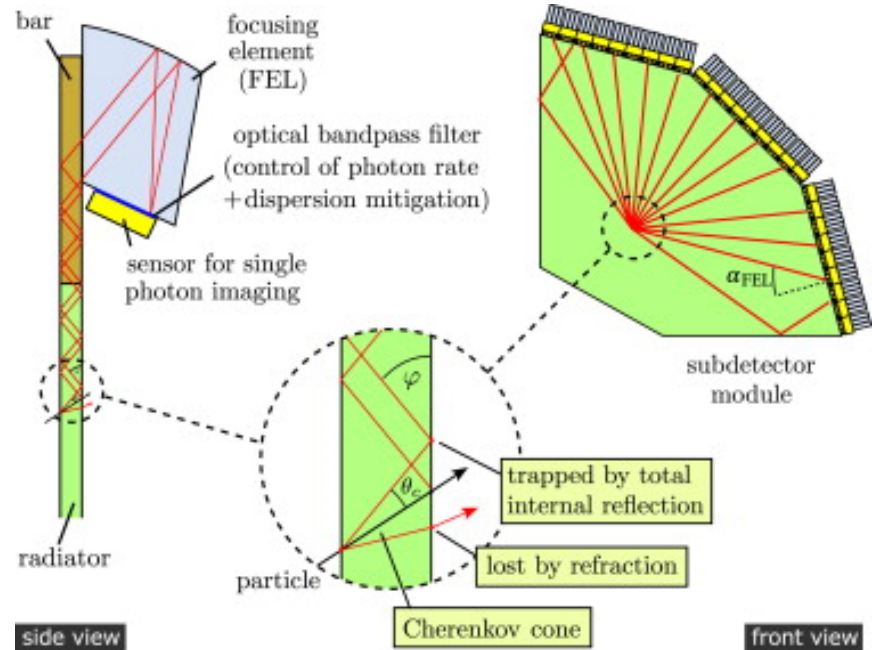
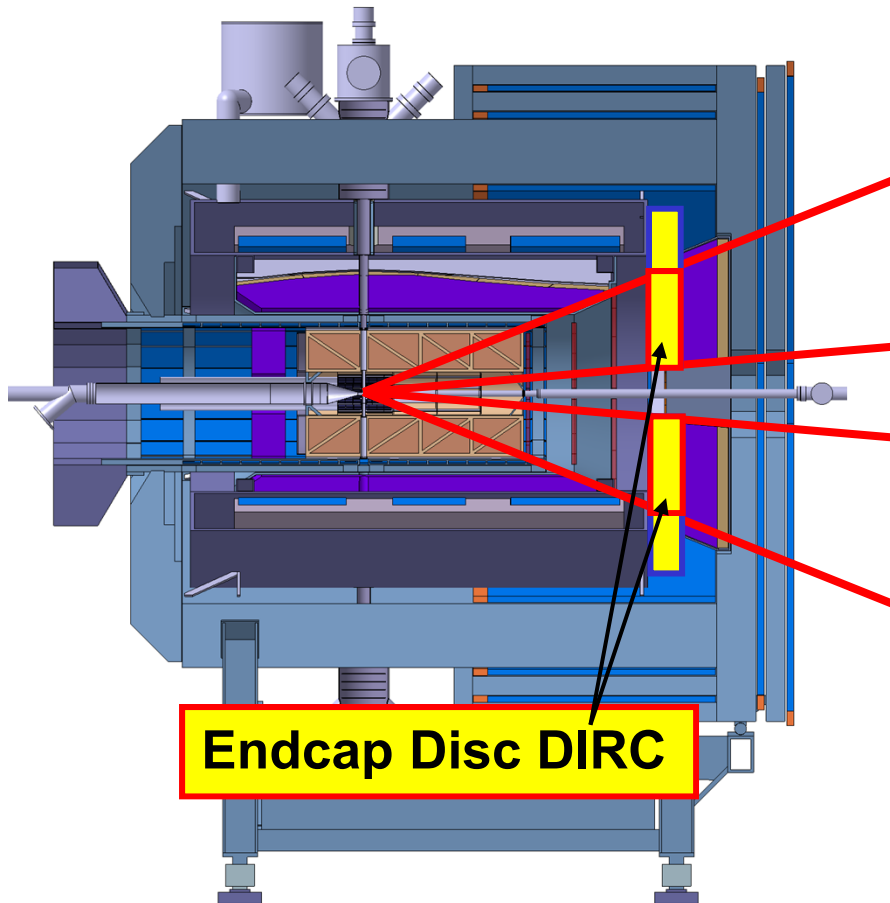


PANDA barrel DIRC

Barrel-DIRC

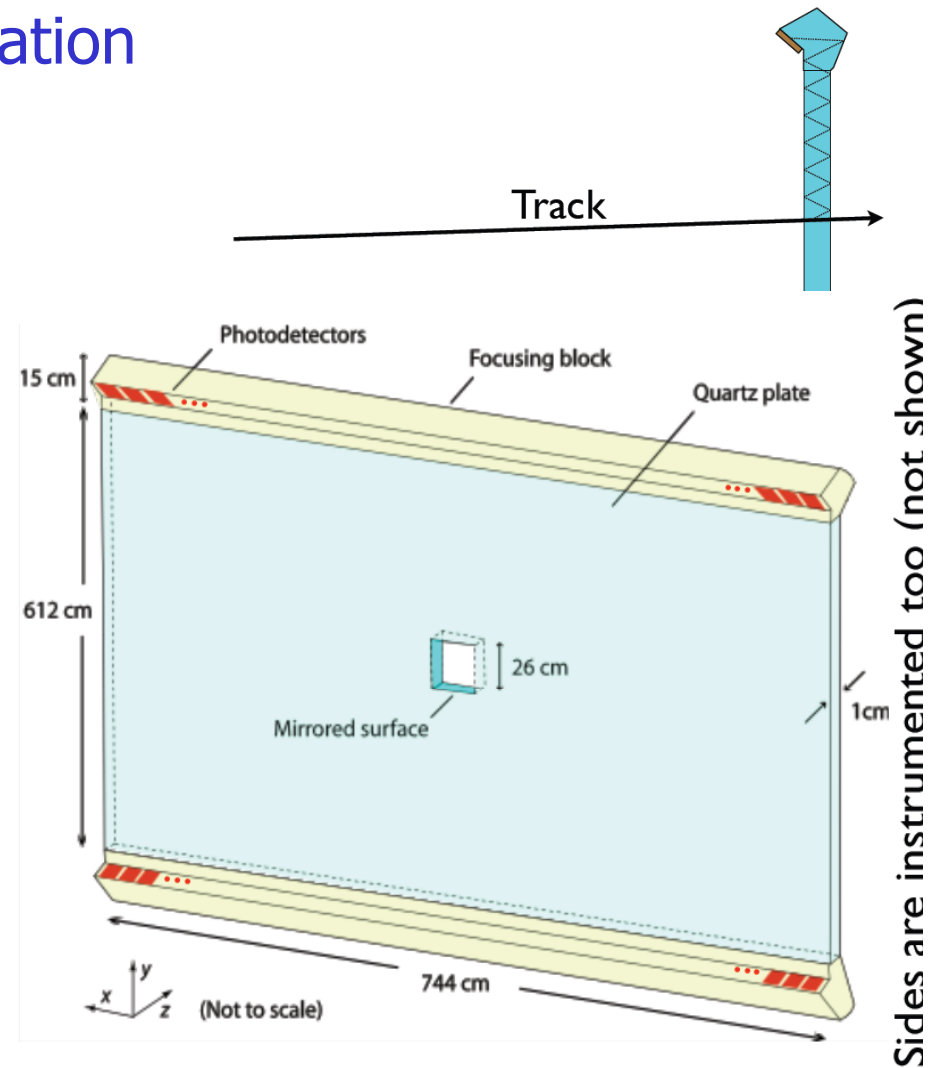
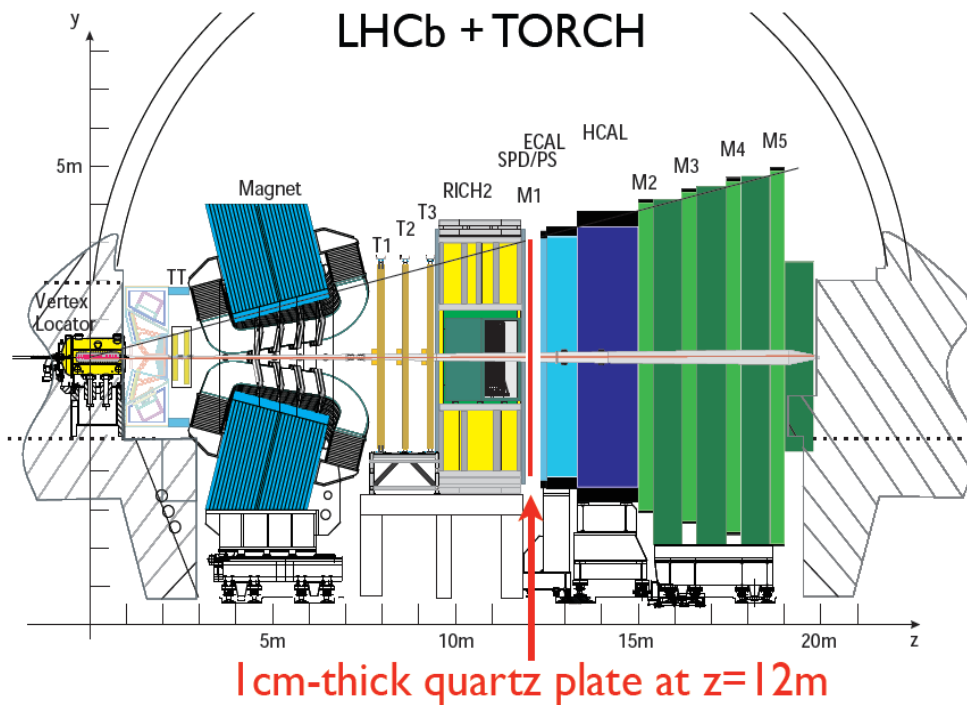


PANDA endcap DIRC



LHCb PID upgrade: TORCH

A special type of Time-of-Propagation counter for the LHCb upgrade



New possibilities in medical imaging: TOFPET with Cherenkov light

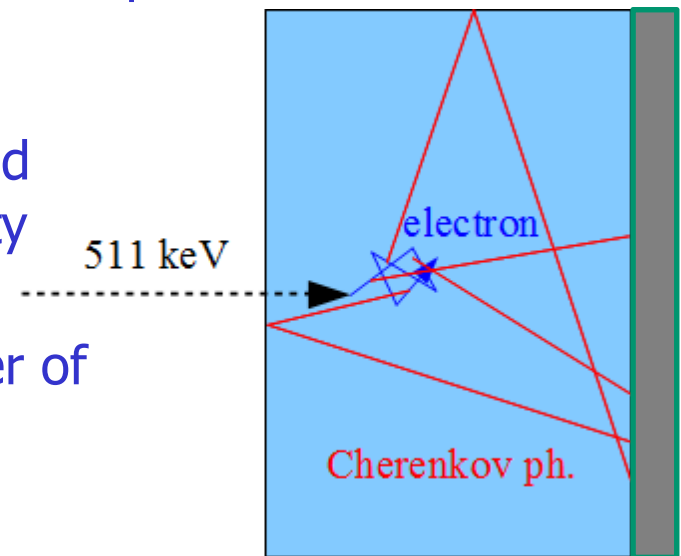
Time-of-Flight difference of annihilation gammas is used to improve the contrast of images obtained with PET:

- localization of source position on the line of response
- reduction of coincidence background
- improvement of S/N

Novel photon detectors – MCP-PMT and SiPM – have excellent timing resolution → TOF resolution limited by the scintillation process

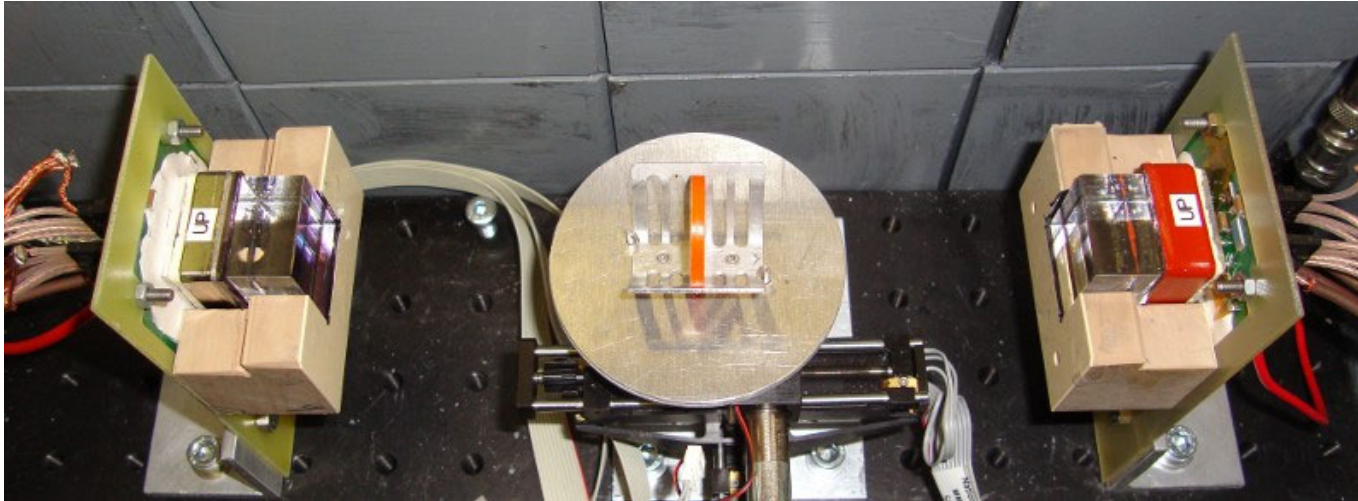
Cherenkov light is **promptly produced** by a charged particle traveling through the medium with velocity higher than the speed of light c_0/n .

Disadvantage of Cherenkov light is a small number of Cherenkov photons produced per interaction → **detection of single photons!**

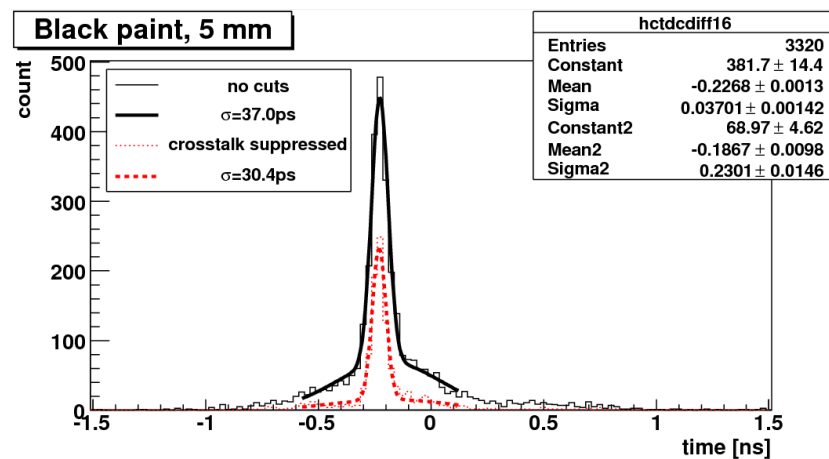


TOF-PET with Cherenkov light

Two detectors in a back-to-back configuration with $25 \times 25 \times 15 \text{ mm}^3$ crystals coupled to MCP-PMT with optical grease.



5 mm long crystal:
→ FWHM $\sim 70 \text{ ps}$



→ NIM A654(2011)532–538

→ Talk by P. Križan - tomorrow

Summary

- Low light level detection is at the hearth of many detectors in particle and nuclear physics
- New methods require very fast timing in radiation harsh environments
- A number of new detectors has been developed recently to cope with these requirements
- **A very active field!**

Back-up slides

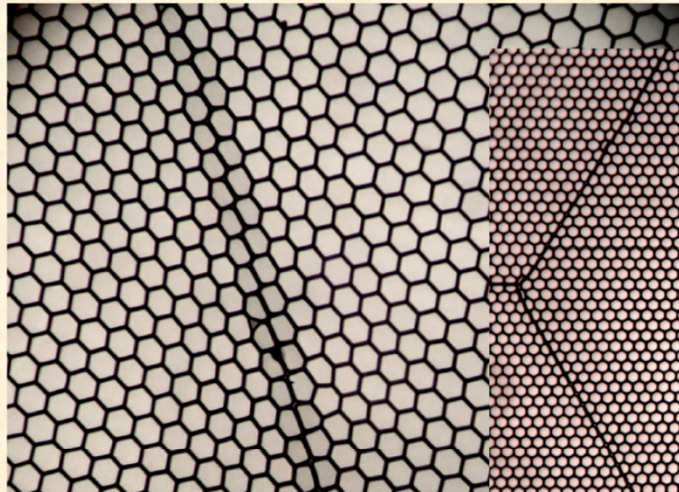
ALD for MCP PMTs: born in Chicago area.

ALD can turn a borosilicate glass substrate into an MCP



Borosilicate Substrate Atomic Layer Deposited Microchannel Plates

Micro-capillary arrays (Incom) with 10 μ m, 20 μ m or 40 μ m pores (8° bias) – borosilicate glass. l/d typically 60:1, but can be much larger. Open area ratios from 60% to 83%. Fabricated with using hollow tubes (no etching). Separate resistive and secondary emissive layers are applied (ANL, Arradance) using atomic layer deposition to allow these to function as MCPs. ALD secondary emissive layers can also be applied to “standard” MCPs to improve yield.



40 μ m pore borosilicate micro-capillary MCP with 83% open area.

Pore distortions at multifiber boundaries, otherwise very uniform.

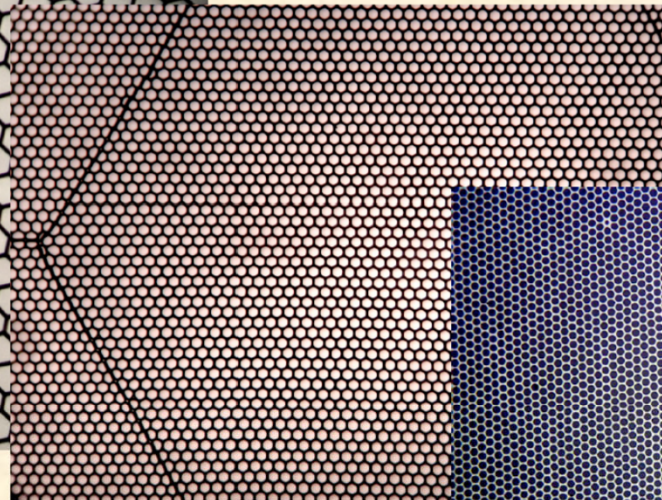


Photo of a 20 μ m pore, 65% open area borosilicate micro-capillary ALD MCP (20cm).

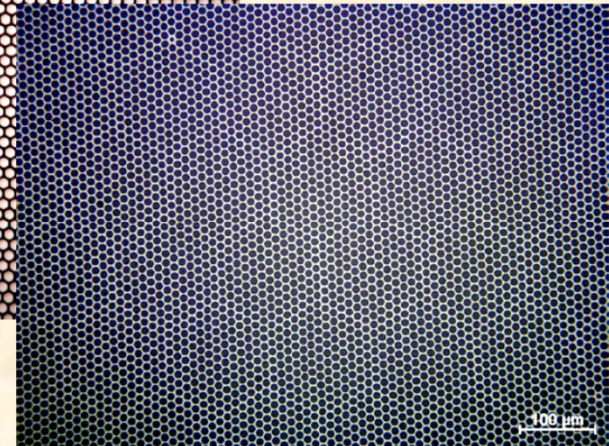
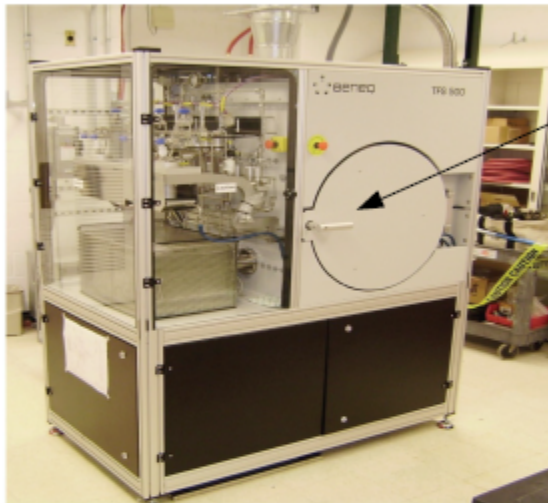


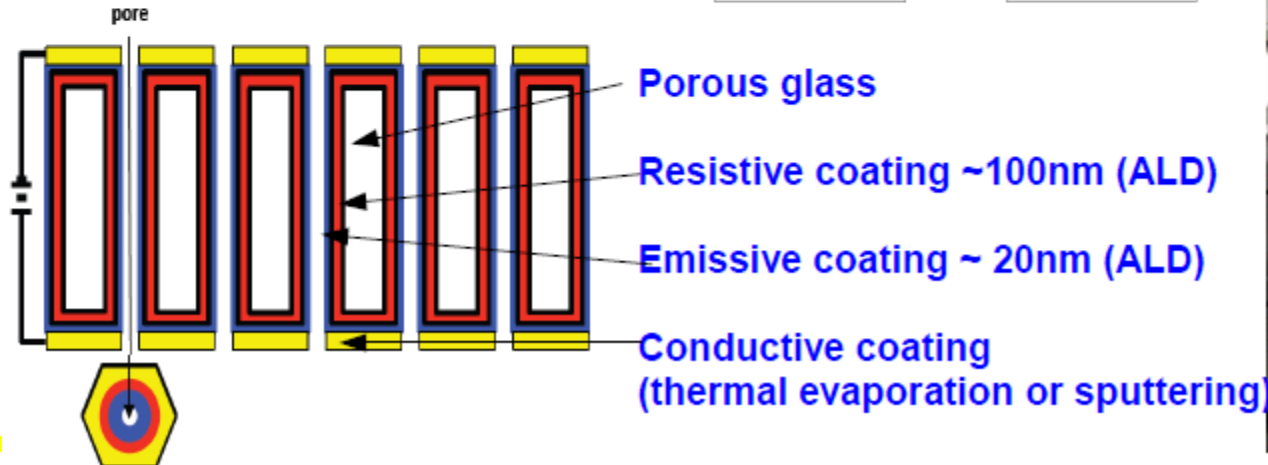
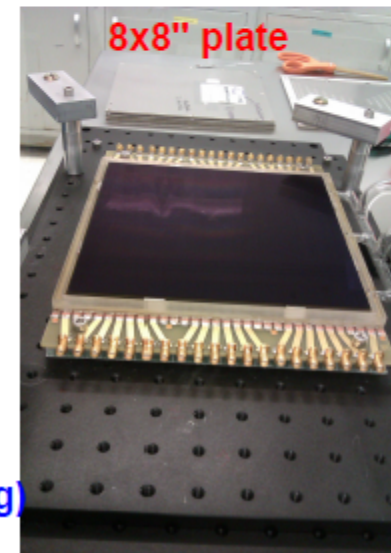
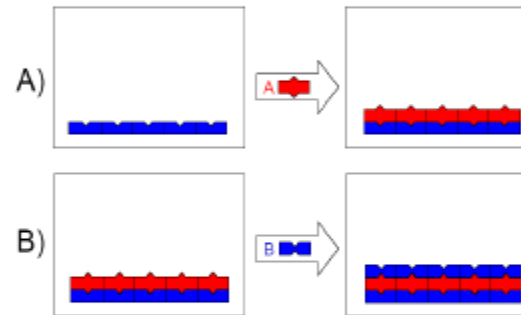
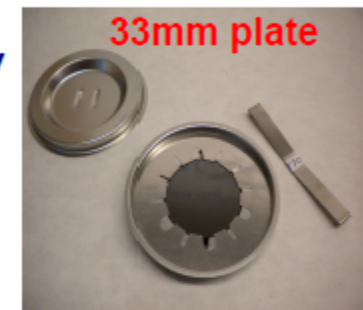
Photo of a 10 μ m pore, 60% open area borosilicate micro-capillary ALD MCP.

LAPPD – Large Area Picosecond Photon Detector

MCP by Atomic Layer Deposition (ALD)



Beneq reactor for ALD
@Argonne National Laboratory
A.Mane, J.Elam





Key Issues for ALD Borosilicate MCPs

Current MCP devices have specific limitations due to the nature of the structure and processing of conventional MCPs. Atomic layer deposited (ALD) MCPs made on borosilicate substrates provide a unique way to improve on current devices or make new device types.

Borosilicate substrate:-

Strong & clean compared with standard MCP glass

Large areas can be made

large detectors for security applications

Larger open area ratios

– higher photon /electron/ion detection efficiency

Low/no radioactive content

lower background for security applications

Low outgassing

longer device lifetimes, shorter process/fab times

High temperatures

deposit materials & cathodes not otherwise possible

Atomic layer deposition:-

Decoupled from substrate, many materials possible

Resistance tailored to suit

can make a wider range than standard MCPs

allowing high local counting rates

High secondary emissive layer

better pulse height at low gain, better gain

Stable secondary emissive layer

faster gain burn-in, or none needed

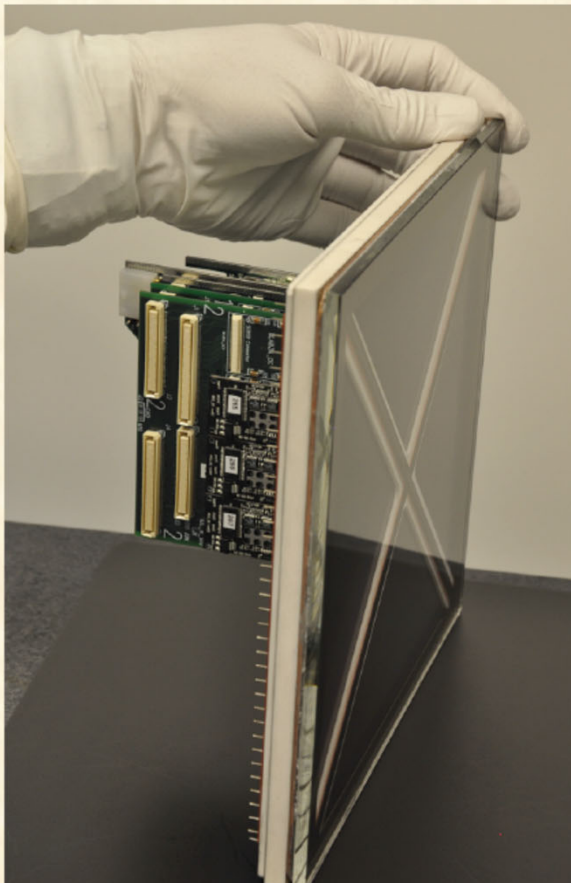
– very long lifetime & durability

– compatibility with alkali cathodes



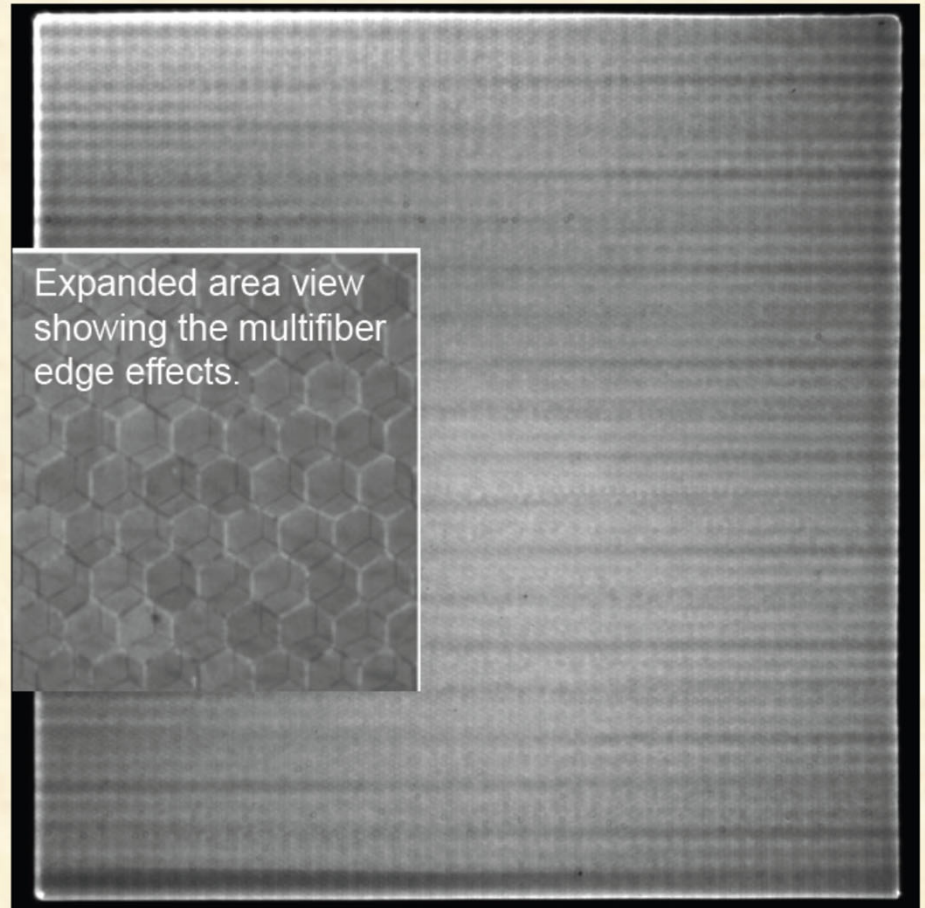
20cm ALD-MCP & Sealed Tube Development

LAPPD collaboration development of 20cm ALD MCPs and sealed tube with bialkali cathode and stripline anode for 2D imaging and $<10\text{ps}$ timing.



Also see Incom poster.

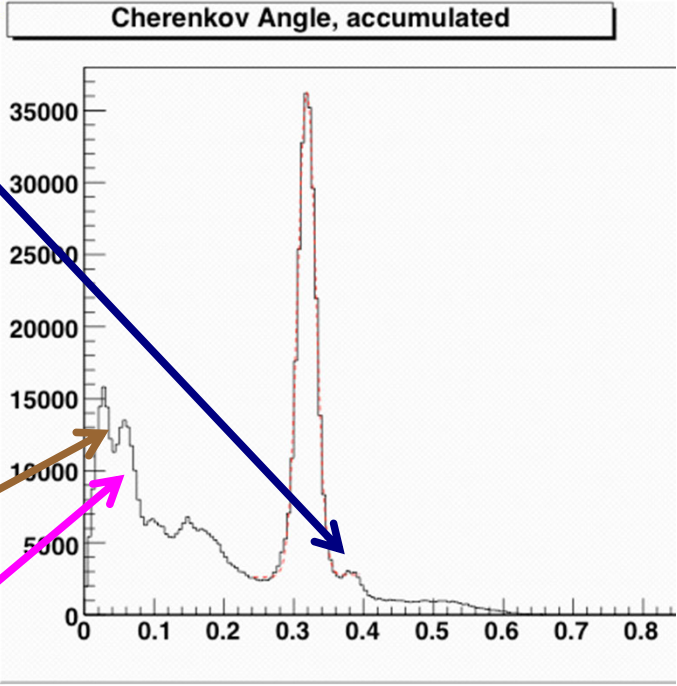
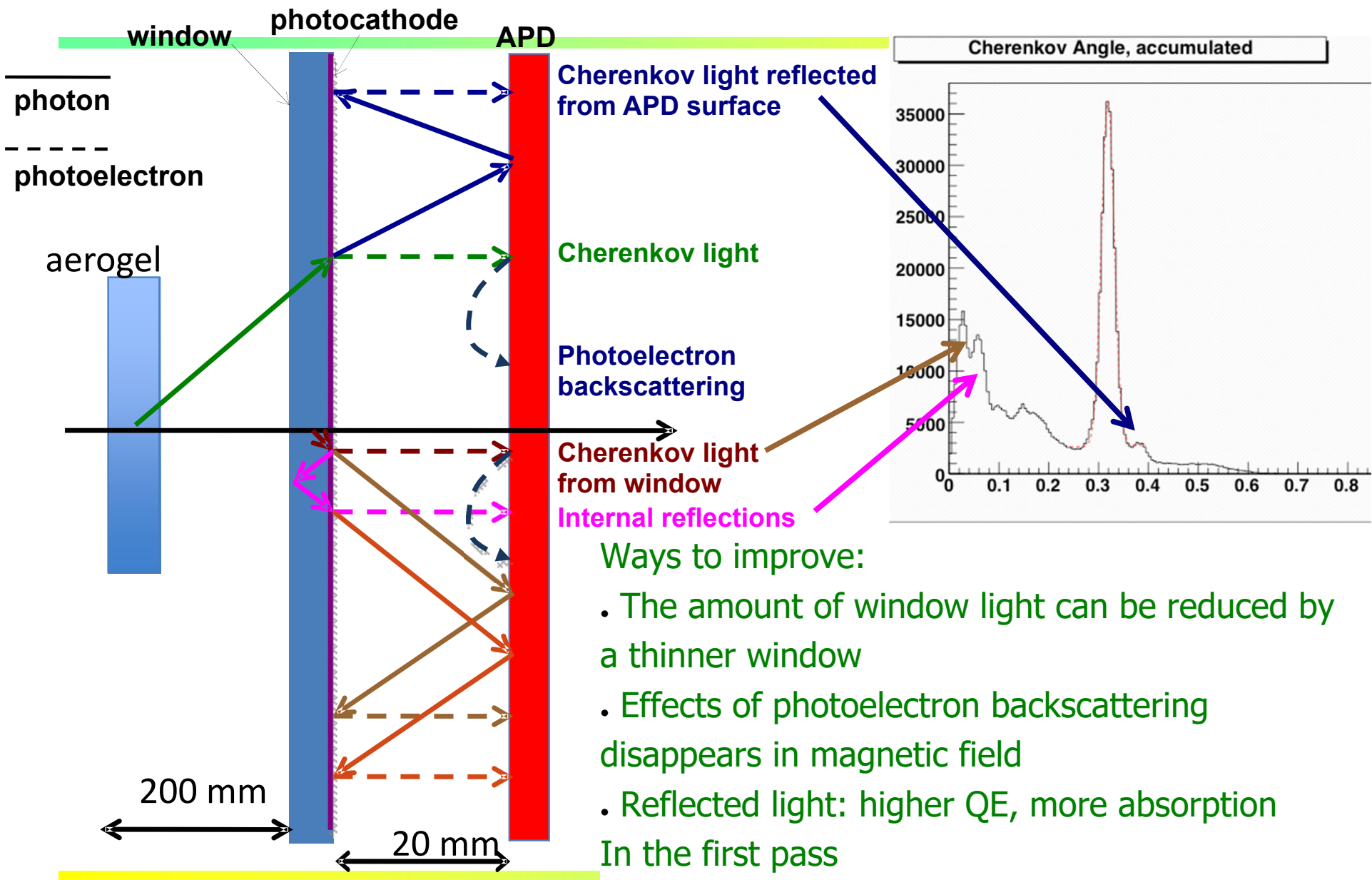
First tube did not seal, making new tubes this summer



20cm, $20\mu\text{m}$ pore, Al_2O_3 SEY, MCP pair image with 185nm non-uniform UV illumination. Cross delay line photon counting anode. Image striping is due to the anode period/charge cloud size modulation.

→ Extremely important development, many talks in this workshop

Ring image, background contributions (B=0T)



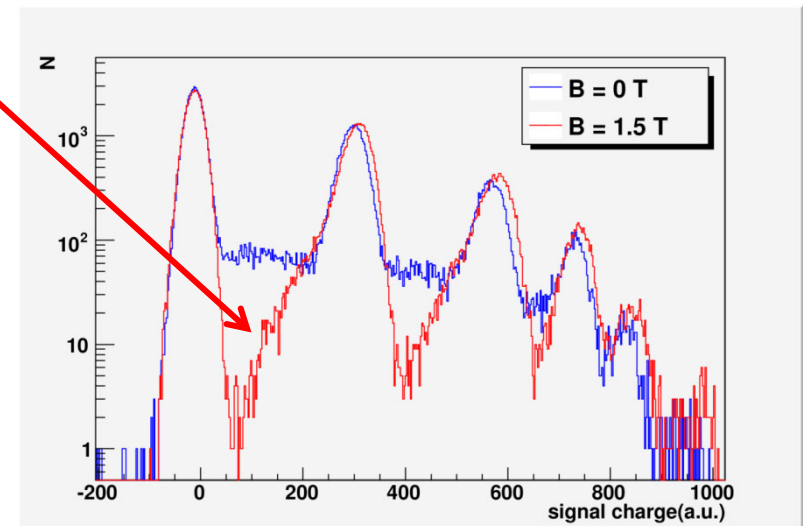
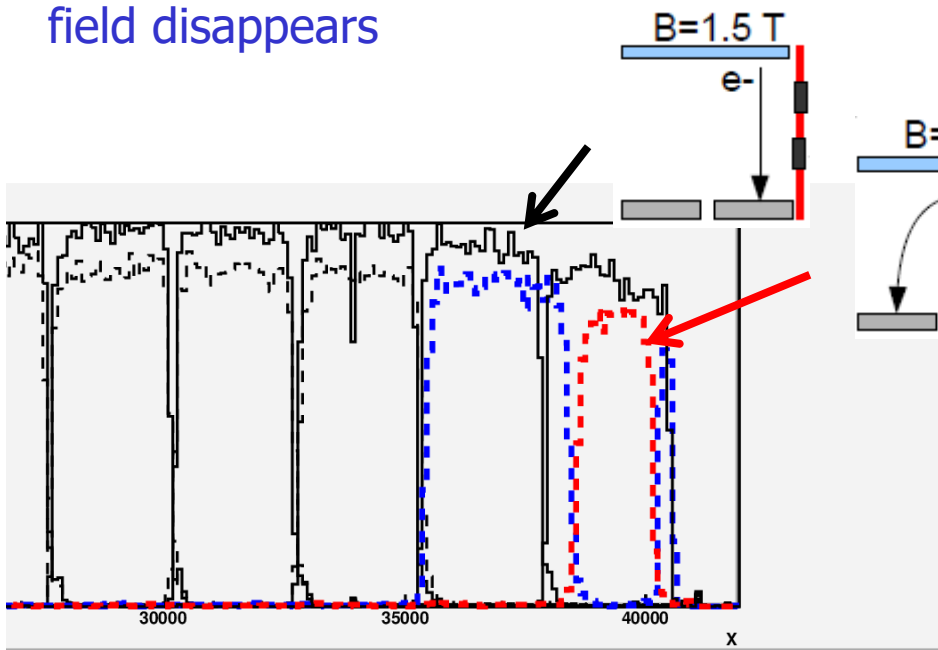
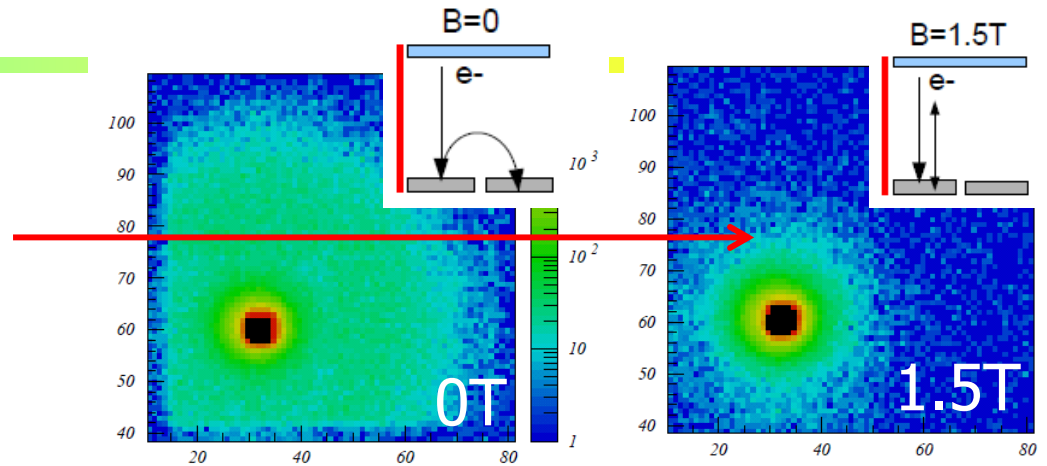
Ways to improve:

- The amount of window light can be reduced by a thinner window
- Effects of photoelectron backscattering disappears in magnetic field
- Reflected light: higher QE, more absorption in the first pass
- Anti-reflective coating?

HAPD: operation in 1.5 T

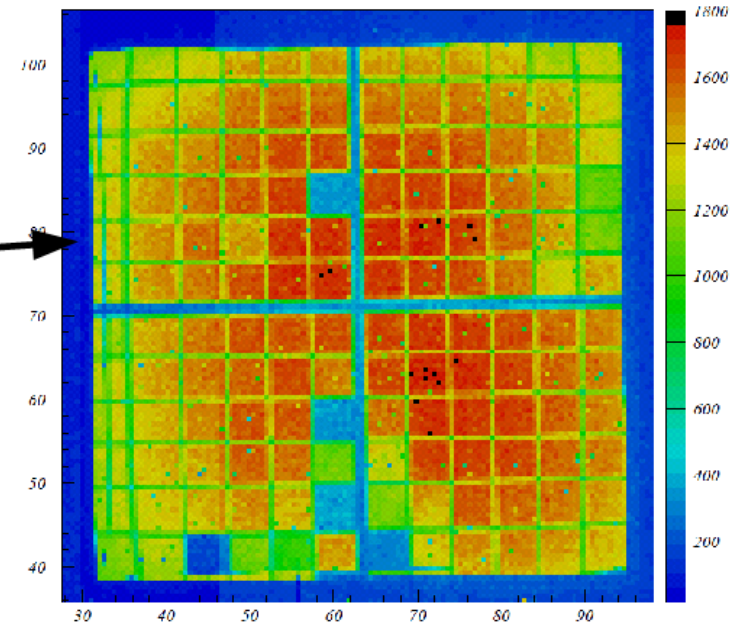
Tests in 1.5 T magnetic field show improved HAPD performance:

- no photoelectron back-scattering cross-talk
- increase of detection efficiency – photoelectron energy deposited at one place
- effect of non-uniformity of electric field disappears



Test in magnetic field 1.5 T

- distortion of electric field lines at HAPD edge produces irregular shapes of areas covered by each channel
- in magnetic field photoelectrons circulate along the magnetic field lines and distortion disappears



no magnetic field

magnetic field 1.5 T

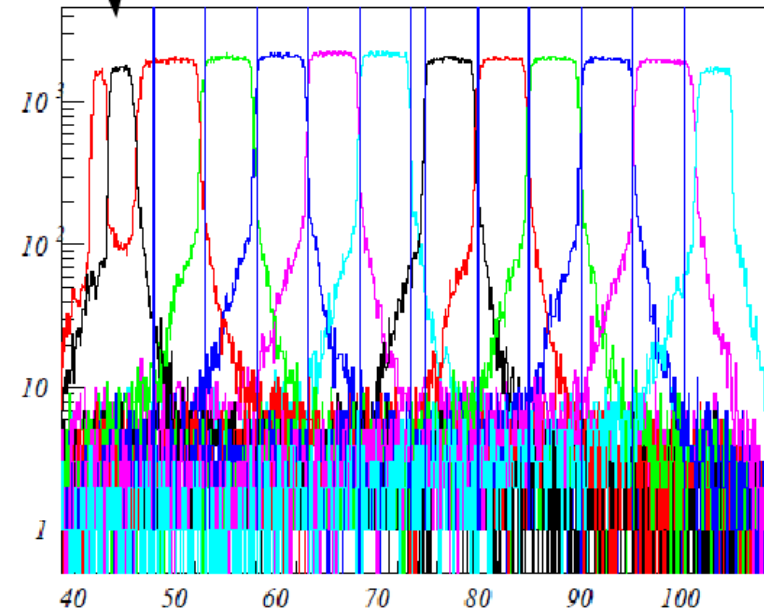
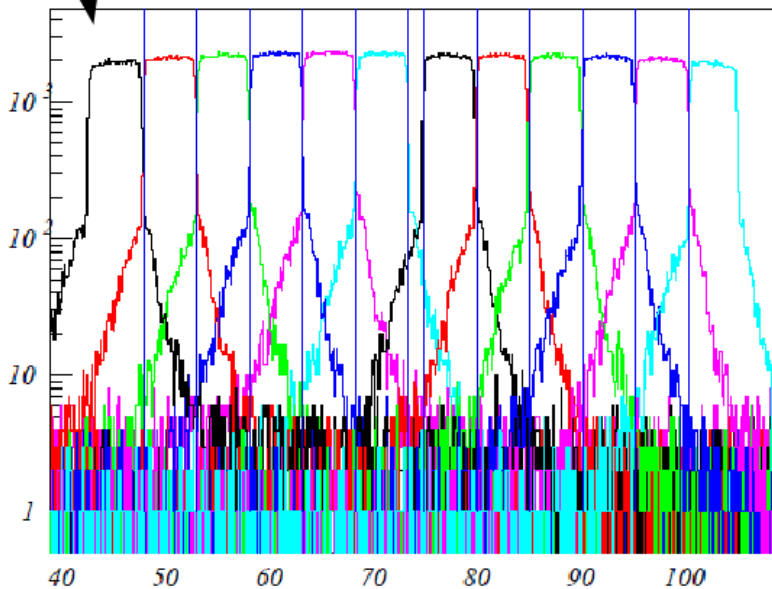
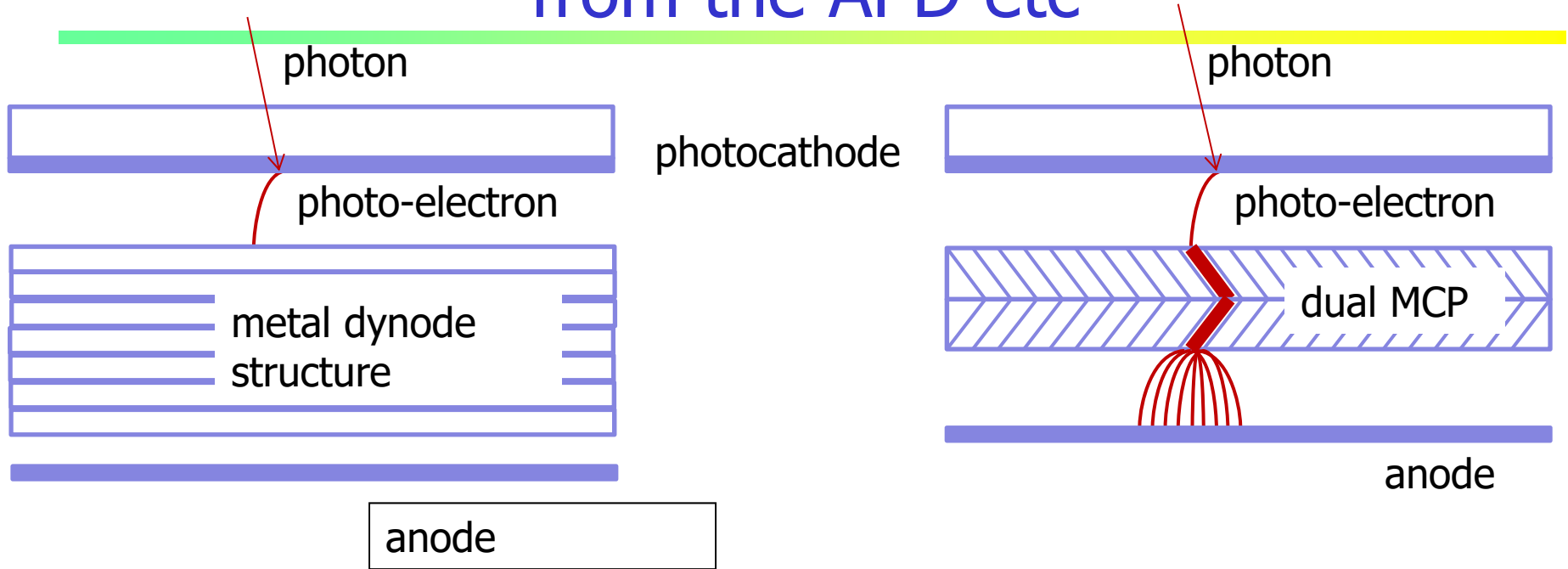


Photo-electron backscattering, light reflection from the APD etc



Similar geometries in the photo-electron step
 → A lot of **similarities** between **prox. focusing HAPD, MCP PMTs and MA-PMTs**

